GEOLOGY AND GENESIS OF THE WOLF PRECIOUS METAL EPITHERMAL PROSPECT AND THE CAPOOSE BASE AND PRECIOUS METAL PORPHYRY-STYLE PROSPECT, CAPOOSE LAKE AREA, CENTRAL BRITISH COLUMBIA

By

KATHRYN PAULINE ELIZABETH ANDREW

B.Sc., The University of British Columbia, 1985

A THESIS SUBMITTED IN PARTIAL FULFILLMENT OF

THE REQUIREMENTS FOR THE DEGREE OF

MASTER OF SCIENCE

in

THE FACULTY OF GRADUATE STUDIES

DEPARTMENT OF GEOLOGICAL SCIENCES

We accept this thesis as conforming to the required standard

.....

.....

.....

.....

THE UNIVERSITY OF BRITISH COLUMBIA

April 1988

Frontispiece above - View of the Wolf Prospect looking west showing the characteristic low relief and tree covered area.

Frontispiece below - View looking northeast to Zone 1 at the Capoose Prospect on Fawnie Range. Recessive lithic wacke units are grass-covered, rhyolite sills are bare. Stratigraphy dips obliquely to the left and toward the fore ground at approximately 40°.

ABSTRACT

The Wolf and Capoose prospects represent two distinctly different types of precious metal deposits in volcanic rocks of the Stikinia terrane, central British Columbia.

At the Wolf prospect, auriferous and argeniferous metallic minerals are in bladed quartz-carbonate veins and heterolithic breccias within Lutetian calc-alkaline rhyolite of the Ootsa Lake Group. Electrum, native silver, and silver sulphosalts occur as inclusions in and adjacent to pyrite in five silicic zones which have eight recognisable phases of veining and brecciation and are bordered by argillic and sericitic altered rhyolite. Fluid inclusions define growth zones in precious metal-bearing quartz-carbonate veins and precious metal-poor drusy quartz veins. The inclusions are primary, two-phase, liquid-rich, low salinity, and low CO_2. Homogenization temperatures of quartz-carbonate veins are 270°C and 170°C and in the late drusy quartz veins, 250°C. Oxygen and hydrogen isotope compositions of vein quartz, rhyolite, and alkali feldspar phenocrysts indicate that depositional fluids were are ^{18}O depleted by 4 to 9 $^{o}/_{oo}$.

Ootsa Lake Group rocks at Wolf are formed by explosive eruptions and flows, related to a ring fault. Flat-lying rhyolite tuffs and flows are intruded by cogenetic stocks and dykes in a maar setting. Precious metal deposition occurred as one event related to quartz-carbonate veins. Later drusy quartz veins precipitated from a different

fluid. Primary fluid inclusion homogenization temperatures show that fluids which deposited quartz-carbonate were boiling and existed under both hydrostatic and near lithostatic pressures at depths of about 96 m. Oxygen and hydrogen isotope compositions indicate a high degree of isotopic exchange between rhyolite and large volumes of low ^{18}O content meteoric fluids. The fluids evolved to a non-boiling, lower salinity, extremely ^{18}O depleted, precious metal-poor variety which precipitated late drusy quartz veins. Geological setting, vein and breccia textures, alteration, metal distribution and depositional fluid composition at Wolf resemble a low sulphur, epithermal hot spring or silicified stockwork deposit.

At the Capoose prospect, auriferous and argeniferous metallic minerals occur as inclusions within disseminated galena and sphalerite in calc-alkaline Maastrichtian rhyolite sills intrusive into Lower and Middle Jurassic Hazelton Group volcanic and sedimentary rocks. Flow-banded, spherulitic rhyolite sills are preserved within a minor horst. Spessartines in the sills are similar in composition to plutonic garnets with less than 5% change in end member composition from rim to core. They occur adjacent to disseminated, aggregate and vein galena, sphalerite, pyrite, arsenopyrite and chalcopyrite. Sulphide and spessartine accummulations are commonly surrounded by muscovite and quartz coronas. Sulphide poor quartz and calcite veining is in hornfelsed Hazelton Group rocks peripheral to the sills.

Phyllic alteration is restricted to the sills and overprints mineralized zones. Primary two-phase, liquid-rich, low salinity, low CO_2 fluid inclusions from late silicate veins homogenize from 285°C to 335°C. Rhyolite sills are not depleted in ^{18}O whereas sericite, quartz and calcite are.

Spessartine in rhyolite sills at Capoose crystallized as late phenocrysts stabilized by high manganese content. They provided a nucleus for sulphide deposition shortly after sill emplacement in groundwater saturated, permeable Hazelton Group rocks. Cooling, crystallization and fracture development in the sills initiated hydrothermal circulation and phyllic alteration with late quartz and calcite veins related to collapse of the hydrothermal system. Lead-zinc mineralization occurred as two events, with only one related to precious metal and copper deposition. Oxygen isotope compositions of quartz-garnet mineral separate pairs indicate crystallization of garnets and sulphides from magmatic fluids at temperatures from 528°C to 725°C. Sericite, quartz and calcite precipitated from meteoric fluids. In summary, hydrothermal fluids at the Capoose prospect evolved from early, high temperature magmatic fluids to late lower temperature, low salinity, meteoric fluids. The geological setting, silicate and sulphide mineralogy, alteration, metal distribution and depositional fluid evolution at Capoose resemble a low-grade, epigenetic, intrusion-related, porphyry-style deposit.

VI

TABLE OF CONTENTS

LIST OF TABLES

LIST OF FIGURES

3.9 Jensen Cation plot for analyses from the Wolf prospect (Table 3.3, boundaries are from Jensen, 1976). Assemblages are calc-alkaline to tholeiitic (section 3.2.2) and are plotted using: squares = mafic volcanics, diamonds = pyroclastic rocks, triangles = rhyolite flows, circles = intrusions.

3.10 Plot of alkalies vs. silica for analyses from the Wolf prospect (Table 3.3, boundaries are from Le Bas et al., 1986). Assemblages are predominantly rhyolites (section 3.2.2) and are plotted using: squares = mafic volcanics, diamonds = pyroclastic rocks, triangles = rhyolite flows and circles = intrusions.

3.11 Triaxial oxide plot (Fe_2O_3 + FeO + 1/2 (MgO + CaO) vs. Al_2O_3/SiO_2) for analyses from the Wolf prospect (Table 3.3) boundaries from Church, 1975). Assemblages are predominantly rhyolites (section 3.2.2) and are plotted using: squares = mafic volcanics, diamonds = pyroclastic rocks, triangles = rhyolite flows, circles = intrusions.

3.12 SiO_2 vs. Nb/Y plot for analyses from the Wolf prospect (Table 3.3, boundaries from Winchester and Floyd, 1977). Assemblages are dominantly rhyolite and rhyodacite (section 3.2.2) and are plotted using: squares = mafic volcanics, diamonds = pyroclastic rocks, triangles = rhyolite flows and circles = intrusions.

3.13 Zr/TiO_2 vs. Nb/Y plot for analyses from the Wolf prospect (Table 3.3, boundaries from Winchester and Floyd, 1977). Assemblages are dominantly rhyolite and rhyodacite (section 3.2.2) and are plotted using: squares = mafic volcanics, diamonds = pyroclastic rocks, triangles = rhyolite flows and circles = intrusions.

3.14 K_2O vs. SiO_2 plot for analyses from the Wolf prospect (Table 3.3, boundaries are from de Rosen-Spence, 1976). Abbreviations are: LK = low potassium, MK = medium potassium, HK = high potassium, VHK = very high potassium, EHK = extremely high potassium. Felsic volcanic assemblages have high (HK) to very high (VHK) potassium (section 3.2.2) and are plotted using: diamonds = pyroclastic rocks, triangles = rhyolite flows and circles = intrusions.

3.15 Zr/Nb vs. Y/Nb plot for analyses from the Wolf prospect (Table 3.3) shows that the Eocene volcanic suite is cogenetic because the variance in conserved element ratios for the data is less than the variance attributable to analytical uncertainty.

precipitation at the Wolf prospect. Shaded area represents subsequently filled vein opening. Data from gold-bearing bladed quartz-carbonate veins (section 3.6.1.5) indicate that conditions alterated between A and C at the boiling point.

3.39 Locations of samples of whole rock, vein and mineral separate samples used for oxygen isotope analyses from the Wolf property. A)west half, and B) east half.

3.40 dD vs. $d^{18}O$ values showing fields for magmatic and metamorphic water and the range of depositional fluid composition at Wolf, central B.C. Values for other Tertiary volcanic-hosted epithermal deposits in B.C., Yukon Territory, and western U.S.A. are also shown.

3.41 dD vs. $d^{18}O$ for quartz vein samples from the Wolf prospect with proposed fluid evolution line.

3.42 Schematic diagram illustrating Ootsa Lake Group volcanic setting at Wolf using a maar model. 1 = conglomerate and tuffs, 2 = pyroclastic assemblage, 3 = rhyolite dome, flows and breccia, and 4 = intrusions.

3.43 Schematic cross-section of low sulphur, hot-spring type silicified stockwork model for the genesis of the Wolf prospect, central British Columbia.

4.1 Geology of the Capoose prospect, Capoose Lake area, central British Columbia. Cross-sections A-A' and B-B' are in Figures 4.2 and 4.3, respectively.

4.2 Cross section A-A' (Fig. 4.1) across the main zone on the Capoose property defining two northeast-trending dip-slip faults which mark the boundaries of a minor horst.

4.3 Cross section B-B' (Fig. 4.1) across the northwestern limb of the Fawnie Range syncline showing stratigraphic relationships

4.4 Whole rock and trace element chemical analyses sample locations, Capoqse property, Capoose Lake area.

4.5 Logarithmic oxide molecular proportion ratio plots (K_2O denominator) for comparison of Capoose volcanic rocks to 'modern' volcanic suites and retrieval of least altered data (Beswick, 1978). Most dots which represent rocks from the Capoose prospect (Appendix 1B) fall predominantly within the limits for 'modern' volcanic suites. Least altered rocks are in Table 3.3.

4.6 Plot of alkalies vs. silica for analyses from the

Capoose property (Table 4.3, boundaries are from MacDonald, 1968, and Irvine and Baragar, 1971). Assemblages are sub-alkaline (section 4.2.2) and are plotted using: squares = mafic volcanics, diamonds = volcaniclastics, triangles = rhyolite sills and circles = dykes.

4.7 AFM diagram with analyses from the Capoose property (Table 4.3, boundaries are from Wager and Deer, 1939). Assemblages are 'calc-alkaline (section 4.2.2) and are plotted using: squares = mafic volcanics, diamonds = volcaniclastics, triangles = rhyolite sills and circles = dykes.

4.8 Jensen Cation plot for analyses from the Capoose prospect (Table 4.3, boundaries are from Jensen, 1976). Assemblages are dominantly calc-alkaline (section 4.2.2) and are plotted using: squares = mafic volcanics, diamonds = volcaniclastics, triangles = rhyolite sills, circles = dykes.

4.9 Plot of alkalies vs. silica for analyses from the Capoose property (Table 4.3, boundaries are from Le Bas et al., 1986). Assemblages are 'rhyolites' (section 4.2.2) and are plotted using: squares = mafic volcanics diamonds = volcaniclastics, triangles = rhyolite sills and circles = dykes.

4.10 Triaxial oxide plot (Fe_2O_3 + FeO + 1/2 (MgO + CaO) vs. Al_2O_3/SiO_2) with analyses from the Capoose prospect (Table 4.3). Assemblages are 'rhyolites' (section 4.2.2) and are plotted using: squares = mafic volcanics diamonds = volcaniclastics, triangles = rhyolite sills and circles = dykes.

4.11 K_2O vs. SiO_2 plot for analyses from the Capoose prospect (Table 4.3, boundaries are from de Rosen-Spence, 1976). Abreviations are: LK = low potassium, MK = medium potassium, HK = high potassium, VHK = very high potassium, EHK = extremely high potassium. Rhyolite sills have high (HK) potassium (section 4.2.2) and are plotted using the following symbols: squares = mafic volcanics, diamonds = volcaniclastics, triangles = rhyolite sills and circles = dykes.

4.12 Line graphs depicting calcium, magnesium, iron and manganese compositional zoning from rim-to-core in three brown garnet and three pink garnet grains from units 6, 7, and 8 (Fig. 4.1, Table 4.7). Sympathetic variation in manganese and iron differs from calcium and magnesium variation. Zonation in pink and brown garnets is distinctive (section 4.5.4.2).Vertical bars are standard deviations of analyses. A) KCP009-RIM6 brown, B) KCP012-RI18 brown, C) KCP054-R208 brown,

D) KCP009-R218 pink, E) KCP012-RI12 pink, F) KCP054 -R202 pink.

4.13 Compositions of Capoose garnets, expressed as the end members: AL (almandine) + PY (pyrope), SP (spessartine), and GR (grossularite) + AN (andradite), are compared with the following environments: plutonic (Troger, 1959; Vennum and Meyer, 1979), volcanic (Bryant, 1975; Fitton, 1972; Green and Ringwood, 1968; Oliver, 1956; Troger, 1959; Wood, 1974), greenschist (Brown, 1969; Fodor and Burt, 1979; Troger, 1959), and amphibolite (Miyashiro, 1953; Troger, 1959). Capoose garnets are similar only to SP-rich plutonic garnets.

4.14 Mineralized zones of the Capoose Prospect, Capoose Lake area, central British Columbia.

4.15 a) Southwest-northeast vertical section (B-B':Fig. 4.1) of the Capoose prospect showing distribution from zones 1 and 2 (Fig 4.14) of A) sphalerite, B) galena, C) arsenopyrite, D) chalcopyrite, and E) pyrite with depth. Refer to Figure 4.3 for geology.

4.16 Qualitative alteration map of the Capoose prospect. Zones of phyllic alteration are indicated by hatched lines; extreme phyllic alteration is indicated by crosshatching.

4.17 Logarithmic probability plots illustrating distribution of A = Ag, B = Cu, C = Pb, and D = Zn from the Capoose prospect. Means and standard deviations are in Table 4.11.

4.18 Line diagram illustrating estimated paragenesis of dominant sulphides and precious metals at Capoose.

4.19 Sample locations of veins used for fluid inclusion analyses from the Capoose prospect. Section B-B' is located in Figure 4.1. Sample descriptions are in Table 4.15.

4.20 Eutectic and last melting temperatures of inclusions from quartz and calcite veins from the Capoose prospect. Freezing data are in Table 4.12.

4.21 A) Homogenization temperature vs. vein type, and B) homogenization temperature vs. origin type for fluid inclusions from quartz and calcite veins from the Capoose prospect. Data are in Table 4.12.

4.22 Sample locations of whole rock, vein and mineral separate samples used for stable isotope analyses from the Capoose prospect. See Figure 4.20 for sample locations from drill core.

XF

4.23 dD vs. $d^{18}O$ values showing fields for magmatic and metamorphic water and the range of deposition of fluid composition at Capoose, central B.C. Values for other well known deposits are also shown.

4.24 Low-grade, epigenetic, intrusion-related, porphyry -style model for genesis of the Capoose prospect, central British Columbia.

LIST OF PLATES

Frontispieces

ACKNOWLEDGEMENTS

Field and financial support for this study was generously provided by Rio Algom Exploration Inc., Vancouver, the British Columbia Ministry of Energy, Mines and Petroleum Resources, Cominco Ltd. and a G.R.E.A.T. Award from the British Columbia Science Council. Granges Exploration Ltd. and Cominco Ltd. are thanked for permission to visit the Capoose property. I am sincerely grateful to Dr. Colin Godwin for his helpful guidance, constant support, and constructive editing. Dr. T.K. Kyser gave considerately of his consultation, hospitality and time; D. Pezerdec, M. Wilson and P. Honovar were extremely helpful in the stable isotope laboratory in Saskatoon. R.M. Cann initiated the Wolf project and was always available for enlightening discussion. D.V. Lefebure generously gave his time and ideas in the field at Capoose. I thank Dr. G. Rouse for allowing access to his laboratory and his perseverence with elusive palynomorphs. Dr. P. Michael and M. Piranian are thanked for undertaking the microprobe analyses. Dr. J.K. Russell provided careful editing and constructive comments. I thank B.N. Church and T.G. Schroeder for allowing use of their data from the Capoose prospect. C. Stanley gave permission and advice on program PEARCE.PLOT. Special thanks go to T. Hoy for inspiring confidence through helpful discussions and advice. I am grateful to R. Light and my friends R. Gaba, K. Hancock, B. Laird and P. Desjardins for their timely drafting assistance and good cheer. My family was an encouraging and unfailing source of moral support.

CHAPTER 3

THE WOLF PRECIOUS METAL EPITHERMAL PROSPECT: GEOLOGY AND GENESIS

3.1 LOCATION AND ACCESS

The Wolf epithermal precious metal vein prospect (Fig 1.1) is near latitude 53°12′ north and longitude 125°26′ west (N.T.S.: 93F/03) in central British Columbia, about 6 kilometres southeast of Entiako Lake and approximately 185 kilometres southwest of Prince George. Access is by helicopter, float plane or four-wheel drive road off kilometre 141 on the main Kluskus-Ootsa logging road running southwest from Vanderhoof.

3.2 GEOLOGY

3.2.1 INTRODUCTION

The Wolf prospect is within Ootsa Lake Group volcanic rocks (Fig 2.1) in an area characterised by approximately 1% rock outcrop. These predominantly felsic volcanic rocks are assigned to the rhyolite member of the Eocene Ootsa Lake Group (Tipper, 1963) which unconformably overlies Jurassic Hazelton Group rocks in the Capoose Lake area. The Ootsa Lake Group is unconformably overlain by mid-Miocene unconsolidated sedimentary rocks (Rouse, pers. comm., 1988).

3.2.2 STRATIGRAPHY AND PETROLOGY

The Ootsa Lake Group rhyolite member is composed predominantly of felsic volcanic and volcaniclastic rocks

(after Tipper, 1963). Intrusive into these rocks are rhyolite domes with associated flows and breccias as well as porphyritic plugs and dykes.

Field relations and petrologic observations define 10 units at a map scale of 1:5000 within the rhyolite member of the Ootsa Lake Group. These are shown on Figure 3.1 and described below and listed in Appendix 1.

Map units on the property are grouped into four assemblages (Table 3.1) based on spatial relationships, similarity of depositional environment, complementary lithologies and associated textures. The assemblages, from oldest to youngest, are: (1) conglomerate and tuffs (Eo_1 and Eo_2), (2) pyroclastics and subordinate flows (Eo_3 to Eo_6), (3) rhyolite flows and breccias (Eo_7 and Eo_8), and (4) intrusions (Eo_9 and Eo_{10}). Units are correlated, where possible, with Ootsa Lake Group subdivisions of Diakow and Mihalynuk (1987) in the Whitesail Lake area.

Conglomerate and tuffs (Eo_1 and Eo_2) crop out in a creek and along a ridge on the northwest side of the property (Fig. 3.1). Boulder conglomerate (Eo_1) is a matrix supported basal unit with 30% well-rounded granodiorite clasts (5 cm to 0.5 m in diameter), 10% angular andesite clasts (up to 15 cm in diameter), and 5% subrounded aplite clasts (20 to 30 cm in diameter). The tuffaceous matrix has up to 60% quartz. Although partly derived from volcanic rocks, the quartzose matrix, and granodiorite and aplite clasts indicate a dominantly granitic provenance. This unit

TABLE 2.1: Correlation among major geological groups and formations from the Capoose Lake area (NTS:093F), Whitesail Lake area (NTS:093E), Smithers area (NTS:093L), Gang ranch-Big bar area (NTS:092O)

			CAPOOSE LAKE AREA (Tipper 1963;, Tipper et al. 1979, this study)		WHITESAIL LAKE AREA (Duffel 1959, Diakow and Mihalynuk 1987; Diakow and Koyanagi 1988)		SMITHERS AREA (Tipper and Richards 1976; MacIntyre and Desjardins 1988)		GANG RANCH - BIG BAR AREA (Tipper 1978; Mathews and Rouse 1984)	
PERIOD	EPOCH	AGE	GROUP	FORMATION	GROUP	FORMATION	GROUP	FORMATION	GROUP	FORMATION
QUATERNARY	HOLOCENE									
	PLEISTOCENE									
TERTIARY	PLIOCENE		unnamed basalt						unnamed basalt	
	MIOCENE L			?						
	MIOCENE M			FRASER BEND					FRASER BEND	
	MIOCENE E									
	OLIGOCENE L								"Blackdome Mtn basalt"	
	OLIGOCENE E				ENDAKO				"Porcupine Ck obsidian"	
	EOCENE L									
	EOCENE M	BARTONIAN								
	EOCENE M	LUTETIAN	OOTSA LAKE		OOTSA LAKE				KAMLOOPS	
	EOCENE E									
	PALEOCENE L									
	PALEOCENE E									
CRETACEOUS	LATE	MAASTRICHTIAN	unnamed rhyolite							
	LATE	CAMPANIAN	QUANCHUS INTRUSIONS		KASALKA		KASALKA			
	LATE	SANTONIAN								
	LATE	CONIACIAN								
	LATE	TURONIAN								
	LATE	CENOMANIAN							?	? SPENCES BRIDGE/ KINGSVALE
	EARLY				SKEENA		? SKEENA	? RED ROSE	JACKASS MTN	
JURASSIC	LATE									
	MIDDLE	CALLOVIAN			BOWSER LAKE	ASHMAN	BOWSER LAKE	ASHMAN		
	MIDDLE	BATHONIAN			?	?				
	MIDDLE	BAJOCIAN	HAZELTON M	SMITHERS	HAZELTON	SMITHERS	HAZELTON	SMITHERS		
	MIDDLE	AALENIAN								
	EARLY	TOARCIAN		NILKITKWA				NILKITKWA		
	EARLY	PLIENSBACHIAN								
	EARLY	SINEMURIAN	L			TELKWA		TELKWA		
	EARLY	HETTANGIAN								

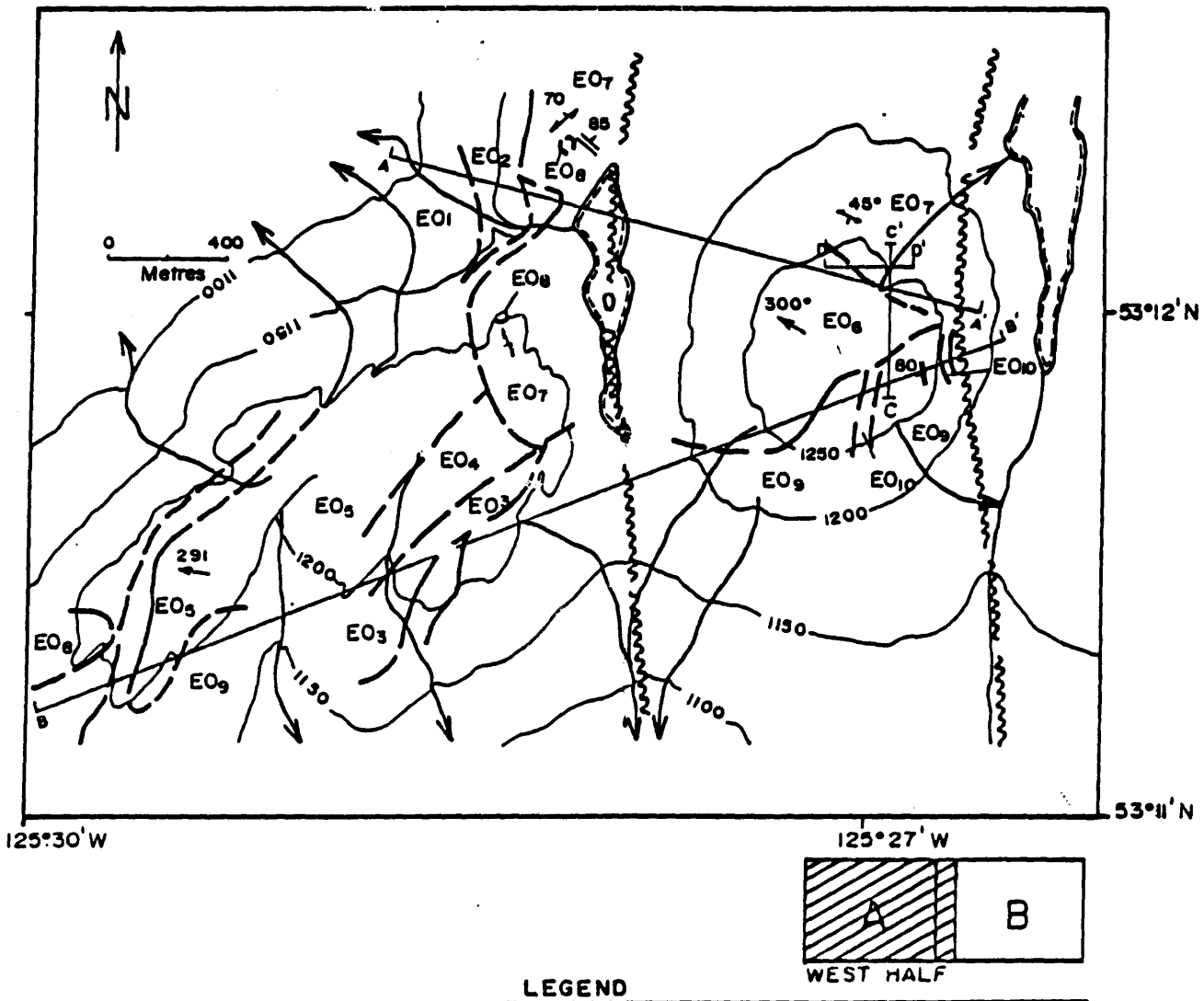

FIGURE 3.1: Geology of the Wolf prospect, Capoose Lake area, central British Columbia. Sections A-A', B-B', C-C' and D-D' are in Figures 3.2, 3.3, 3.20 and 3.21, respectively.

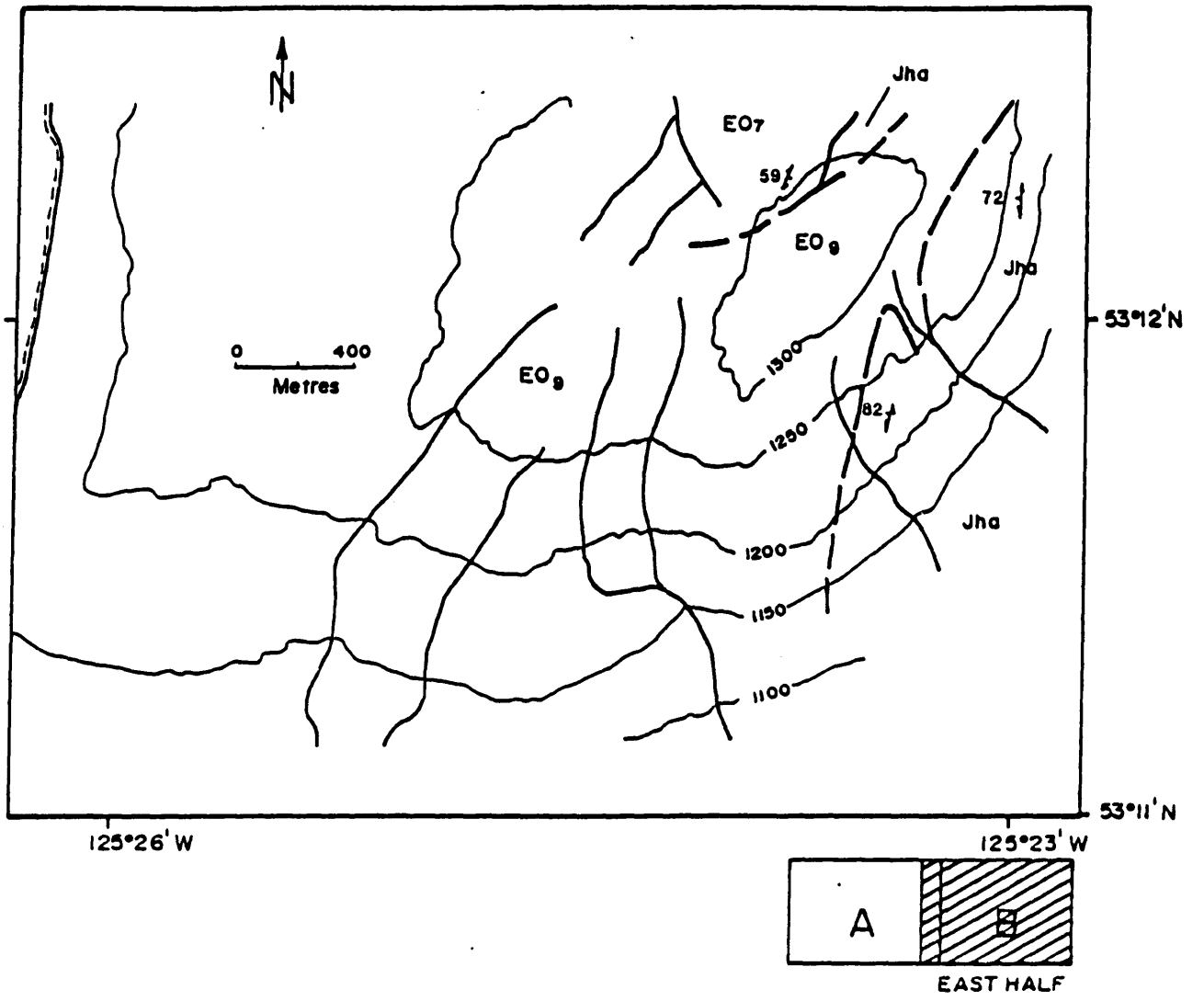

LEGEND

Ms	SILTSTONE, TUFFACEOUS SANDSTONE	EO_4	ASH TUFF	EO_8	VOLCANIC BRECCIA
EO_1	CONGLOMERATE	EO_5	RHYOLITE FLOWS	EO_9	RHYLITE PORPHYRY
EO_2	FELSIC LAPILLI TUFF	EO_6	CRYSTAL TUFF	EO_{10}	QUARTZ PORPHYRY
EO_3	LITHIC, CRYSTAL TUFF	EO_7	RHYOLITE	Jha	ANDESITE FLOWS, FLOW BRECCIA

SYMBOLS

geological contact; known, assumed
fault; known, assumed
20 foliation
10 lineation
vein, with dip

FIGURE 3.1: Geology of the Wolf prospect, Capoose Lake area, central British Columbia. Sections A-A', B-B', C-C' and D-D' are in Figures 3.2, 3.3, 3.20 and 3.21, respectively.

TABLE 3.1: Grouping of Ootsa Lake Group map units based on spatial relationship, complementary lithology, similarity of depositional environment, and associated textures, Wolf prospect, central British Columbia.

MAP UNIT	LITHOLOGY	TEXTURES	DEPOSITIONAL ENVIRONMENT	ASSEMBLAGE	
Eo1	conglomerate	boulder clasts	fluvial	conglomerate and tuffs	
Eo2	rhyodacite lapilli tuff	20% lithic fragments	subaerial	conglomerate and tuffs	
Eo3	lithic crystal tuff	25% lithic fragments	subaerial	pyroclastic rocks	
Eo4	ash tuff	aphanitic, microspherulitic	subaerial	pyroclastic rocks	
Eo5	rhyolite flows	massive, aphanitic	subaerial	subordinate flows	
Eo6	crystal tuff	porphyritic	subaerial	pyroclastic rocks	49.9±1.7 Ma
Eo7	rhyolite	flow banding spherulitic	subaerial	rhyolite flows and breccias	48.3±1.7
Eo8	volcanic	35% lithic fragments	subaerial	rhyolite flows and breccias	
Eo9	rhyolite porphyry	porphyritic	-	intrusions	47.6±1.7
Eo10	quartz porphyry	porphyritic	-	intrusions	

could represent the basal conglomerate, reported by Duffel (1959), which marks the unconformity with Jurassic Hazelton Group rocks. (The type section described by Duffel (1959) on the eastern shores of Whitesail Lake is now submerged.) Pale green to grey rhyodacite lapilli tuff (Eo_2), rests conformably on the conglomerate. The fine ash tuff groundmass of this unit supports up to 20% pyroclasts (1 to 10 mm in size). Most of the fragments are accidental with a variety of compositions. Less than 5% of the fragments are cognate, derived from previous eruptions of the same volcano.

Pyroclastics and subordinate flows (Eo_3 to Eo_6) crop out over much of the west-central part of the property (Fig. 3.1). These are predominantly lapilli and ash tuffs with pyroclasts of cognate origin where associated with minor flows. Grey to green lithic crystal tuff (Eo_3), forms the basal unit of the shallowly westward dipping pyroclastic sequence. This tuff has an aphanitic groundmass that supports 10% quartz and sanidine crystals, and 25% lithic fragments. Textures in the tuff vary from flow-banded to agglomeratic. Cream ash tuff (Eo_4), conformably overlying unit 4, is aphanitic with up to 20% microspherulites, but locally contains 2 to 5% broken quartz phenocrysts 1 mm across. Columnar jointed, mauve rhyolitic flows (Eo_5), are volumetrically subordinate to the pyroclastics. The flows have a pronounced slabby parting developed parallel to flow layering. Quartz and sanidine phenocrysts, each up to 5% of

the overall volume, are suspended in a felsic cryptocrystalline groundmass. Grey to maroon crystal tuff (Eo_6), marks the top of the pyroclastic package. It is characterised by a 'crowded' phenocryst assemblage (Plate 3.1) of 30% euhedral sanidine (1 to 3 mm across) and 10% broken quartz (1 mm in diameter).

Rhyolite flows and breccias (Eo_7 and Eo_8) crop out over most of the northern part of the map area (Fig. 3.1). Rhyolite (Eo_7), is commonly flow banded (Plate 3.2) and spherulitic (Plate 3.3) and unconformably overlies units 1 to 6 (Fig. 3.2). The rock generally contains 10% anhedral sanidine phenocrysts (1 to 2 mm in diameter) and 5% irregular quartz crystals (1 mm in diameter). Volcanic breccia (Eo_8), occurs as small irregular and pod-shaped bodies within Eo_7. This breccia consists of 35% accidental lithic fragments of varying sizes, and of 5% subhedral orthoclase crystals suspended in an aphanitic black matrix (Plate 3.4). Eo_7 and Eo_8 are tentatively correlated with rhyolitic flows of Diakow and Mihalynuk (1987: their unit 8). However, Diakow and Mihalynuk make no mention of heterolithic breccia.

Intrusions (Eo_9 and Eo_{10}) crop out over most of the southern part of the property (Fig. 3.1). Coarse grained rhyolite porphyry (Eo_9) contains up to 60% euhedral orthoclase and 10% quartz phenocrysts. Quartz porphyry (Eo_{10}) occurs within Eo_9, but is distinguished from it by up to 10% stubby, commonly embayed, quartz phenocrysts, and up

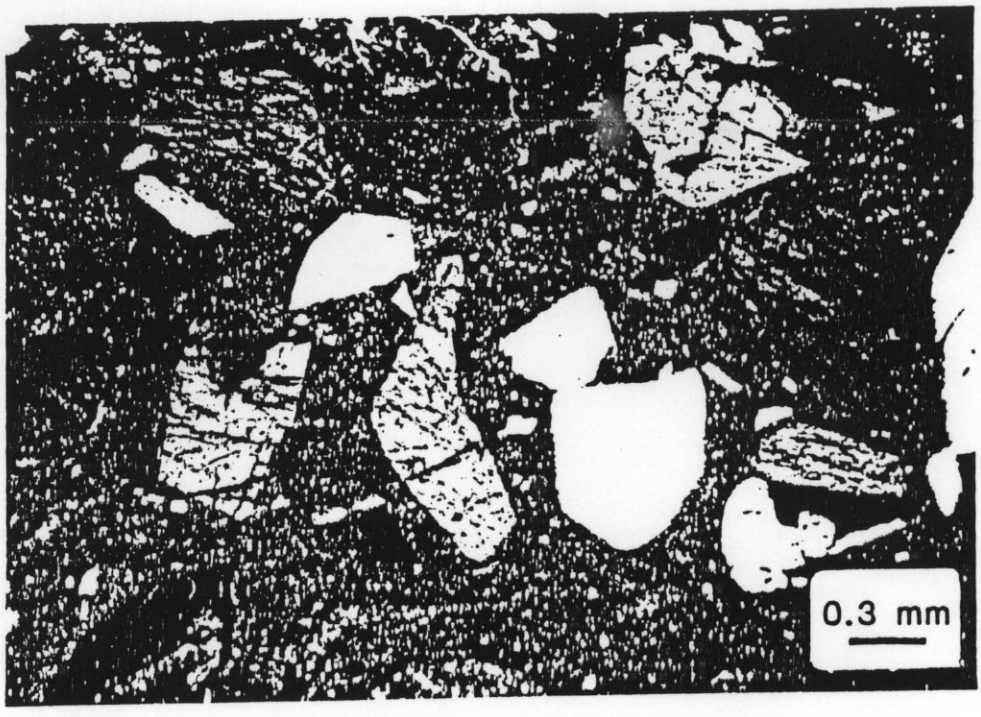

PLATE 3.1: Photomicrograph of broken orthoclase and quartz crystals typical of Ootsa Lake Group crystal tuff (Eo_6; Fig. 3.1). Sample KA133, Wolf prospect. Transmitted light, crossed polars.

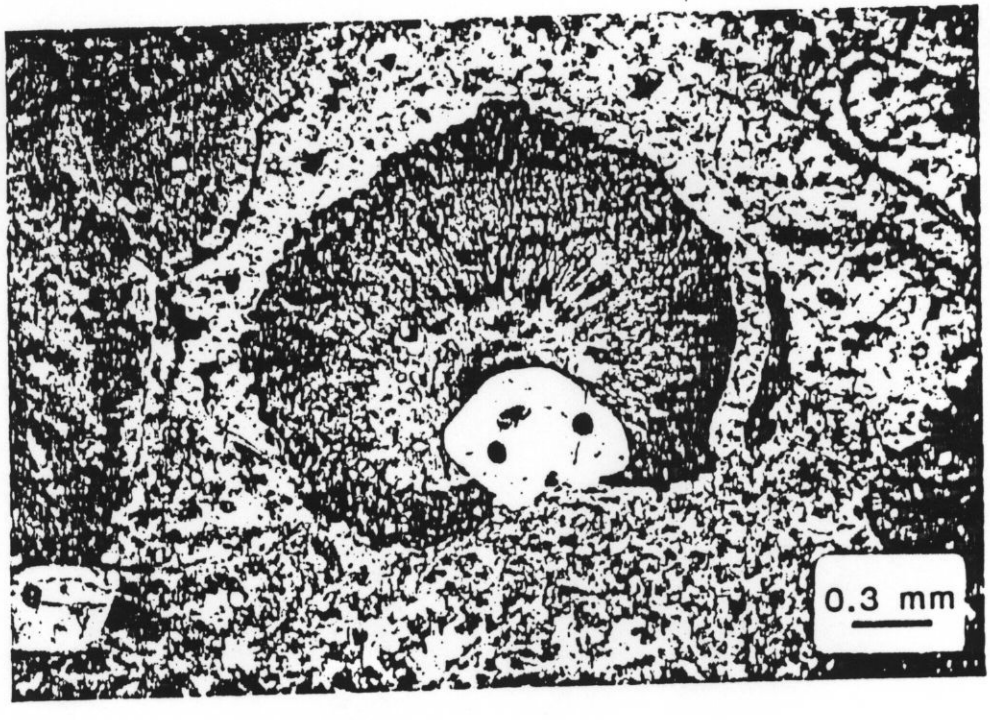

PLATE 3.2: Photomicrograph of a spherulite from Ootsa Lake Group rhyolite (Eo_7; Fig. 3.1). Sample KA104, Wolf prospect. Transmitted light, plane polarized light.

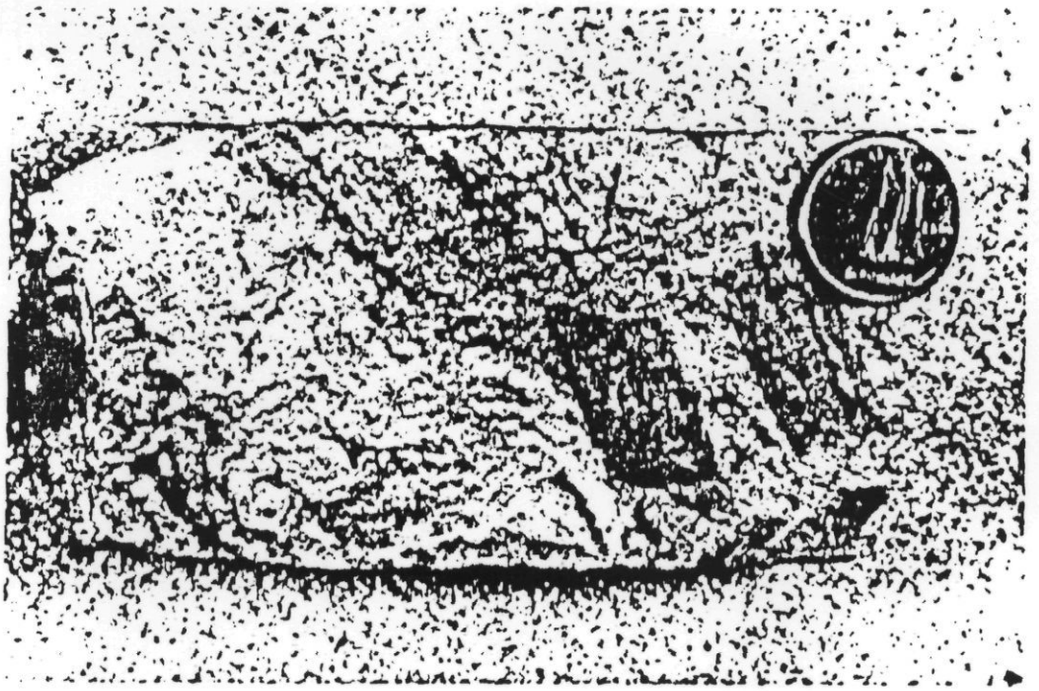

PLATE 3.3: Photomicrograph of flow banding in Ootsa Lake Group rhyolite (Eo_7; Fig. 3.1). Sample KA104, Wolf prospect. Transmitted light, plane polarized light.

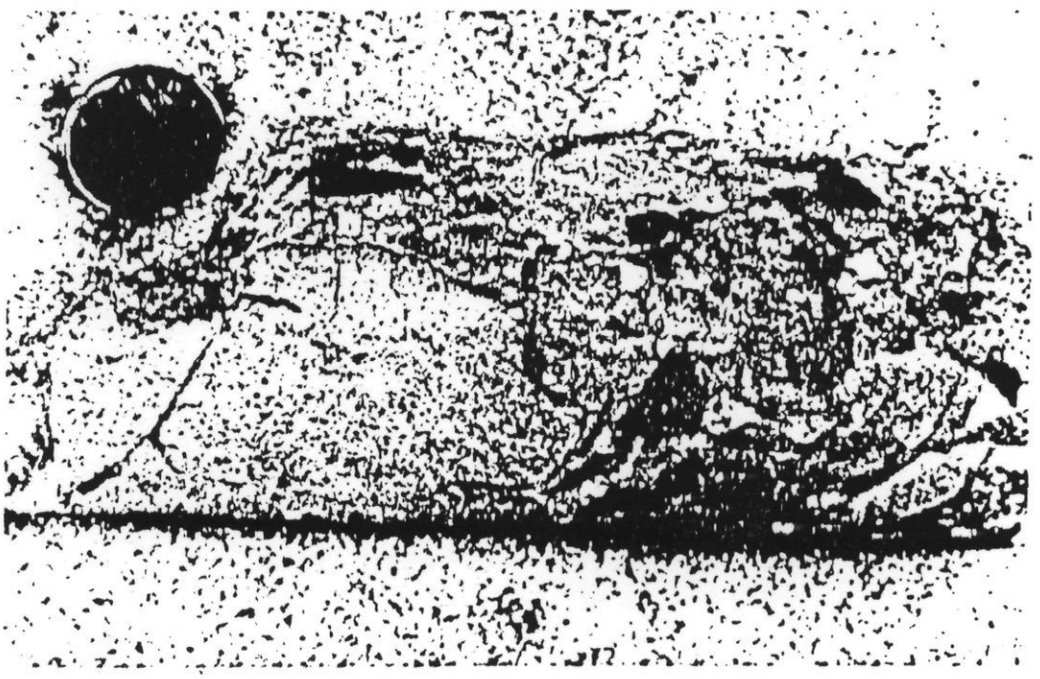

PLATE 3.4: Black chalcedony and felsic volcanic fragments in heterolithic breccia (Eo_9; Fig. 3.1). Sample KA1-11, Wolf prospect.

to 3% euhedral orthoclase phenocrysts (Plate 3.5). This unit might represent a late magmatic stage of the plutonism which formed Eo_9.

Jurassic Hazelton Group Andesite flows are restricted to the eastern edge of the property (Fig. 3.1). They are dark green to black, amygdaloidal, and mainly plagioclase porphyritic with minor massive and brecciated textures. The matrix is felted and comprises 50 to 60% plagioclase laths. The phenocryst assemblage consists of 5 to 25% anhedral chloritized augite, 5 to 10% euhedral plagioclase (An_{75-82}), and 2 to 10% opaques. Amygdales are infilled with calcite and agate. These rocks appear to correlate with the Kotsine subaqueous facies amygdaloidal basalt flows and breccias of Tipper and Richards (1976).

Mid-Miocene epiclastic rocks (Rouse, pers. comm., 1988) do not outcrop in the Wolf area (Fig. 3.1); however, these recessive weathering rocks occur in drill core. Drill holes on the central ridge of the property (Fig. 3.2) encountered epiclastic rocks at least 30 metres thick (Fig. 3.3) composed of siltstone, tuffaceous sandstone, coarse ash tuff, lithic tuff and tuffaceous breccia (Plate 3.6). The deposits are poorly consolidated and poorly sorted. Graded bedding, cross-bedding, scour marks, angular heterolithic fragments, and broken quartz and feldspar crystals with corroded rims are common textures.

3.2.3 STRUCTURE

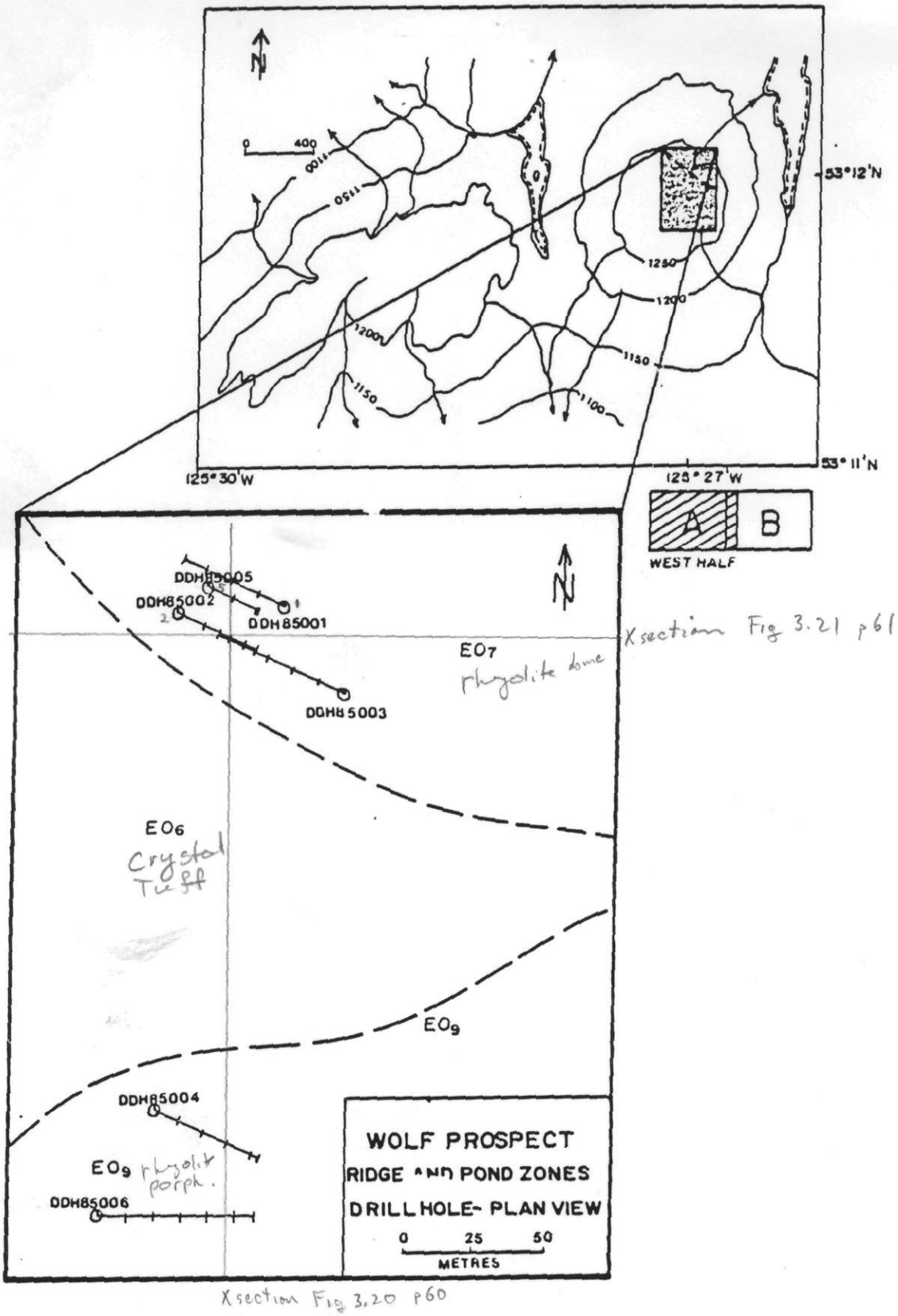

Xsection Fig 3.21 p61

Xsection Fig 3.20 p60

FIGURE 3.2: Diamond drill hole plan of the Wolf prospect, central British Columbia. Map is keyed to Figure 3.1A.

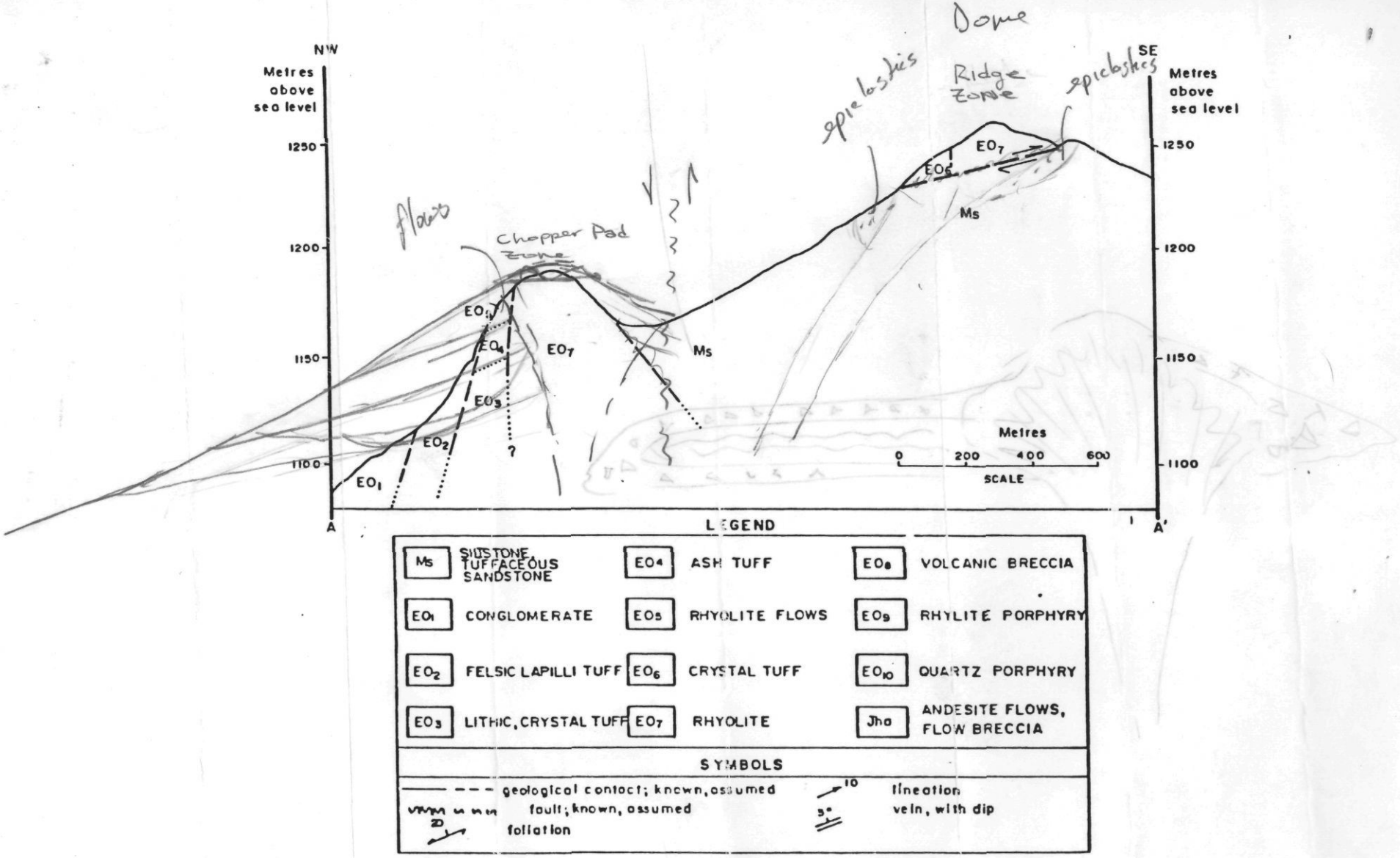

FIGURE 3.3: Cross section A-A' across the central ridge on the Wolf prospect (Fig. 3.1A) showing mid-Eocene Ootsa Lake Group rocks thrust over mid-Miocene epiclastic rocks.

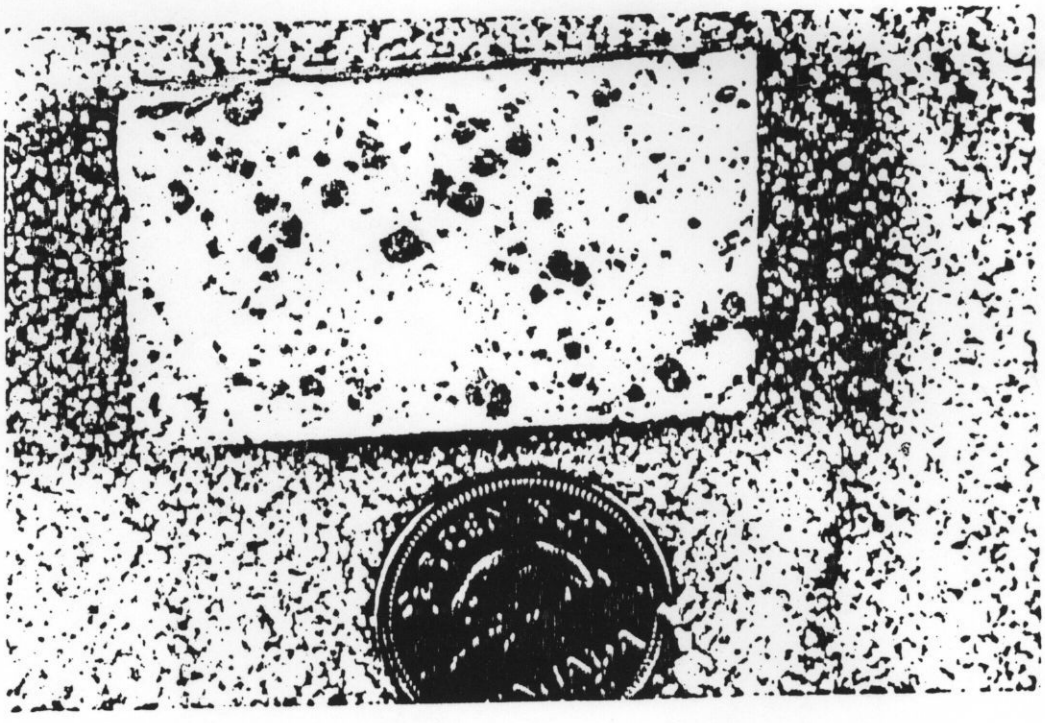

PLATE 3.5: Prominant euhedral quartz crystals in quartz porphyry (Eo_{10}; Fig. 3.1). Sample KA141, Wolf prospect.

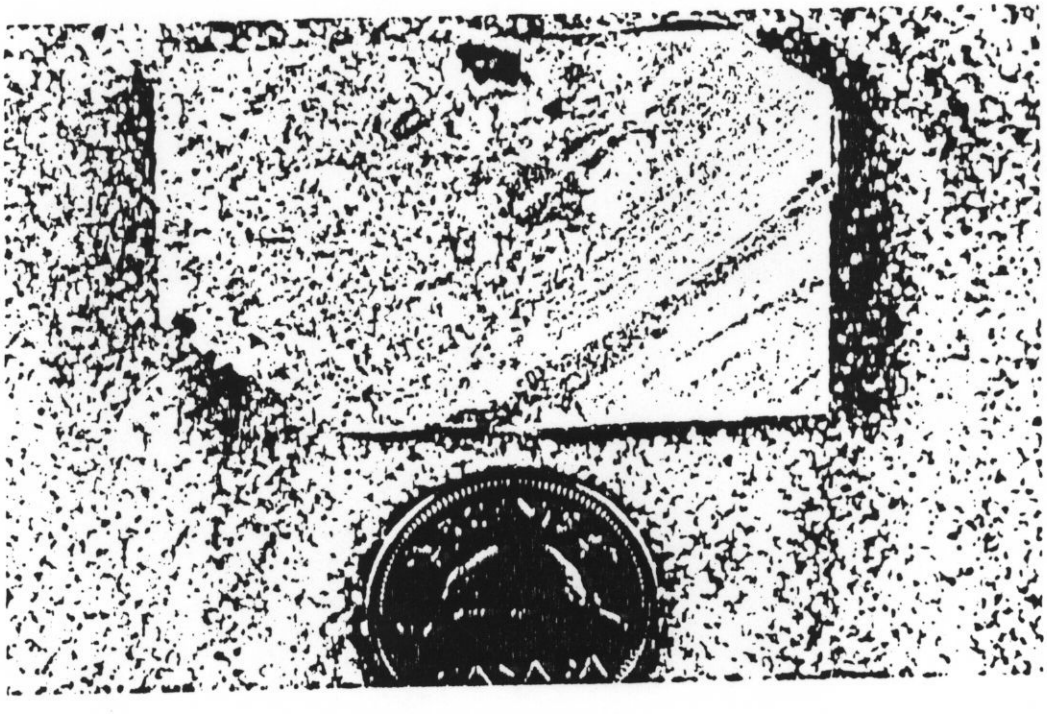

PLATE 3.6: Poorly consolidated mid-Miocene siltstone and tuffaceous sandstone (Ms; Fig. 3.2). Sample KA5-10, Wolf prospect. Discordant saw mark to right of sample.

Mesozoic and Cenozoic strata are extensively block-faulted in the Nechako Plateau (Diakow and Koyanagi, 1988). Ootsa Lake Group rocks characteristically are warped gently and preserved as open folds with dips less than 45 degrees (Tipper, 1963; Diakow and Mihalynuk, 1986). Although the deformation of these rocks is not generally intense, Tipper (1963) suggested that commonly featureless volcanic rocks could mask complex fold patterns. The scarcity of well-exposed rock and the minimal structural information observable in outcrops makes structural interpretations difficult.

Ootsa Lake Group rocks in the Wolf area, however, appear to be little disturbed. Bedding measurements in drill core on the Ridge zone (Fig. 3.4) suggests flat lying units are disrupted only slightly by intrusion of rhyolite porphyry and by block faulting. Measurement of columnar jointing in flow units in the southwestern part of Figure 3.3 indicates shallowly westward dipping strata. Flow banding is irregular.

A low angle north-south thrust fault displaces mid-Eocene over mid-Miocene stratigraphy at Wolf (Figs. 3.1, 3.3 and 3.4). Similar displacements are noted in the Gang Ranch-Big bar area by Mathews and Rouse (1984). The ridge zone fault is characterized by intense shearing and gouge in drill core. Displacement on this fault is obscure because of extensive drift and poor stratigraphic information.

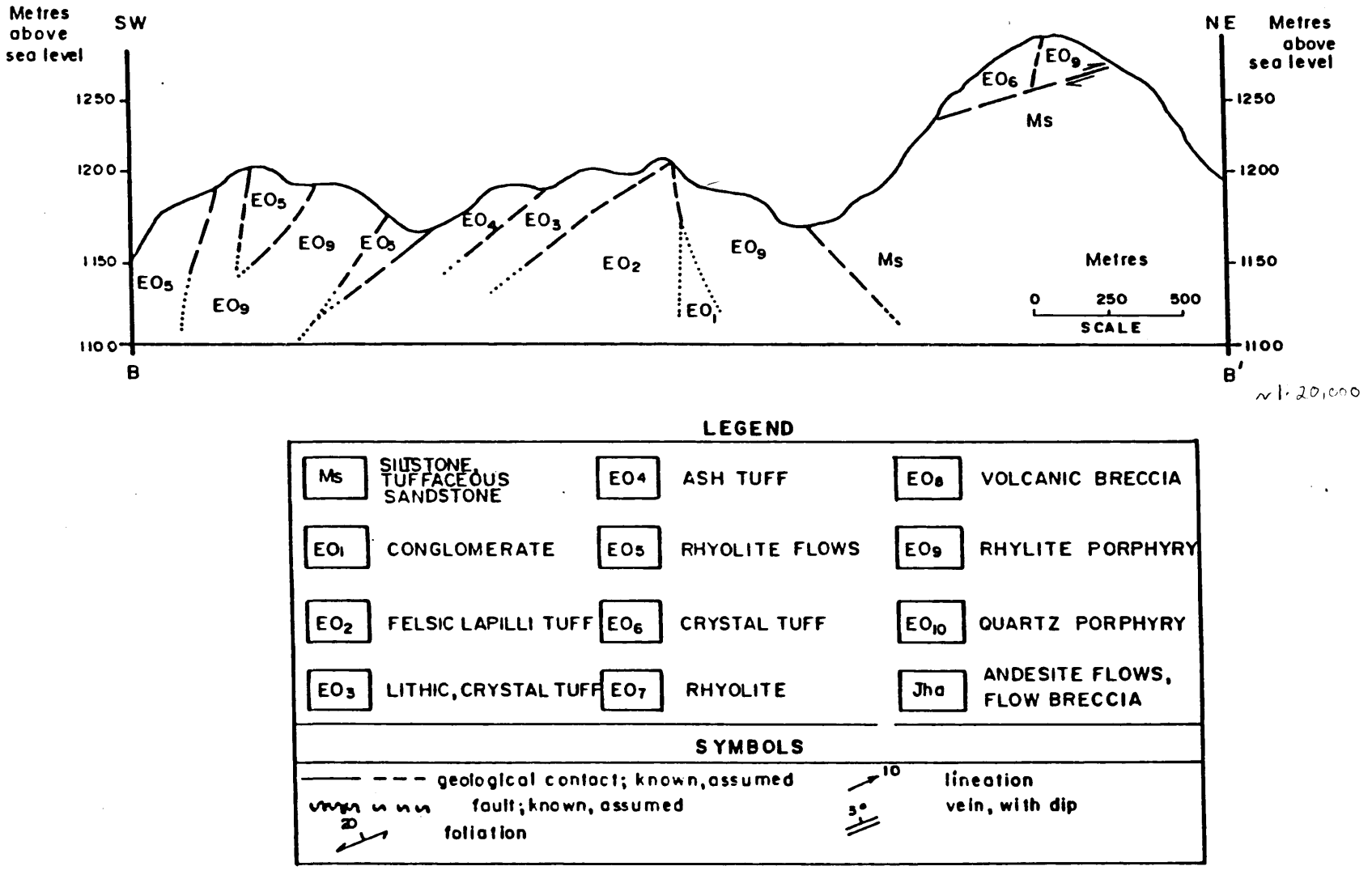

FIGURE 3.4: Cross section B-B′ across the southwestern portion of the Wolf prospect (Fig. 3.1A) showing stratigraphic relationships.

KATHRYN ANDREW 1988 MSc U.B.C

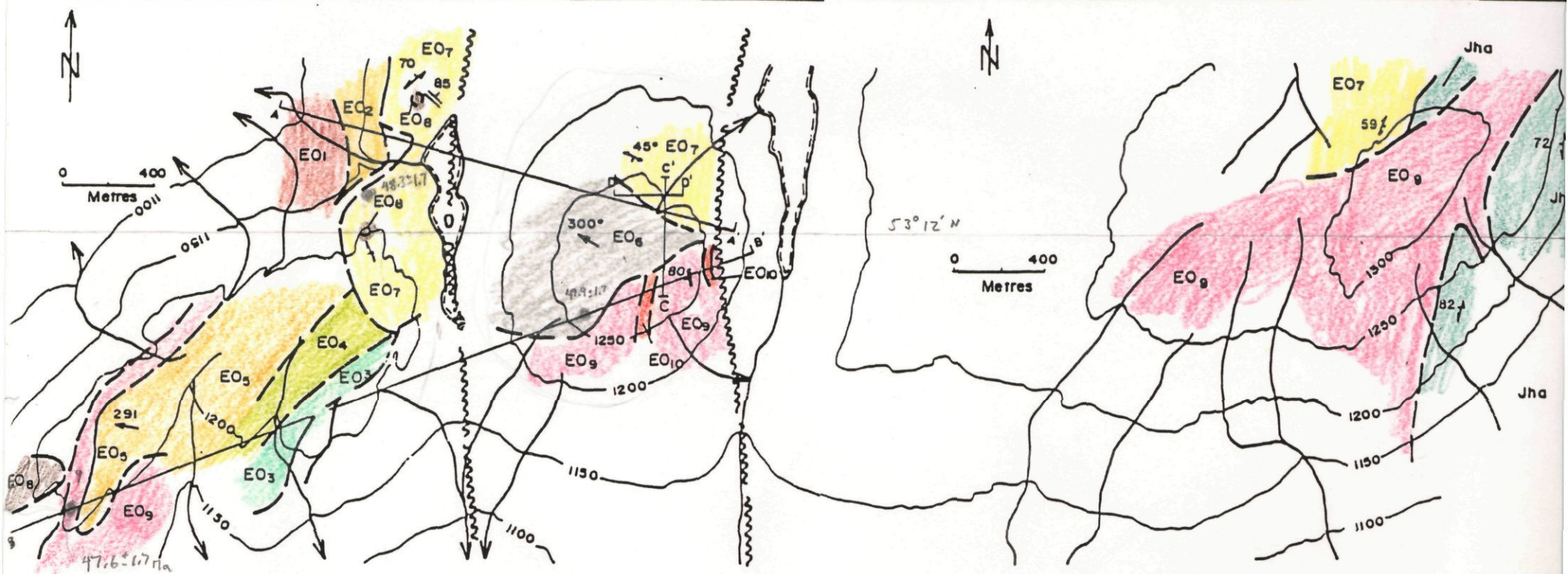

Ms	SILTSTONE, TUFFACEOUS SANDSTONE	EO4	ASH TUFF	EO8	VOLCANIC BRECCIA
EO1	CONGLOMERATE	EO5	RHYOLITE FLOWS	EO9	RHYLITE PORPHYRY
EO2	FELSIC LAPILLI TUFF	EO6	CRYSTAL TUFF	EO10	QUARTZ PORPHYRY
EO3	LITHIC, CRYSTAL TUFF	EO7	RHYOLITE	Jha	ANDESITE FLOWS, FLOW BRECCIA

3.2.4 METAMORPHISM

Low grade regional greenschist metamorphism characterises rocks of the Nechako Plateau. Jurassic mafic volcanic rocks on the east side of the Wolf property (Fig. 3.1) show breakdown of primary pyroxene to amphibole and chlorite. However, Eocene felsic volcanic rocks appear to be relatively fresh with virtually no saussuritization of plagioclase. Although the deformation of these rocks is not generally intense, Tipper (1963) suggested that commonly featureless volcanic rocks could mask complex fold patterns.

3.3 PETROCHEMISTRY

Twenty-eight rock samples from the Wolf property were analysed for major, minor and trace element concentrations. Sample locations are plotted in Figure 3.5 and petrographic descriptions are found in Appendix 2A.

3.3.1. SAMPLE PREPARATION AND ANALYSIS

All rock samples were broken to chip-size in a jaw crusher, split and pulverized to <200 mesh in a tungsten carbide ring mill. Approximately 100 g of sample was sent to Maurette Resources and Services Ltd., Calgary, Alberta, for X-ray fluorescence (XRF) at Midland Earth Science Associates, Nottingham, U..

Analyses of major and minor elements were undertaken by XRF and reported (Appendix 1A) as weight percent oxide; water and CO_2 *etc*. were reported as loss on ignition (LOI). Trace elements determined include: Ag, As, Ba, Cl, Cr, Nb,

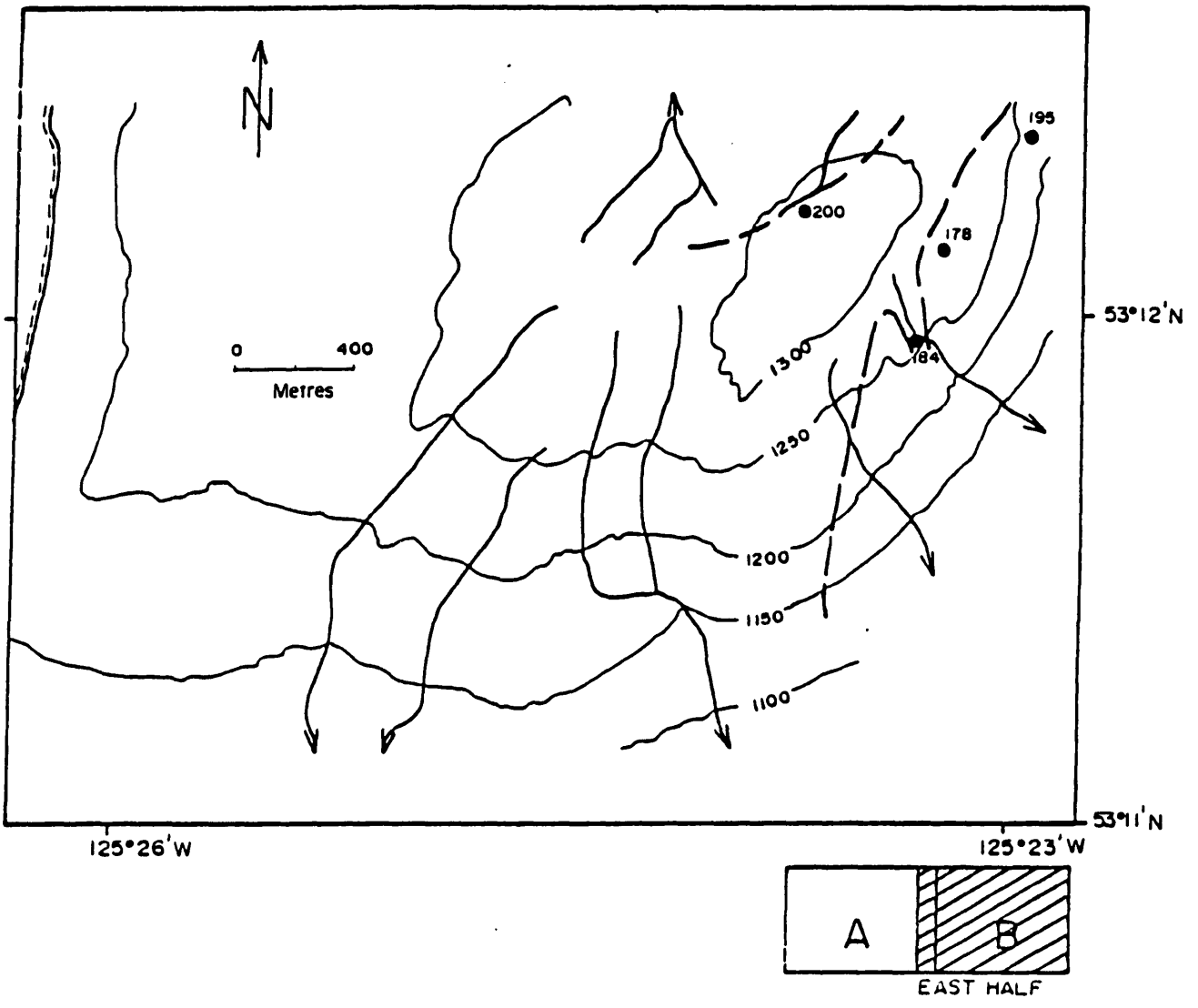

FIGURE 3.5: Sample locations for whole rock and trace element chemical analyses and X-ray diffraction analyses, Wolf prospect, central British Columbia. A) west half, and B) east half.

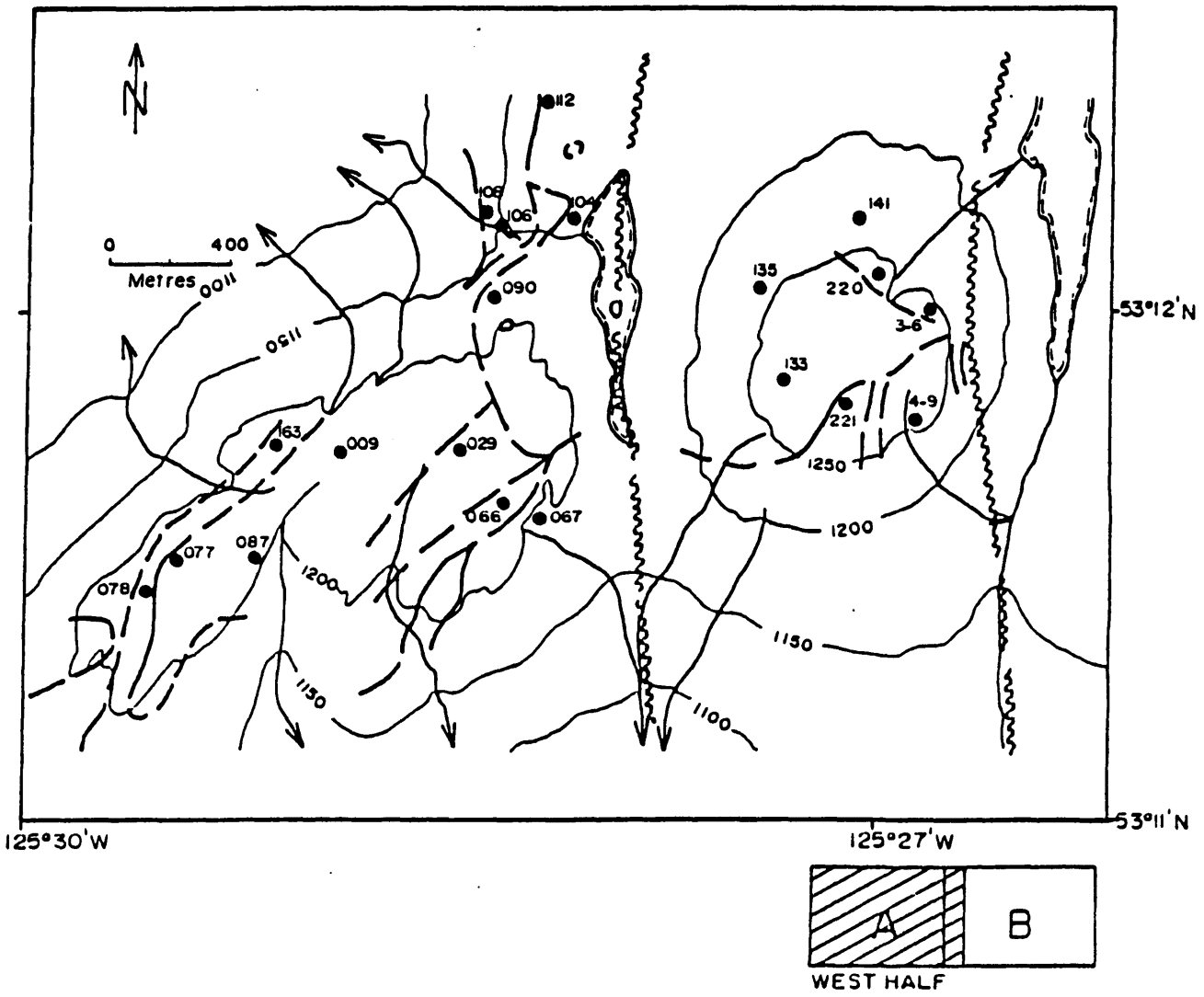

FIGURE 3.5: Sample locations for whole rock and trace element chemical analyses and X-ray diffraction analyses, Wolf prospect, central British Columbia. A) west half, and B) east half.

Ni, Rb, S, Sb, Se, Sr, Te, U, V, Y and Zr. Elemental data were reported in ppm (Appendix 2A). Detection limits are 1 ppm.

Control samples consist of three pairs of field duplicates and two UBC internal standards (Table 3.2). The field duplicate samples were used to determine the amount of combined sampling, preparation and analytical error for each analysis. The internal standard samples were used to determine analytical accuracy.

3.3.2. ERROR ANALYSIS

Samples collected as duplicates are evaluated, below, to determine the precision of the geochemical analyses. Internal standard samples were used to test analytical accuracy.

The duplicate analyses have excellent precision. Combined relative errors for most elements are below 5%. Errors for major, minor and trace elements are 3%, 5%, and 10% respectively. Thus, sampling variation within an outcrop does not seem to be significantly large. Preparation error associated with the analyses probably includes trace Fe contamination from the jaw crusher and trace Cr contamination from the tungsten carbide ring mill (Hickson and Juras, 1986). Analytical error such as contamination and analytical drift cannot be determined because duplicate samples were analysed sequentially.

TABLE 3.2: Control samples analysed together with geochemical sample suite, Wolf prospect, Capoose Lake Area.

	SAMPLE NO.							
	KA077A D1	KA077B D2	KA200A D1	KA200B D2	KA3-6A D1	KA3-6B D2	WP1 S	P1 S
OXIDES wt. %								
SiO2	76.05	76.88	75.78	76.45	76.92	76.72	66.01	69.43
Al2O3	12.10	12.34	13.54	13.20	12.86	13.25	15.49	14.50
TiO2	0.20	0.20	0.24	0.23	0.16	0.16	0.52	0.39
Fe2O3	1.73	1.73	2.55	2.46	1.19	1.18	4.63	4.29
MgO	0.01	0.00	0.35	0.38	0.02	0.00	1.67	1.09
CaO	0.10	0.10	0.21	0.20	0.12	0.11	4.91	3.51
Na2O	3.23	3.33	1.27	1.28	1.78	1.84	4.43	3.79
K2O	4.81	4.87	4.26	4.08	6.23	6.29	1.64	2.21
MnO	0.02	0.02	0.06	0.06	0.00	0.00	0.09	0.08
P2O5	0.00	0.00	0.04	0.04	0.00	0.00	0.14	0.08
ELEMENTS: ppm								
Ag	0	0	0	0	0	0	-	-
As	20	17	11	12	43	23	-	-
Ba	24	32	156	159	20	182	631	782
Cl	0	0	0	0	0	11	-	-
Cr	5	8	0	0	9	51	60	41
Nb	23	24	21	21	23	11	5	4
Ni	3	0	2	6	0	0	46	4
Rb	196	199	235	232	295	203	8	13
S	69	69	94	97	117	83	60	121
Sb	1	1	1	3	4	4	-	-
Se	0	0	0	0	0	0	-	-
Sr	4	5	34	34	10	15	752	229
Te	0	0	0	3	0	0	-	-
U	8	6	6	6	6	4	-	-
V	3	4	15	17	5	16	76	57
Y	79	80	83	81	58	46	18	23
Zr	592	587	500	501	340	379	124	115

3.3.3. ELIMINATION OF MOST ALTERED DATA

Altered rocks from the Wolf property were identified by plotting major oxide data from Appendix 2A on diagrams monitoring metasomatism (Beswick, 1978). This approach was necessary because deuteric and metamorphic processes can affect the alkalies, magnesium, calcium and possibly the contents of other elements upon which chemical classifications depend.

Most samples from the Wolf property plot within the tightly defined trends of modern volcanic rocks (Fig 3.6). These trends are insensitive to the differences in the detailed fractionation history of suites (Beswick, 1978). Samples, established as altered, following the above analyses, were deleted from Appendix 2A and from chemical classification plots in section 3.3.4. Least altered samples are in Table 3.3.

3.3.4. CHEMICAL ROCK CLASSIFICATION

Rocks on the Wolf property were named conventionally in section 3.2, using descriptive field terms combined with modal petrographic information (Table 3.1). Least altered rocks are classified more fully on the basis of major and trace element geochemistry.

Wolf volcanic rocks are dominantly hypersthene-corundum normative with similar normative compositions (Table 3.3).

Wolf volcanic rocks are subalkaline (Fig. 3.7; MacDonald, 1968; Irvine and Baragar, 1971). Major elements

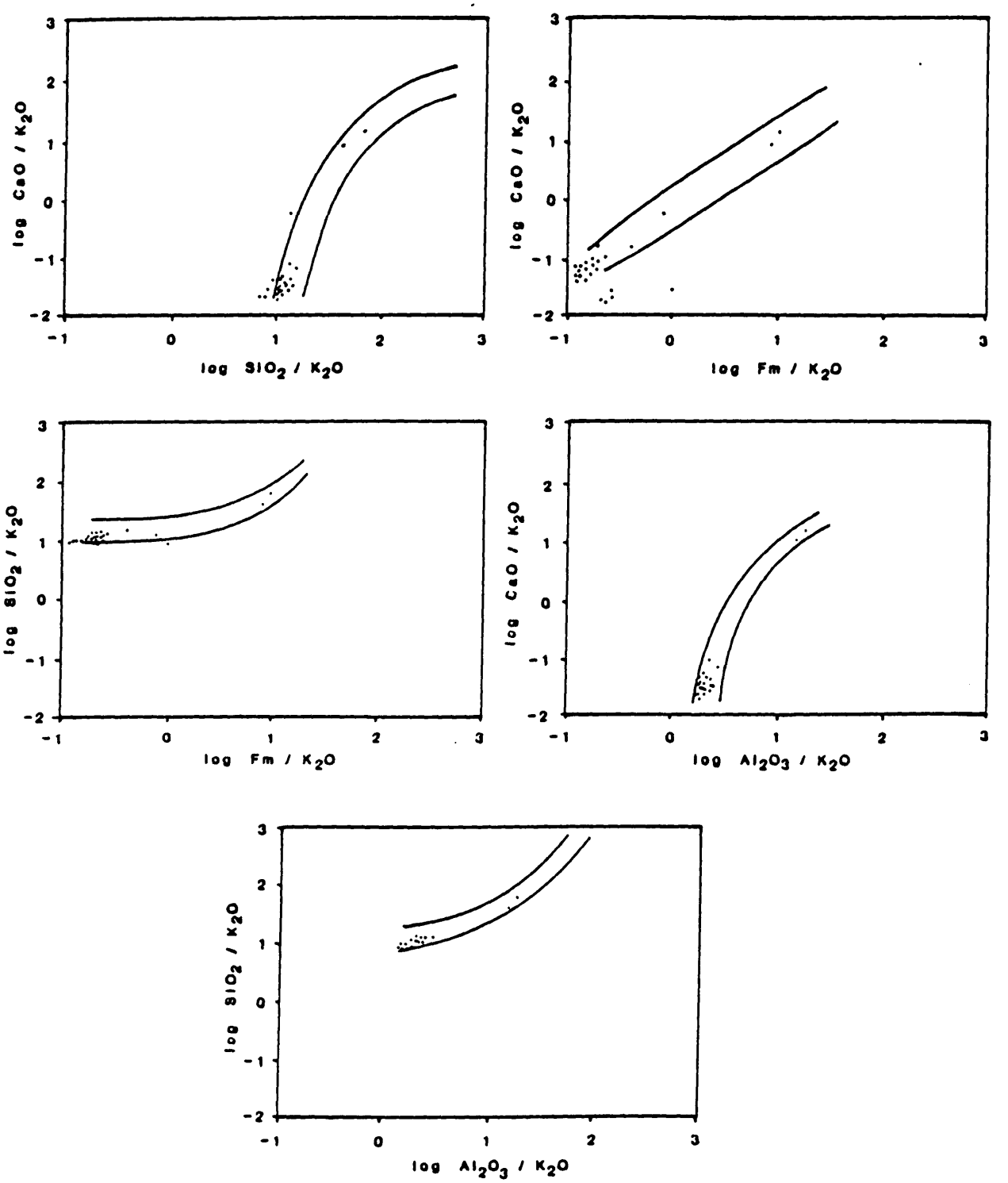

FIGURE 3.6: Logarithmic oxide molecular proportion ratio plots (K_2O denominator) for comparison of Wolf volcanic rocks to 'modern' volcanic suites and retrieval of least altered data (Beswick, 1978). Most dots which represent rocks from the Wolf prospect (Appendix 1A) fall predominantly within the limits for 'modern' volcanic suites. Least altered rocks are in Table 3.3.

TABLE 3.3: Least altered samples used for rock classification and chemical classification, Wolf prospect, Capoose Lake Area.

	SAMPLE NUMBER							
	KA009	KA029	KA066	KA077	KA078	KA087	KA090	KA104
OXIDES (wt. %)								
SiO_2	77.89	78.57	74.21	76.05	76.46	76.87	79.40	79.82
Al_2O_3	11.01	11.65	14.41	12.10	12.14	12.56	11.31	10.91
TiO_2	0.22	0.09	0.36	0.20	0.21	0.23	0.12	0.14
Fe_2O_3[1]	1.59	0.78	0.96	1.73	1.83	1.42	0.57	1.01
MgO	0.01	0.04	0.02	0.01	0.02	0.04	0.08	0.03
CaO	0.10	0.15	0.17	0.10	0.13	0.11	0.12	0.11
Na_2O	2.95	2.25	2.97	3.23	3.38	2.13	0.33	0.11
K_2O	4.45	5.32	6.13	4.81	4.62	6.17	6.04	7.17
MnO	0.01	0.01	0.01	0.02	0.02	0.02	0.01	0.00
P_2O_5	0.02	0.01	0.02	0.02	0.00	0.01	0.00	0.00
LOI	0.79	0.67	0.78	0.43	0.44	0.76	0.80	0.58
total	99.04	99.54	100.05	98.70	99.26	100.32	98.79	99.90
ELEMENTS (ppm)								
Nb	21	12	16	23	23	18	8	22
Y	65	22	59	79	83	72	18	40
Zr	65	69	456	592	600	564	84	313
CIPW NORM								
Q	41.97	42.91	31.26	37.03	36.27	38.62	53.01	49.93
C	1.37	2.19	2.92	1.58	1.29	2.47	4.64	3.17
Or	27.36	32.52	36.88	29.41	29.54	37.44	37.83	44.37
(Ab)	27.57	20.91	27.16	30.02	0.66	19.64	3.14	1.03
(An)	0.38	0.70	0.73	0.51	31.36	0.49	0.63	0.57
(En)	0.00	0.11	0.06	0.03	0.06	0.11	0.23	1.61
(Fs)	0.00	0.00	0.00	3.23	3.38	0.00	0.00	0.09
Il	0.00	0.00	0.02	0.03	0.03	0.03	0.00	0.00
Hm	1.15	0.56	0.68	1.25	1.31	1.02	0.42	0.74
Ru	0.16	0.06	0.25	0.13	0.13	0.15	0.09	0.10
Ap	0.04	0.02	0.04	0.00	0.00	0.02	0.00	0.00

1. Total iron is expressed as Fe_2O_3

TABLE 3.3: (continued p2.)

	SAMPLE NUMBER							
	KA106	KA112	KA133	KA135	KA141	KA163	KA178	KA184
OXIDES (wt. %)								
SiO_2	78.11	80.45	73.02	73.15	80.42	74.65	46.92	76.87
Al_2O_3	12.31	10.73	13.23	14.05	10.62	14.77	14.88	11.79
TiO_2	0.18	0.15	0.28	0.36	0.18	0.10	0.77	0.14
Fe_2O_3[1]	1.50	0.80	1.75	1.87	1.81	1.41	10.97	1.31
MgO	0.24	0.00	0.14	0.08	0.06	0.13	8.51	0.07
CaO	0.15	0.11	0.18	0.19	0.12	0.15	9.96	0.27
Na_2O	0.09	0.92	3.44	3.60	0.14	1.48	1.79	3.36
K2O	5.39	6.00	5.23	6.35	5.38	6.00	0.92	4.70
MnO	0.04	0.00	0.04	0.03	0.02	0.05	0.22	0.02
P_2O_5	0.00	0.00	0.04	0.09	0.02	0.00	0.32	0.02
LOI	1.93	0.69	0.63	0.34	1.19	1.16	3.22	0.52
total	99.94	99.86	97.98	100.11	99.97	99.91	98.49	99.07
ELEMENTS (ppm)								
Nb	18	21	14	13	17	22	0	16
Y	51	61	54	48	71	36	23	38
Zr	256	320	400	377	348	134	38	146
CIPW NORM								
Q	55.46	50.21	31.28	25.86	57.68	41.02	2.44	36.94
C	7.03	2.88	1.90	1.24	5.09	6.44	0.00	0.82
Or	33.88	37.02	32.09	37.89	33.70	36.76	5.78	28.61
(Ab)	0.86	8.63	32.08	32.65	1.33	13.78	18.12	31.08
(An)	0.79	0.57	0.66	0.36	0.49	0.43	33.44	1.25
(Wo)	0.00	0.00	0.00	0.00	0.00	0.00	6.99	0.00
(En)	0.70	0.00	0.40	0.00	0.18	0.37	6.99	0.00
Di	0.00	0.00	0.00	0.00	0.00	0.00	13.97	0.00
(En)	0.00	0.00	0.00	0.00	0.00	0.00	16.01	0.20
Il	0.07	0.00	0.07	0.05	0.03	0.00	0.33	0.03
Hm	1.11	0.58	1.27	1.32	1.34	1.02	7.99	0.94
Ru	0.10	0.11	0.17	0.23	0.12	0.07	1.27	0.08
Ap	0.00	0.00	0.09	0.19	0.04	0.11	0.65	0.04

1. Total iron is expressed as Fe_2O_3

TABLE 3.3: (continued p3.)

	SAMPLE NUMBER KA195	KA221	KA3-6	KA4-9
OXIDES (wt. %)				
SiO_2	48.21	48.21	77.33	76.92
Al_2O_3	11.43	11.43	12.69	12.86
TiO_2	0.66	0.66	0.10	0.16
Fe_2O_3 [1]	8.27	8.27	0.66	1.19
MgO	11.97	11.97	0.04	0.02
CaO	10.24	10.24	0.17	0.12
Na_2O	1.72	1.72	0.83	1.78
K_2O	0.58	0.58	7.79	6.23
MnO	0.15	0.15	0.00	0.00
P_2O_5	0.18	0.18	0.01	0.00
LOI	5.76	5.76	0.57	0.63
total	99.15	99.15	100.20	99.92
ELEMENTS (ppm)				
Nb	0	13	25	11
Y	32	24	56	58
Zr	54	87	339	379
CIPW NORM				
Q	2.69	40.41	40.55	36.21
C	0.00	2.94	3.35	2.97
Or	3.64	47.48	37.97	37.72
(Ab)	16.42	7.69	16.49	21.41
(An)	23.13	0.80	0.61	0.53
(Wo)	11.13	0.00	0.00	0.00
(En)	11.13	0.00	0.00	0.00
Di	22.25	0.00	0.00	0.00
(En)	24.01	0.11	0.06	0.08
Il	0.25	0.00	0.00	0.00
Hm	6.13	0.47	0.86	0.79
Ru	1.09	0.07	0.11	0.25
Ap	0.40	0.02	0.00	0.04

1. Total iron is expressed as Fe_{2-3}

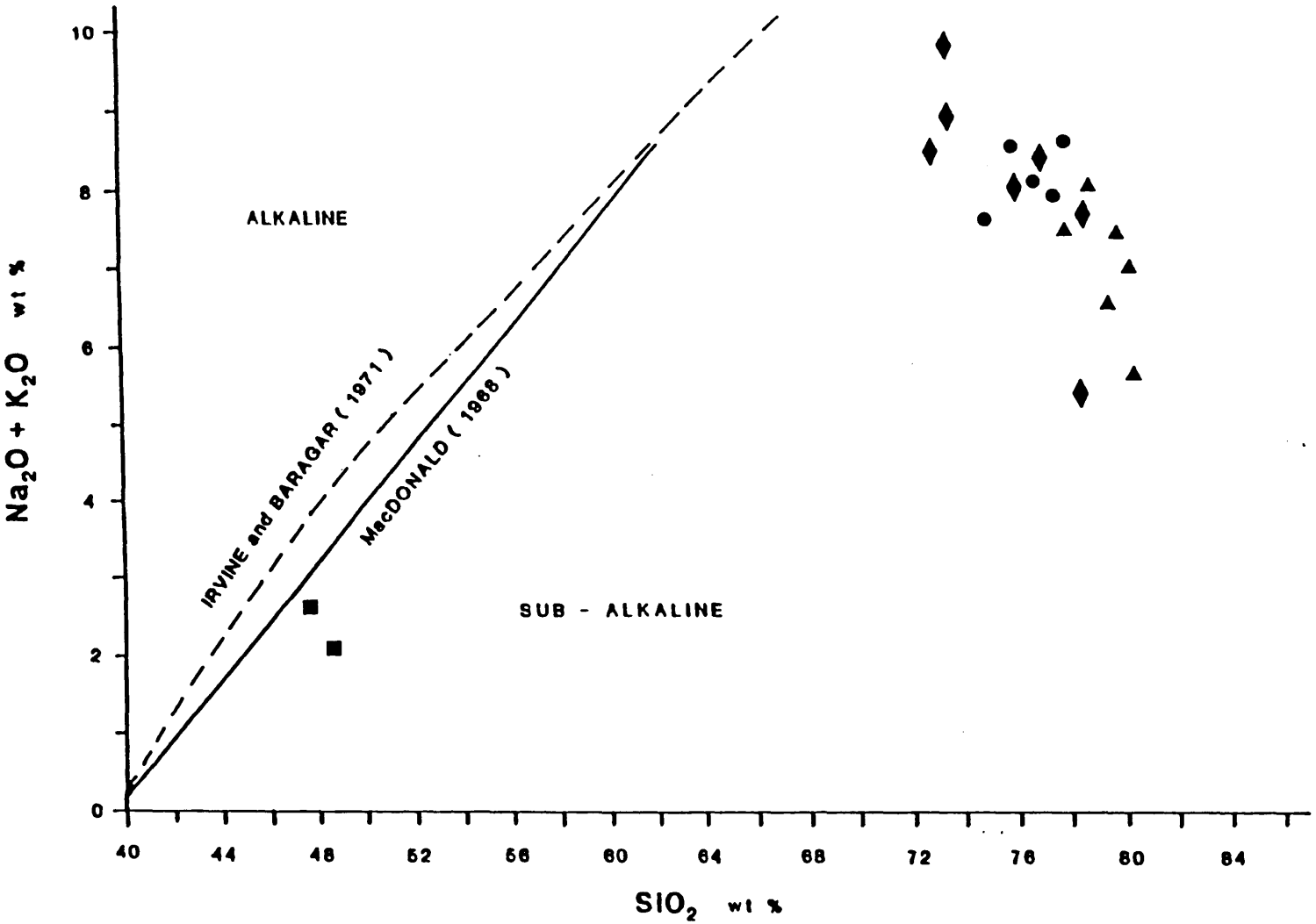

FIGURE 3.7: Plot of alkalies vs. silica for analyses from the Wolf prospect (Table 3.3, boundaries are from MacDonald, 1968, and Irvine and Baragar, 1971). Assemblages are sub-alkaline (section 3.2.2), and are plotted using: squares = mafic volcanics, diamonds = pyroclastic rocks, triangles = rhyolite flows and circles = intrusions.

plotted on the AFM diagram of Figure 3.8 demonstrates the calcalkaline affinity. A calcalkaline trend is also evident in Figure 3.9, the Jensen plot (Jensen, 1976). Total iron, analysed as Fe_2O_3, was converted to weight percent FeO and Fe_2O_3 using the method of Sack et al. (1980). The calculations were made at 800°C and $lnfO_2$ of 10^{-14} (from figure 6-12 in Carmichael et al., 1974).

Rocks from the Wolf property plot as oversaturated acid volcanics dominantly within the rhyolite field on the TAS plot (Fig. 3.10) after LeBa- et al. (1986). Samples cluster as rhyolites on the Jensen plot and the "triaxial oxide" plot in Figure 3.11 (Church, 1975).

Samples from the Wolf property fall well within the rhyolite field using immobile element plots from Winchester and Floyd (Figs. 3.12. and 3.13). Selected minor and trace elements such as Ti, Zr, Y and Nb are relatively immobile during deuteric and metamorphic processes. Therefore diagrams monitoring these elements are reliable chemical classifiers. Since SiO_2 can be mobile during alteration, its use in chemical classification plots such as Figure 3.12 can be limited. Wolf data plotted on a Zr/TiO_2 - Nb/Y diagram (Fig. 3.13) shows that the volcanic rocks from Wolf vary from andesitic to rhyolitic in composition.

Most tectonic descrimination diagrams, defined generally for basaltic rocks, cannot be applied to felsic volcanic rocks from the Wolf property. However, the K_2O vs. SiO_2 diagram of Gill (1981), modified to include rhyolites

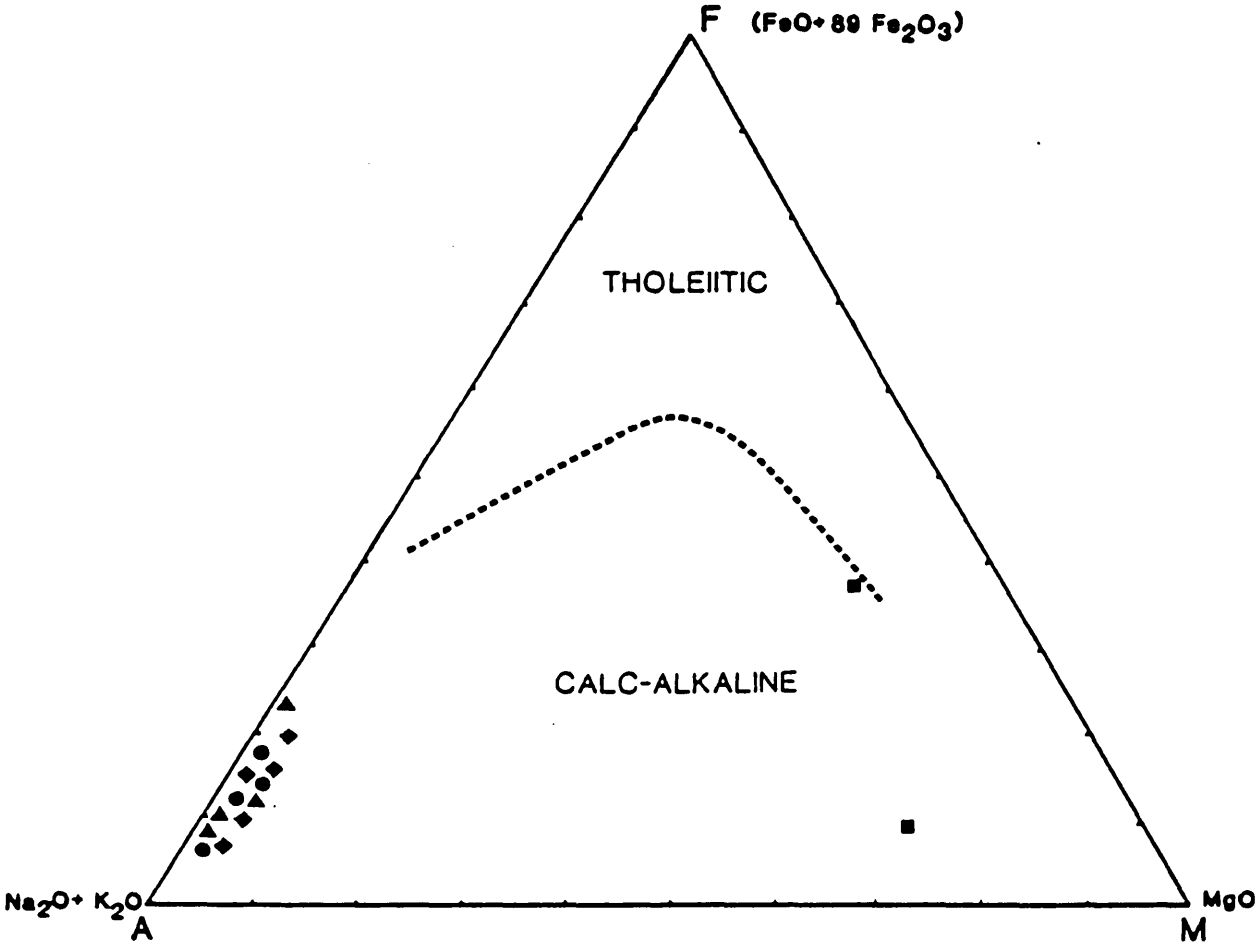

FIGURE 3.8: AFM diagram with analyses from the Wolf prospect (Table 3.3, boundaries are from Wager and Deer, 1939). Assemblages are calc-alkaline (section 3.2.2), and are plotted using squares = mafic volcanics, diamonds = pyroclastic rocks, triangles = rhyolite flows and circles = intrusions.

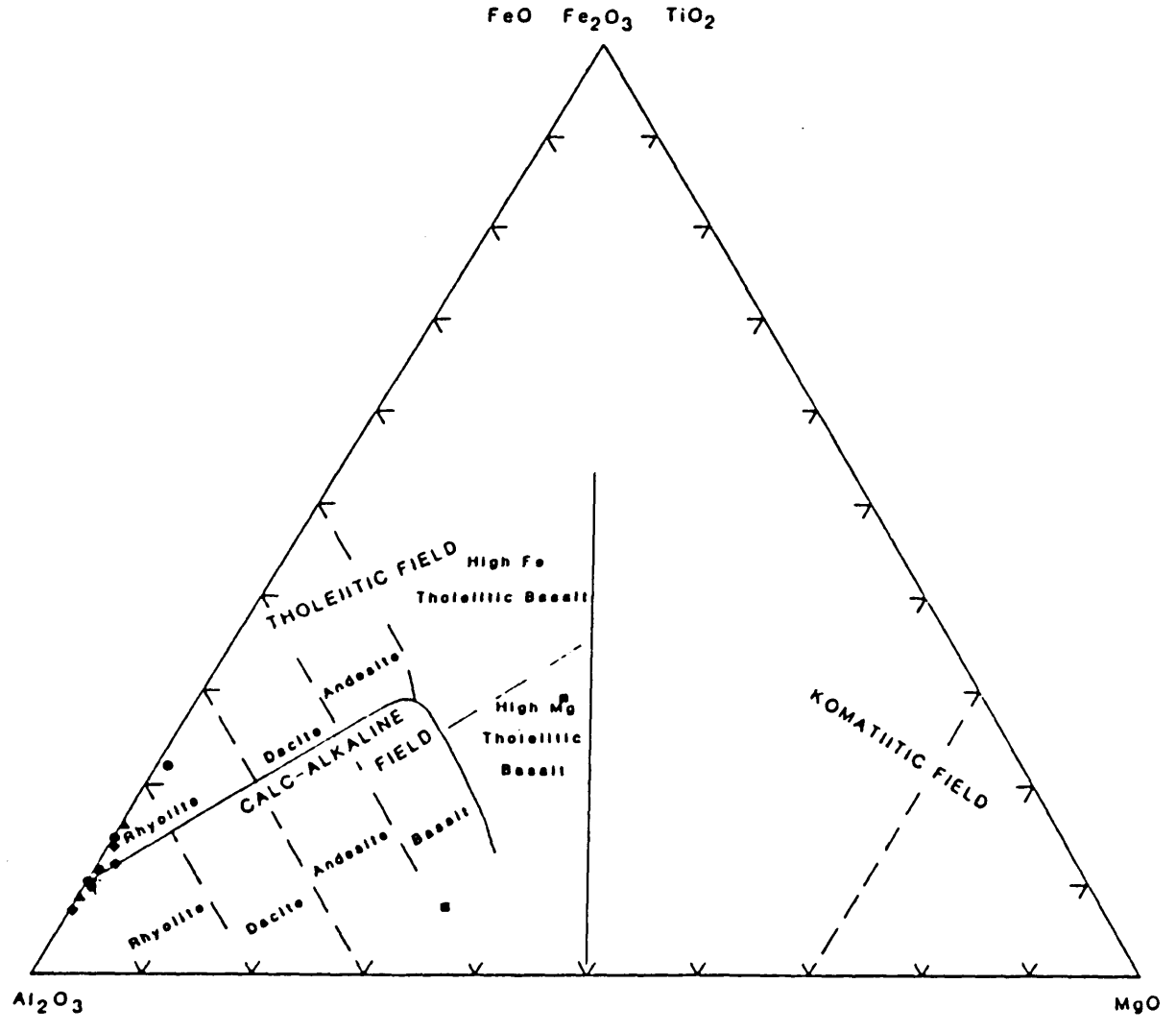

FIGURE 3.9: Jensen Cation plot for analyses from the Wolf prospect (Table 3.3, boundaries are from Jensen, 1976). Assemblages are calc-alkaline to tholeiitic (section 3.2.2) and are plotted using: squares = mafic volcanics, diamonds = pyroclastic rocks, triangles = rhyolite flows, circles = intrusions.

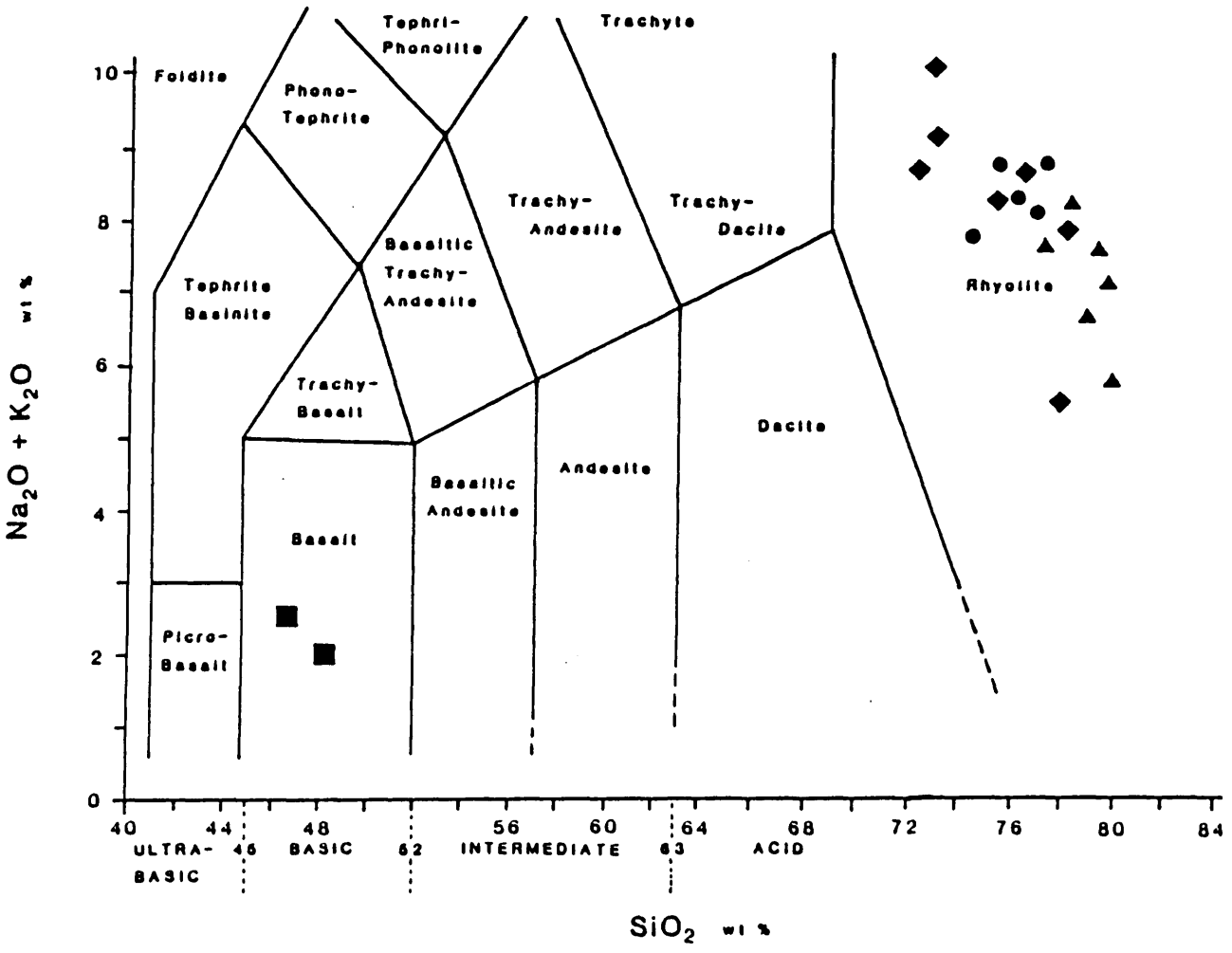

FIGURE 3.10: Plot of alkalies vs. silica for analyses from the Wolf prospect (Table 3.3, boundaries are from Le Bas et al. 1986). Assemblages are predominantly rhyolites (section 3.2.2) and are plotted using: squares = mafic volcanics, diamonds = pyroclastic rocks, triangles = rhyolite flows and circles = intrusions.

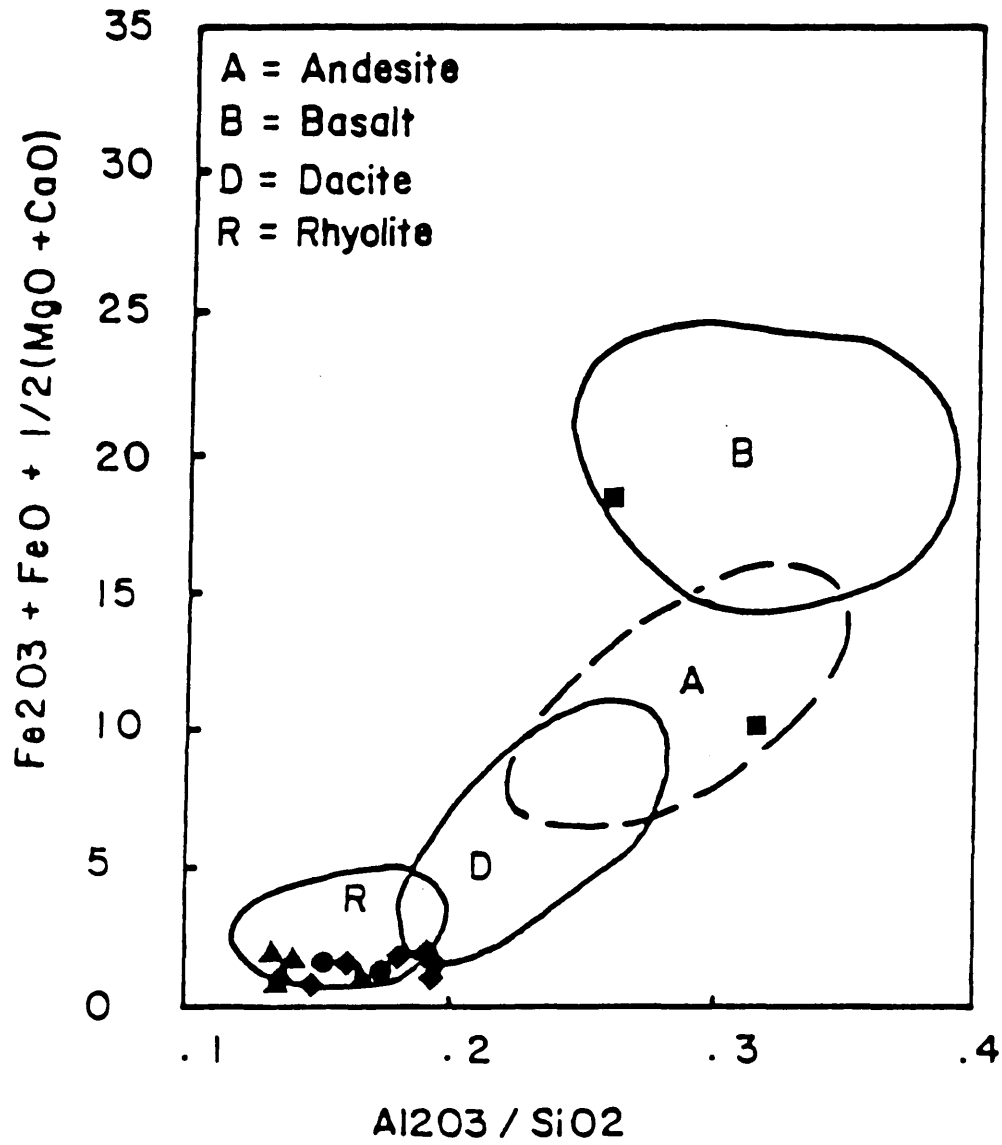

FIGURE 3.11: Triaxial oxide plot (Fe_2O_3 + FeO + 1/2 (MgO + CaO) vs. Al_2O_3/SiO_2) for analyses from the Wolf prospect (Table 3.3) boundaries from Church, 1975). Assemblages are predominantly rhyolites (section 3.2.2) and are plotted using: squares = mafic volcanics, diamonds = pyroclastic rocks, triangles = rhyolite flows, circles = intrusions.

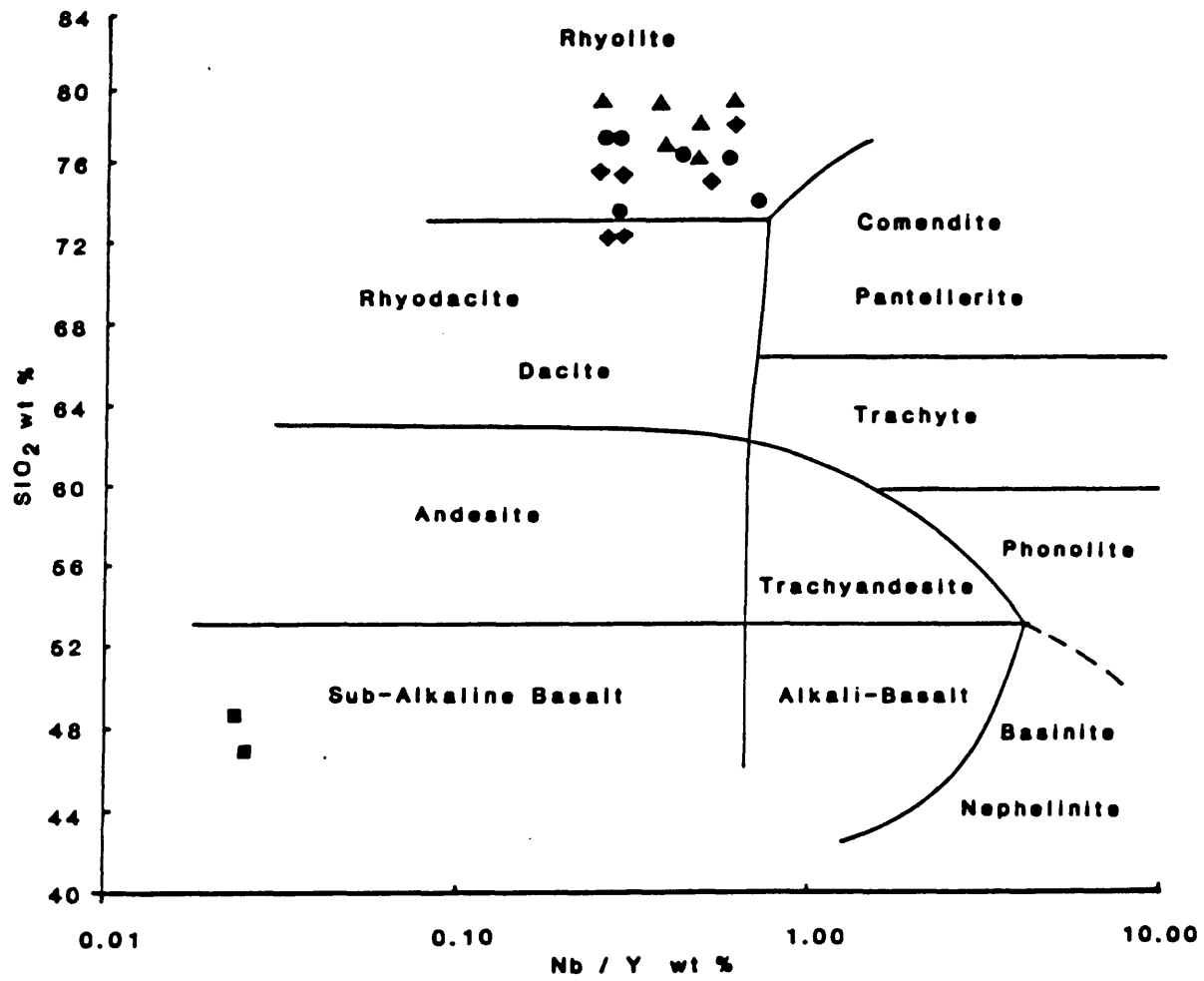

FIGURE 3.12: SiO_2 vs. Nb/Y plot for analyses from the Wolf prospect (Table 3.3, boundaries from Winchester and Floyd, 1977). Assemblages are dominantly rhyolite and rhyodacite (section 3.2.2) and are plotted using: squares = mafic volcanics, diamonds = pyroclastic rocks, triangles = rhyolite flows and circles = intrusions.

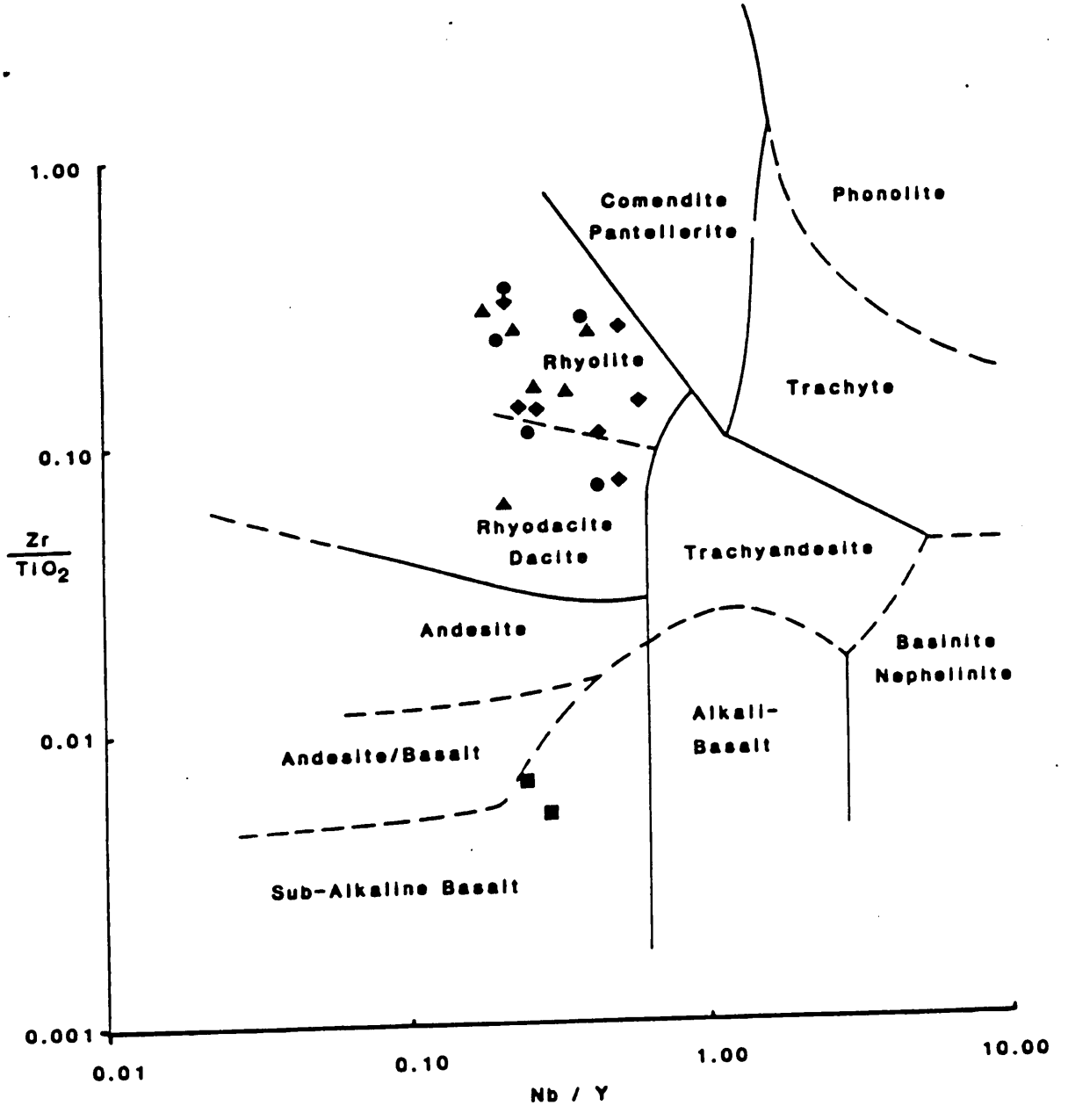

FIGURE 3.13: Zr/TiO_2 vs. Nb/Y plot for analyses from the Wolf prospect (Table 3.3, boundaries from Winchester and Floyd, 1977). Assemblages are dominantly rhyolite and rhyodacite (section 3.2.2) and are plotted using: squares = mafic volcanics, diamonds = pyroclastic rocks, triangles = rhyolite flows and circles = intrusions.

(Spence, 1985), and the K_2O vs. Na_2O (for 70% SiO_2) diagram of Spence (1987) can be applied to Wolf felsic volcanic rocks. Wolf volcanics plot as high-K to very high-K (Fig. 3.14), calcalkaline (Fig. 3.8 and 3.9), and Fe-poor (Fig. 3.8). This relates them to a Type III arc classified as "less sodic" than Type I and II arcs (Spence, 1987). Type III arcs are considered to be intracontinental arcs deposited on thick continental crust, possibly above subducted continental crust (Channel and Horvath, 1976).

Whole rock and trace element chemistry of Ootsa Lake Group rocks has not been reported in the literature. This thesis chemically classifies the rhyolite member of the Ootsa Lake Group using volcanic rock samples from the Wolf property. These samples are predominantly oversaturated felsic volcanic rocks of calcalkaline affinity. SiO_2 values are between 65 and 80%, consequently, a unimodal suite is indicated.

Wolf Ootsa Lake Group rhyolites contrast with Kasalka Group and Hazelton Group volcanic rocks. The latter two are Type II arcs (Spence, 1987), which are distinctly bimodal in character. However, Wolf volcanics, classified as Type III arcs by Spence (1987), compare with South Fork volcanic rocks, Yukon Territory (Wood and Armstrong, 1982) which are a subaerial intracontinental arc sequence composed of calcalkaline, potassic and Fe-poor differentiated flows and tuffs.

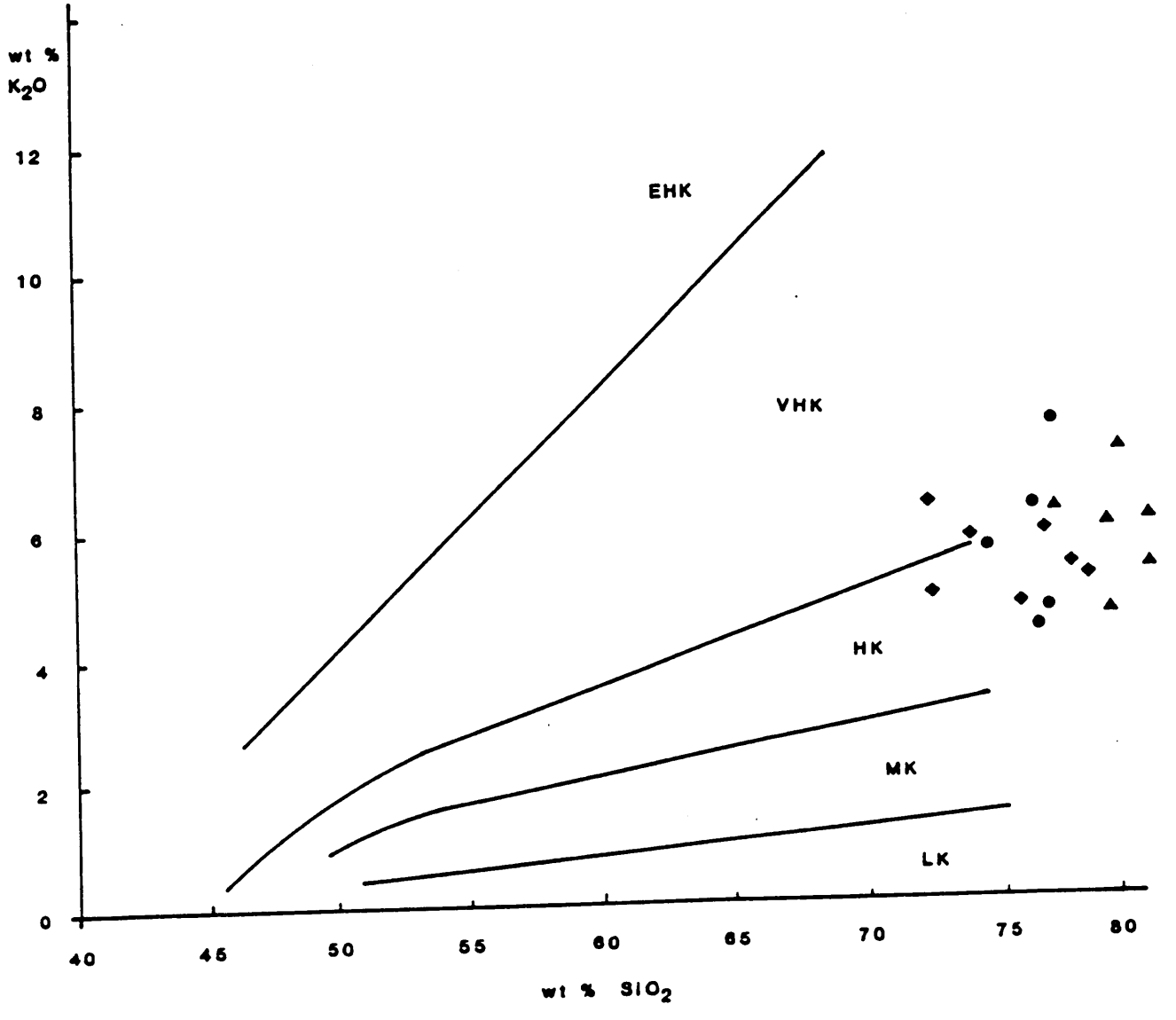

FIGURE 3.14: K_2O vs. SiO_2 plot for analyses from the Wolf prospect (Table 3.3, boundaries are from de Rosen-Spence, 1976). Abbreviations are: LK = low potassium, MK = medium potassium, HK = high potassium, VHK = very high potassium, EHK = extremely high potassium. Felsic volcanic assemblages have high (HK) to very high (VHK) potassium (section 3.2.2) and are plotted using diamonds = pyroclastic rocks, triangles = rhyolite flows and circles = intrusions.

3.3.5. PETROGENESIS

Wolf volcanic rocks may have originated from one or more igneous processes. Pearce element ratio diagrams (Pearce, 1968) are used below to recognise cogenetic rock analyses and to evaluate a hypothesis of feldspar crystal fractionation.

True relationships among variables are shown by dividing the variables by a parameter that remains constant throughout the variation (Pearce, 1968). Chemical data reported in weight percent (wt.%) or parts per million (ppm) are intensive variables (independent of the total quantity of matter in the system under consideration). In order to examine extensive chemical variation (dependent on the total amount of matter in the system under consideration), oxides and elements are converted to moles and ratioed using a common divisor, which is assumed to remain constant throughout the variation. Variations between Pearce element ratios can be directly related to mineral formulae. Thus Pearce variation diagrams illustrate the spatial, mineralogic and chemical variation in rock suites, and are used to evaluate processes involved in their formation.

Pearce element ratios of incompatible trace data are used to test whether rocks from the Eocene volcanic suite at Wolf (Table 3.3) are cogenetic. Pearce plots were generated using PEARCE.PLOT a turbo-pascal program (Stanley and Russell, 1988). Plots of Zr/Nb vs. Y/Nb as well as Y/Nb vs. Ti/Nb show that the variance in the conserved element ratios

for the data is less than the variance attributable to analytical uncertainty (Figs. 3.15 and 3.16). Thus, the Ootsa Lake Group volcanic suite at Wolf could represent a single magma series. Jurassic Hazelton Group rocks cluster separately from the Ootsa Lake Group volcanic suite (Figs. 3.15 and 3.16). These andesites are unrelated to the Ootsa Lake Group volcanic series at Wolf.

The observed chemical diversity of the Wolf volcanic suite could be the result of feldspar differentiation since the Ootsa Lake Group flows and tuffs can be derived from a single magma. The affects of feldspar fractionation are modelled on a Pearce element ratio diagram with the axes Y = 2Ca + Na + K/i and X = Al/i, where i = a conserved element. This figure examines feldspar differentiation alone; rock compositions that are related through accumulation or loss of plagioclase or potassium feldspar define a trend with a slope of one on this diagram.

The element Ti is used as a conserved element because it is probably not involved in crystallization of rhyolites at Wolf (Fig. 3.16). Data from wolf plotted on the Pearce plot for feldspar differentiation defines a trend of slope 1.00 with strong correlation of $r^2 = 0.89$; N = 23 (Fig. 3.17). Thus, the hypothesis of feldspar differentiation cannot be rejected, and the chemical variability of Wolf volcanic rocks is probably the result of accumulation and loss of plagioclase and potassium feldspar.

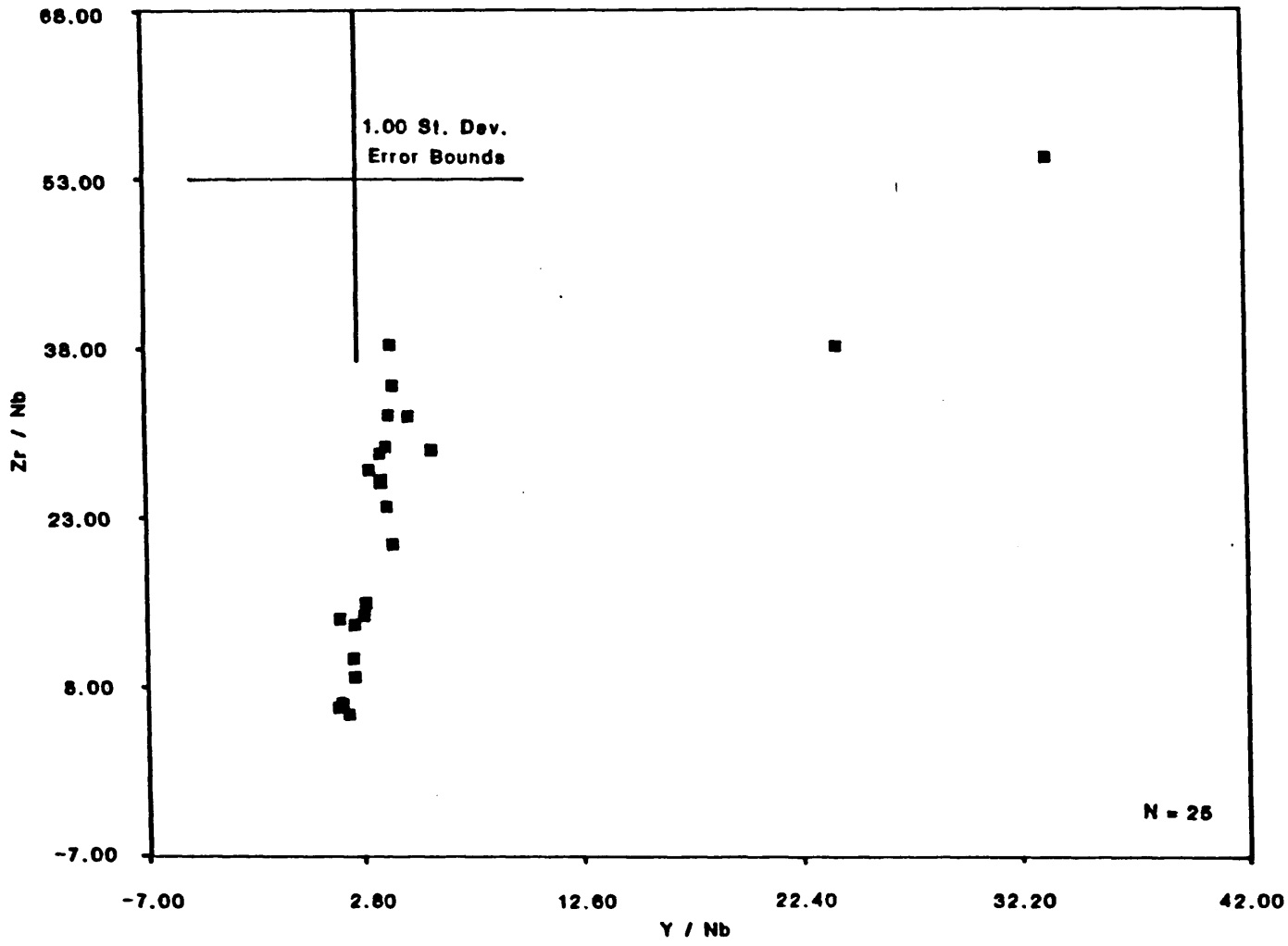

FIGURE 3.15: Zr/Nb vs. Y/Nb plot for analyses from the Wolf prospect (Table 3.3) shows that the Eocene volcanic suite is cogenetic because the variance in conserved element ratios for the data is less than the variance attributable to analytical uncertainty.

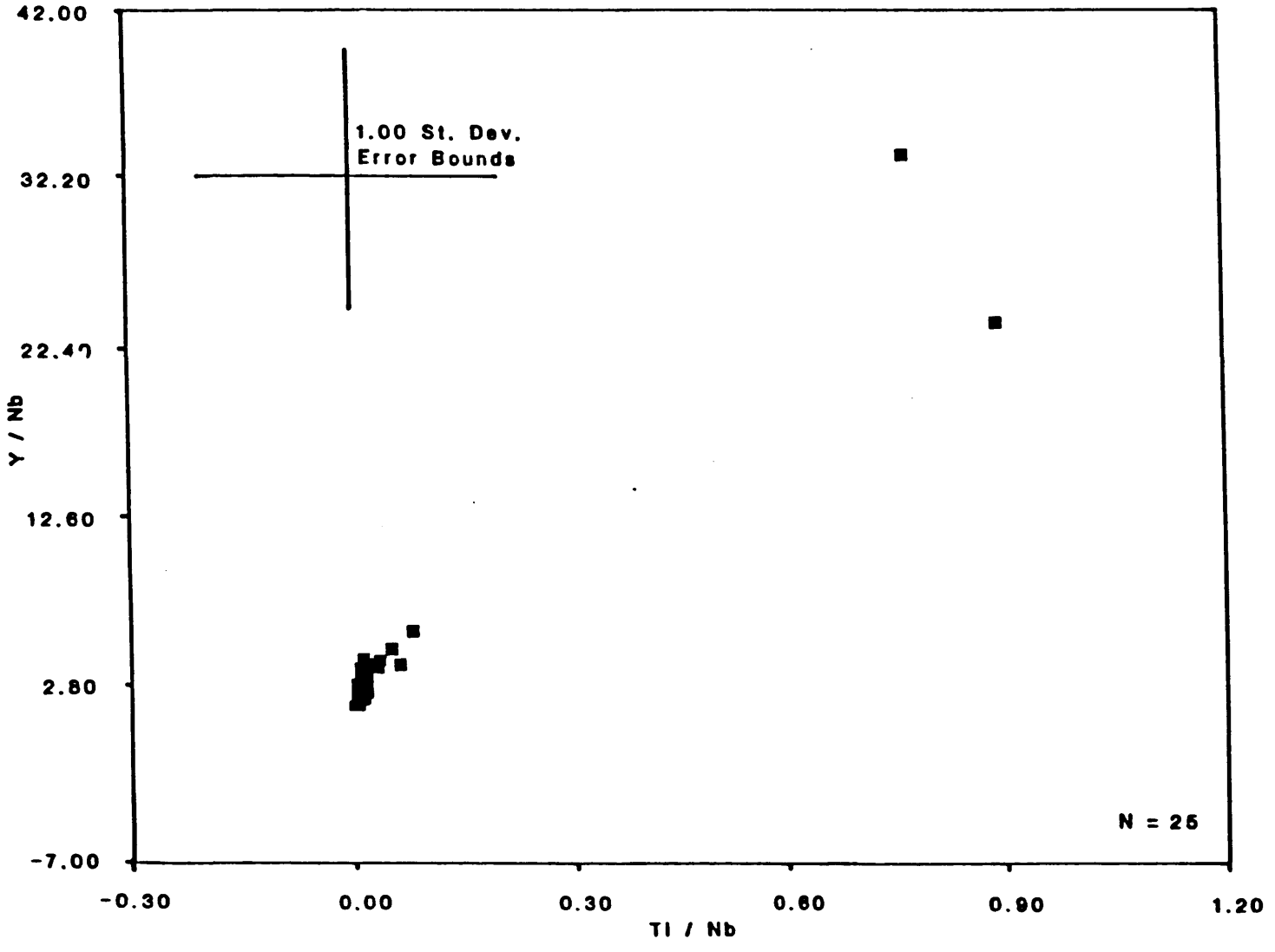

FIGURE 3.16: Y/Nb vs. Ti/Nb plot for analyses from the Wolf prospect (Table 3.3) shows that the Eocene volcanic suite is cogenetic because the variance in conserved element ratios for the data is less than the variance attributable to analytical uncertainty.

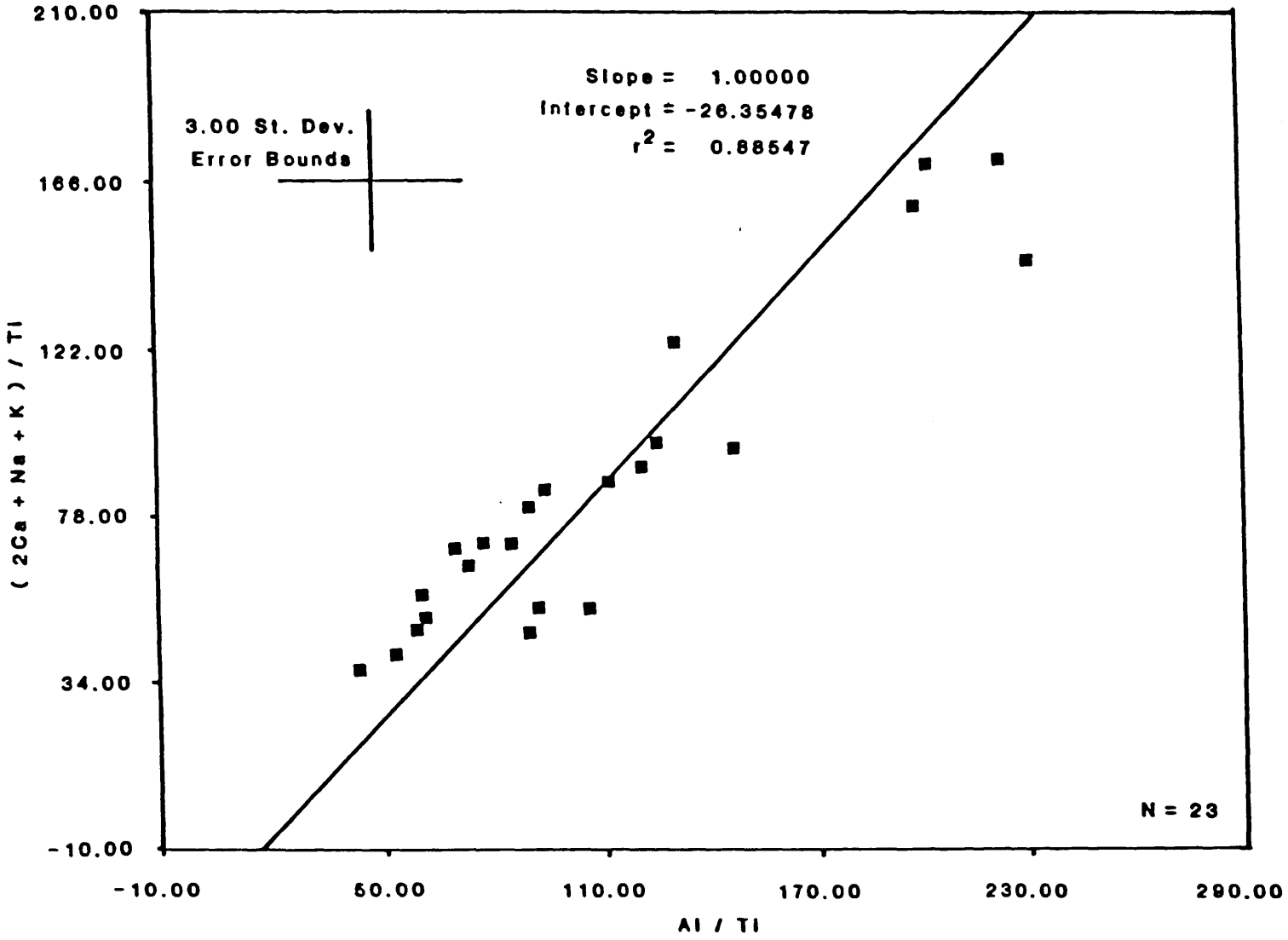

FIGURE 3.17: 2Ca+Na+K/Ti vs. Al/Ti plot of data from the Wolf property (Table 3.3) to test the hypothesis of feldspar fractionation.

3.4 DATING

3.4.1 K-AR

Three samples from the Wolf property were dated by whole rock K-Ar (Table 3.4). They consisted of: (1) a crystal tuff (KA135: Eo_6) which marks the top of the pyroclasitic package at Wolf, (2) a spherulitic and flow banded rhyolite flow (KA112: Eo_7), and (3) a coarse-grained rhyolite porphyry (KA078: Eo_9). The purpose of the dating was to obtain an age for the volcanic and intrusive rocks at Wolf to confirm that they are Ootsa Lake Group rocks.

The K analyses were by atomic absorption (by K.R. Scott), and the Ar analyses were by isotope dilution using conventional procedures (by J. Harakal). The decay constants used are $\lambda_e + \lambda_{e'} = 0.581 * 10^{-10}$ year^{-1}; $\lambda_\beta = 4.962 * 10^{-10}$ year^{-1}; and $^{40}K/K = 1.167 * 10^{-2}$ atomic percent (Steiger and Jager, 1977).

All three whole rock K-Ar dates confirm a mid-Eocene (Lutetian) age (46 to 50 Ma) for volcanic rocks at the Wolf property. This date is within the age limits assigned to Ootsa Lake Group volcanic rocks by Tipper (1963).

The cessation of pyroclastic volcanism and commencement of rhyolite doming is bracketed by the ages of Eo_6 and Eo_7 (49.9 ± 1.7 to 48.3 ± 1.7 Ma). Intrusion of Eo_9 (rhyolite porphyry) into the volcanic succession (Fig. 3.1) took place at the same time or up to a million years later at 47.6 ± 1.7 Ma.

TABLE 3.4: K-Ar ages for Ootsa Lake Group volcanic rocks from the Wolf prospect, central British Columbia. Samples are located on Figure 3.5.

SAMPLE NUMBER	LATITUDE/ LONGITUDE	K (wt.%)	$^{40}Ar_{rad}$*10^{-10} (moles/g)	$^{40}Ar_{rad}$ (%)	DATE[1] (Ma)	AGE[2]
KA 078 rhyolite porphyry whole rock	53°11'15" 125°29'30"	4.22	3.530	67.4	47.6±1.7	Middle Eocene
KA 112 rhyolite whole rock	53°12'10" 125°28'10"	5.35	4.538	89.5	48.3±1.7	Middle Eocene
KA 135 crystal tuff whole rock	53°11'50" 125°27'15"	5.38	4.722	75.7	49.9±1.7	Middle Eocene

1. Analyses were carried out at The University of British Columbia, Department of Geological Sciences, by K.R. Scott (K) and J. Harakal (Ar).
2. Age is based on date and time scale of the DNAG 1983 Time Scale (Palmer, 1983).

The Capoose batholith, a quartz monzonite intrusive 7 km north of the property has been dated as Late Cretaceous (67 Ma) by the K-Ar technique using biotite (section 4.4). Such evidence precludes a genetic relationship between the intrusive at Capoose and volcanism at Wolf.

3.4.2 PALYNOLOGY

Epiclastic rocks on the Wolf property do not outcrop (Fig. 3.1) but were intersected in drill core. These poorly consolidated siltstones, sandstones, and tuffs are at least 30 metres thick (Fig. 3.2). Four samples were systematically collected from the siltstones for a study of fossil spores. The study was undertaken to determine the relative age of the epiclastic unit with respect to overlying Ootsa Lake Group volcanic rocks.

Samples were crushed with a steel mortar and dissolved in strong hydrofluoric acid overnight. Remaining carbonate and organic debris was sieved to minus 10 and plus 20 mesh. Strong hydrochloric acid was used to dissolve carbonates and test for pyrite--most solutions turned green which is diagnostic of the presence of iron. Palynomorphs were isolated by immersing samples in zinc bromide which induces minerals to settle and organic debris to float. Samples of the separated organic debris were pipetted into different containers and rinsed with strong nitric acid followed by water. Samples were then placed in solution for eight hours to make the palynomorphs less opaque. Saframine was used to

stain the samples in preparation for petrographic observation.

A small but well-preserved assemblage of palynomorphs (Table 3.5) were identified by G.E. Rouse at The University of British Columbia. The epiclastic rocks at Wolf correlate closely with assemblages from the Fraser Bend Formation along the Fraser River, and equivalents along and flanking Nechako River which are Middle Miocene. This age is estimated to be 17-13.5 Ma, or Barstovian on the mammalian scale (Rouse and Mathews, 1979; Mathews and Rouse, 1984,. The climate is estimated to have been warm temperate, with an annual precipitation between 100 and 1300 mm and mean annual temperature of about 12-16^{o}C (Rouse, pers. comm. 1988). The epiclastic rocks were subjected to paleo-temperatures near 200^{o}C as indicated by the required length of time (at least 8 Hours) needed to bleach palynomorphs in Schultz's solution (Rouse, pers. comm., 1988).

3.5 MINERALIZATION AND ALTERATION

The Wolf epithermal prospect is characterized by low-sulphide zones in quartz veins and breccias containing electrum, native silver, silver sulphides and sulphosalts. Wallrock alteration is typically argillic or sericitic bordering the silicified zones near veins. Also near the veins are disseminated fine-grained potassium feldspar or chlorite. Mineral and alteration assemblages resemble those of adularia-sericite epithermal systems described by Hayba et al. (1985).

TABLE 3.5: Palynomorphs in Fraser-Bend equivalent mid-Miocene epiclastic rocks at the Wolf prospect, central British Columbia (G. E. Rouse, pers. comm. 1988).

FERN SPORES:

Laevigato sporites ovatus
Polypodiisporites favus
Deltoidospora diaphana
Polypodiaceae spore cf. Dryopteris austriaca (spreading wood fern)

CONIFER POLLEN:

Pinus cf. contorta
P. haploxylon - type
P. diploxylon - type
Tsuga heterophyllites
T. mertensiana
Pseudotsuga cf. menziesii
Abies sp.
Taxodiaceaepollenites hiatus

ANGIOSPERM POLLEN:

Pterocarya stellata
Fraxinoipollenites variabilis
F. medius
Alnus vera
cf. Quercus shiabensis
Quercoidites microhenrici
Corylus/Carpinus

But what's the possible age range that this allows?

Five distinct mineralized zones have been delineated on the property: (1) the Chopper Pad zone, (2) the Lookout zone, (3) the Ridge zone, (4) the Pond zone, and (5) the East zone (Fig. 3.18). The main deposit area comprises the Ridge and Pond zones in the central part of the property. A trench in the Ridge zone returned 8.49 g/tonne gold and 42.41 g/tonne silver over 7.5 m (Holmgren and Cann, 1984). Surface samples from the Pond zone are typified by gold values greater than 0.5 g/tonne; the highest gold and silver values obtained were 1.4 g/tonne and 19 g/tonne respectively (Holmgren and Cann, 1984). Detailed description of the nature and occurrence of mineralized zones with distribution of ore minerals and statistical analyses of metals follow.

3.5.1 DESCRIPTION OF ZONES

Surface samples from all five zones were examined in detail in 1985. Gold and silver mineralization is associated with vein and breccia textures all each zones. Individual veins at Wolf have characteristic features of high-level emplacement such as chalcedonic quartz, brecciated wallrock fragments cemented by chalcedony, colloform layering, cockscomb growth of well-formed quartz, and drusy cavities.

Relative timing of hydrothermal events on the property (section 3.5.2) was estimated from cross-cutting relationships best displayed in trenches on the Ridge Zone (Fig. 3.19). Block faulting preceeded formation of veins

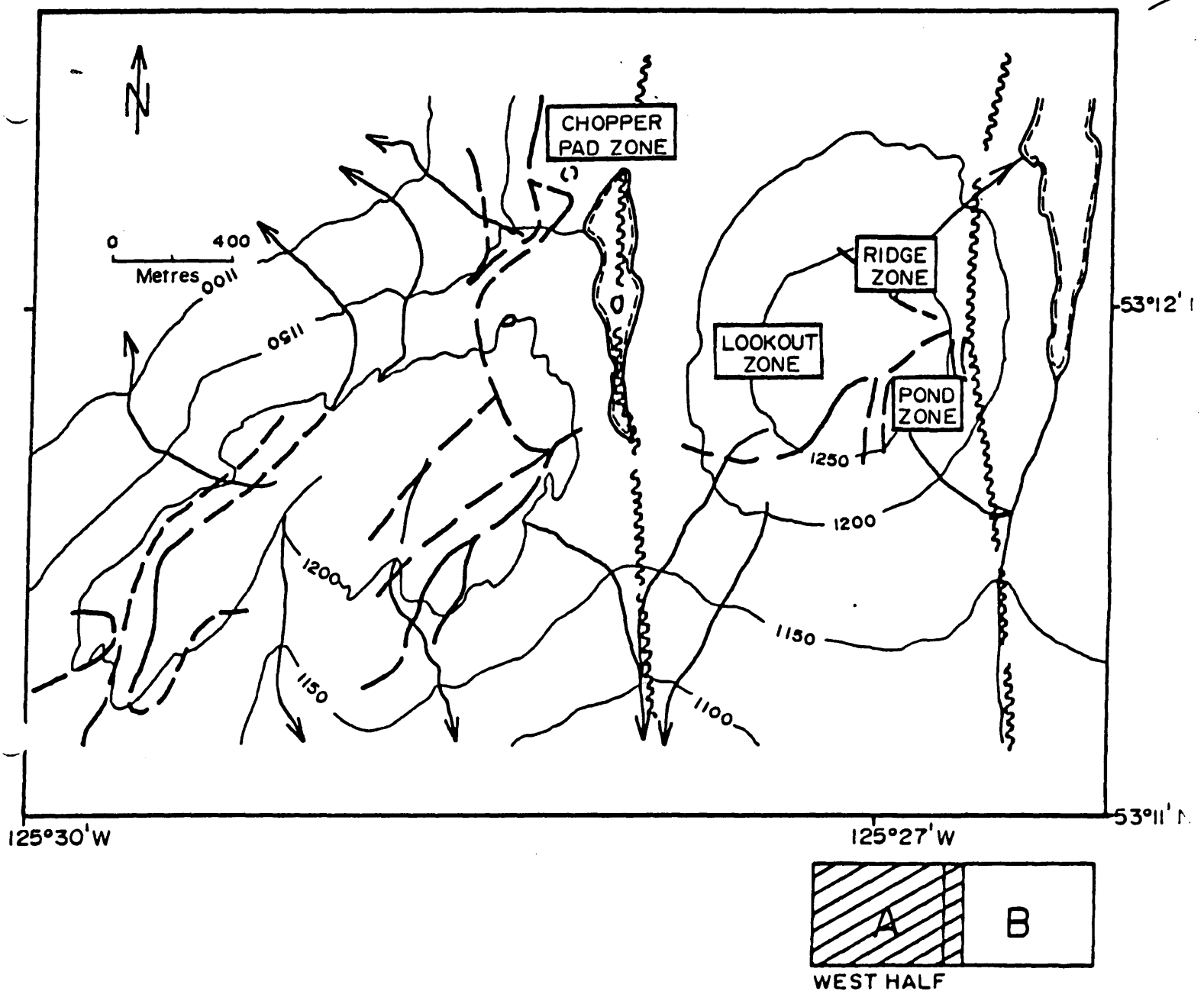

FIGURE 3.18: Mineralized zones of the Wolf prospect, Capoose Lake area, central British Columbia. A)west half, and B) east half.

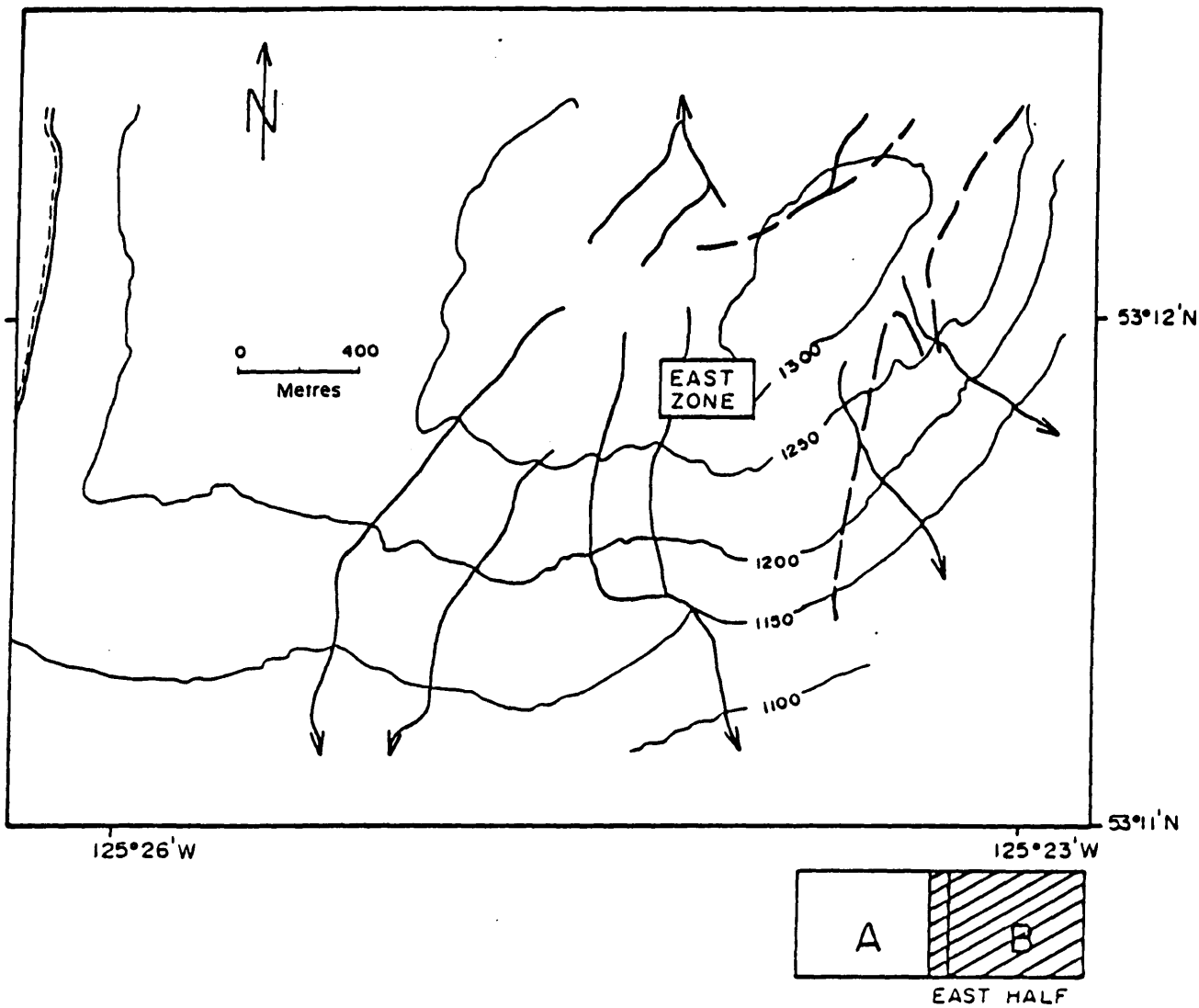

FIGURE 3.18: Mineralized zones of the Wolf prospect, Capoose Lake area, central British Columbia. A)west half, and B) east half.

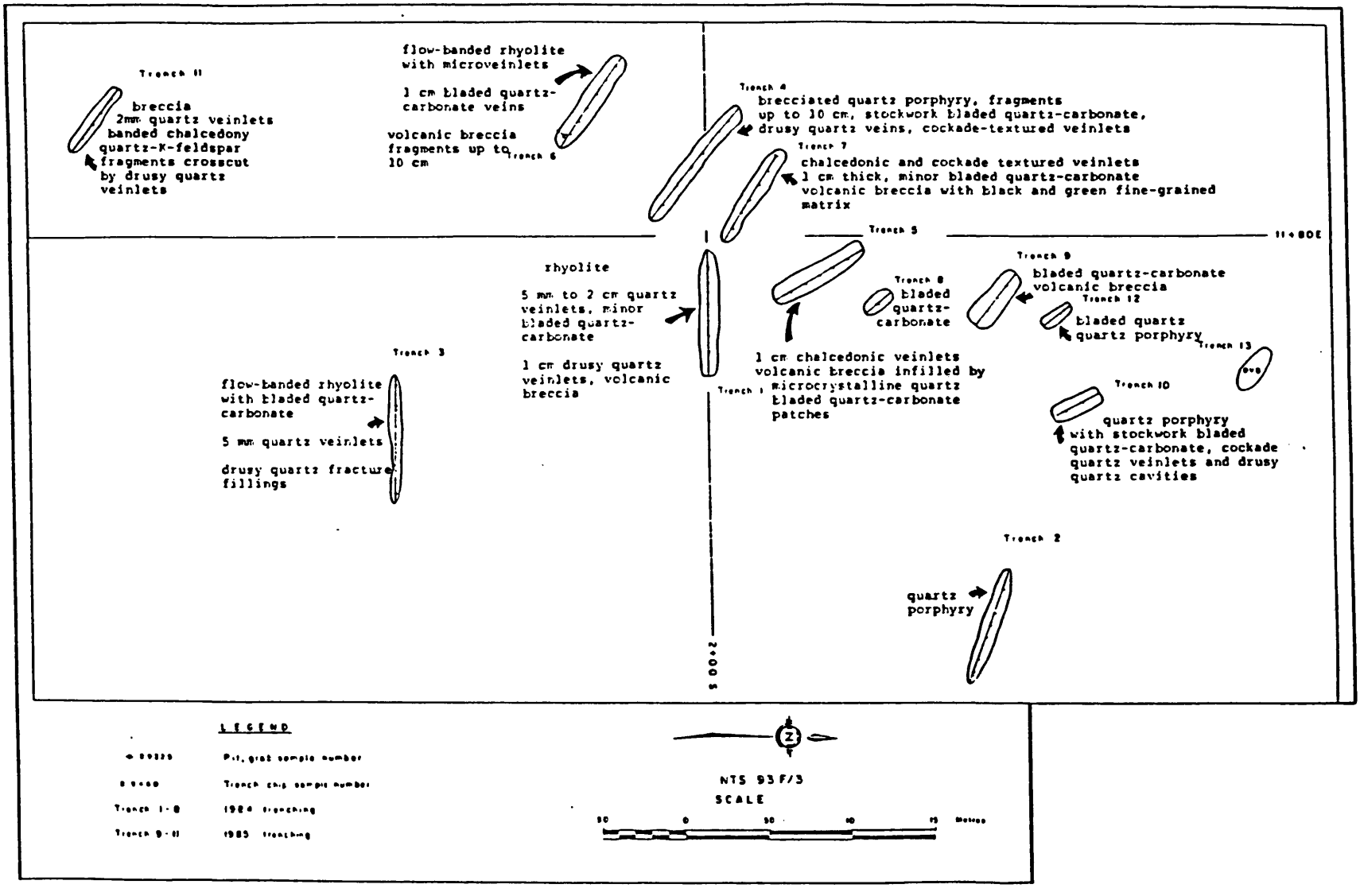

FIGURE 3.19: Trench map of the Ridge Zone (Figure 3.18) showing distribution of vein and breccia types from the Wolf prospect, central British Columbia. Gold and silver grades are in Figure 3.24.

and breccias on the property and provided conduits for hydrothermal fluids at Wolf (section 3.2.3). The extent and nature of the Ridge and Pond zones with depth is displayed in the vertical cross-sections of Figures 3.20 and 3.21 constructed from logged core and the aid of the GEOLOG system (name registered by International Geosystems Corporation, Vancouver, B.C.).

The Chopper Pad zone, in the northwestern part of the property (Fig 3.18A), is an irregular north-south trending zone up to 500 m long. It is characterized by pervasive silicification of massive and brecciated rhyolite (unit 8, Fig 3.1). Silicification is mainly in fractures filled with grey-white chalcedony or in breccias cemented by translucent quartz (Plate 3.7). However, massive replacement of rhyolite by silica occurs as pods up to 2 m across. A bladed quartz-carbonate texture is often developed within these pods (Plate 3.8). This texture, described as lamellar ore by Lingren (1933), is characteristic of many epithermal deposits (cf. McDonald, 1987) and may reflect quenching due to boiling and rapid cooling.

The Lookout, Ridge and Pond zones, separated by less than 200 m on a hill in the central part of the property, are texturally similar. Specifically, bladed quartz carbonate patches from 10 cm to 0.5 m in size (Plate 3.8) commonly occur with diffuse boundaries in each zone. The nature of this quartz carbonate texture, which contains the

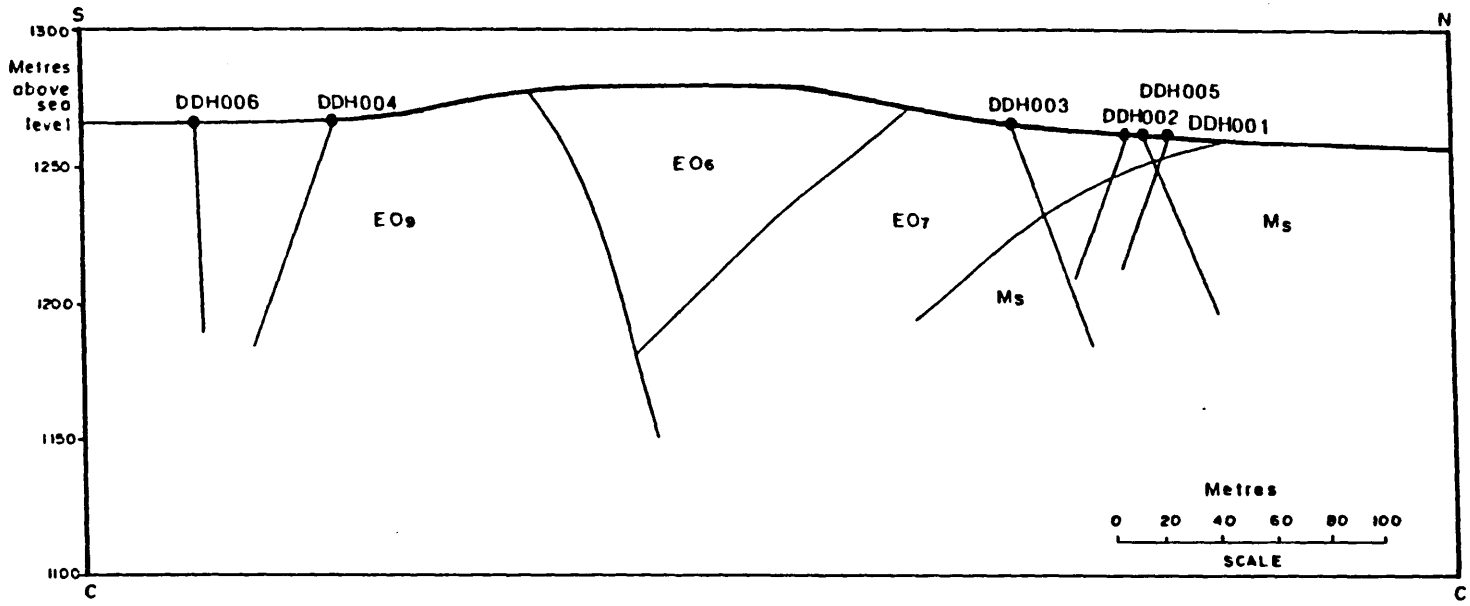

LEGEND

Ms	SILTSTONE, TUFFACEOUS SANDSTONE	EO_4	ASH TUFF	EO_8	VOLCANIC BRECCIA
EO_1	CONGLOMERATE	EO_5	RHYOLITE FLOWS	EO_9	RHYLITE PORPHYRY
EO_2	FELSIC LAPILLI TUFF	EO_6	CRYSTAL TUFF	EO_{10}	QUARTZ PORPHYRY
EO_3	LITHIC, CRYSTAL TUFF	EO_7	RHYOLITE	Jha	ANDESITE FLOWS, FLOW BRECCIA

SYMBOLS

geological contact; known, assumed
fault; known, assumed
foliation
lineation
vein, with dip

FIGURE 3.20: North-south vertical section (C-C':Fig. 3.1A) of the Wolf prospect from surface mapping and core logging of the Ridge and Pond zones, Wolf prospect, central British Columbia.

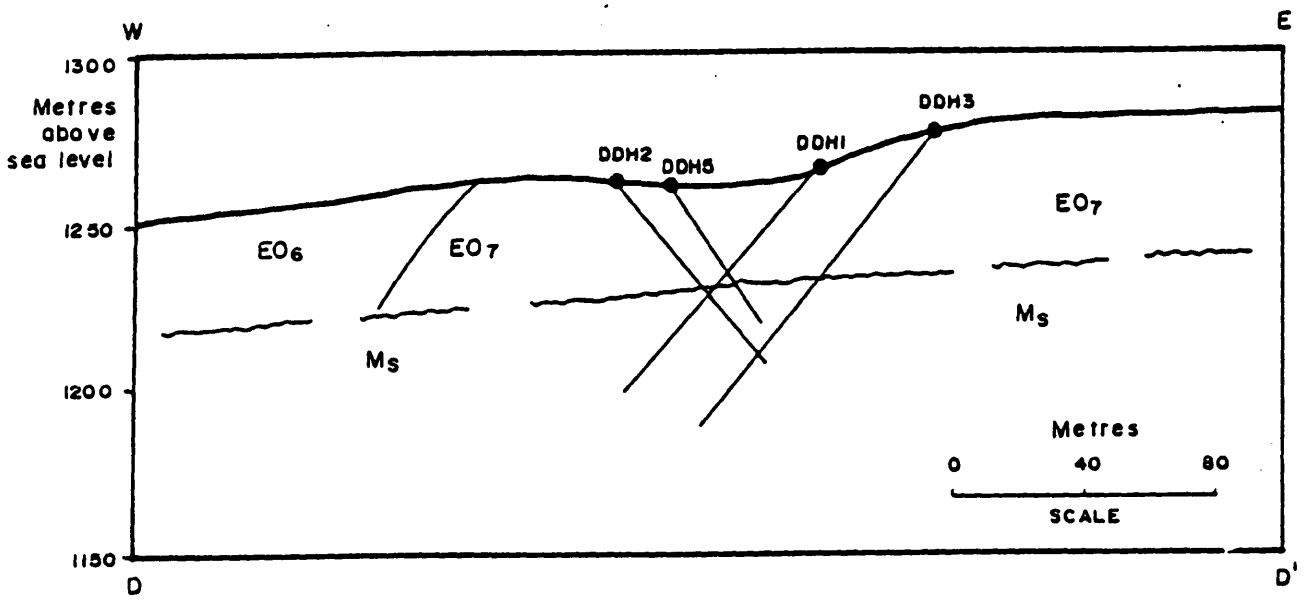

LEGEND

Ms	SILTSTONE, TUFFACEOUS SANDSTONE	EO4	ASH TUFF	EO8	VOLCANIC BRECCIA
EO1	CONGLOMERATE	EO5	RHYOLITE FLOWS	EO9	RHYOLITE PORPHYRY
EO2	FELSIC LAPILLI TUFF	EO6	CRYSTAL TUFF	EO10	QUARTZ PORPHYRY
EO3	LITHIC, CRYSTAL TUFF	EO7	RHYOLITE	Jha	ANDESITE FLOWS, FLOW BRECCIA

SYMBOLS

geological contact; known, assumed	lineation
fault; known, assumed	vein, with dip
20 foliation	diamond drill hole (DDH)
	DDH trace

FIGURE 3.21: East-west vertical section (D-D':Fig. 3.1A) of the wolf prospect from surface mapping and core logging of the Ridge and Pond zones system, Wolf prospect, central British Columbia.

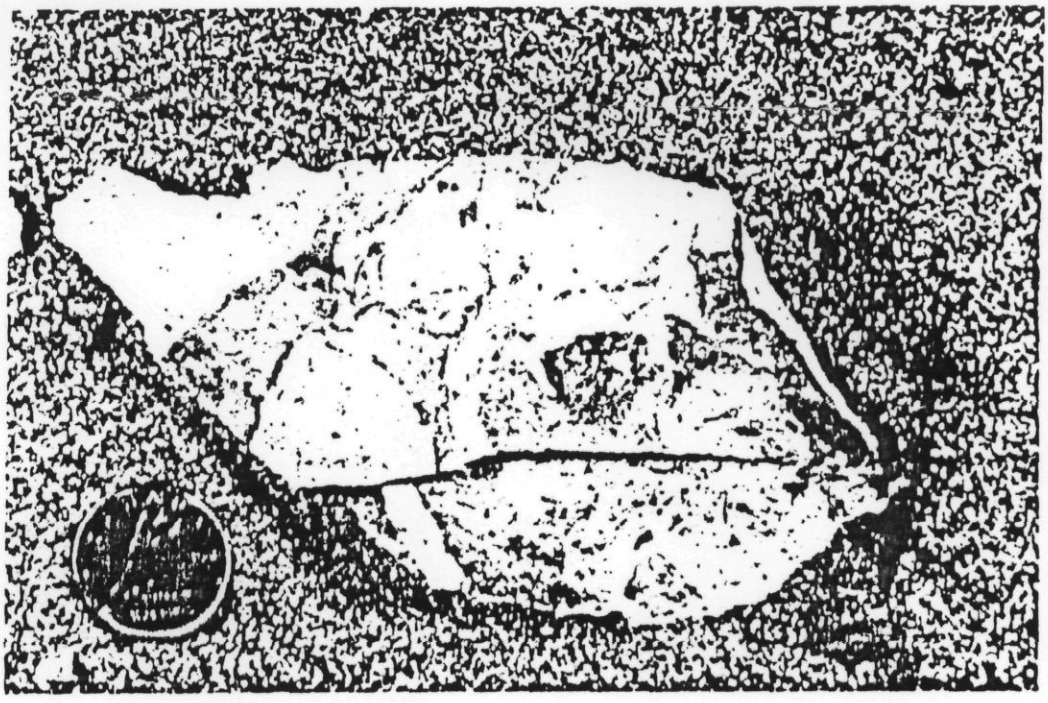

PLATE 3.7: Monolithic quartz-cemented volcanic breccia from the Ridge zone. Sample KATR7-3, Wolf prospect.

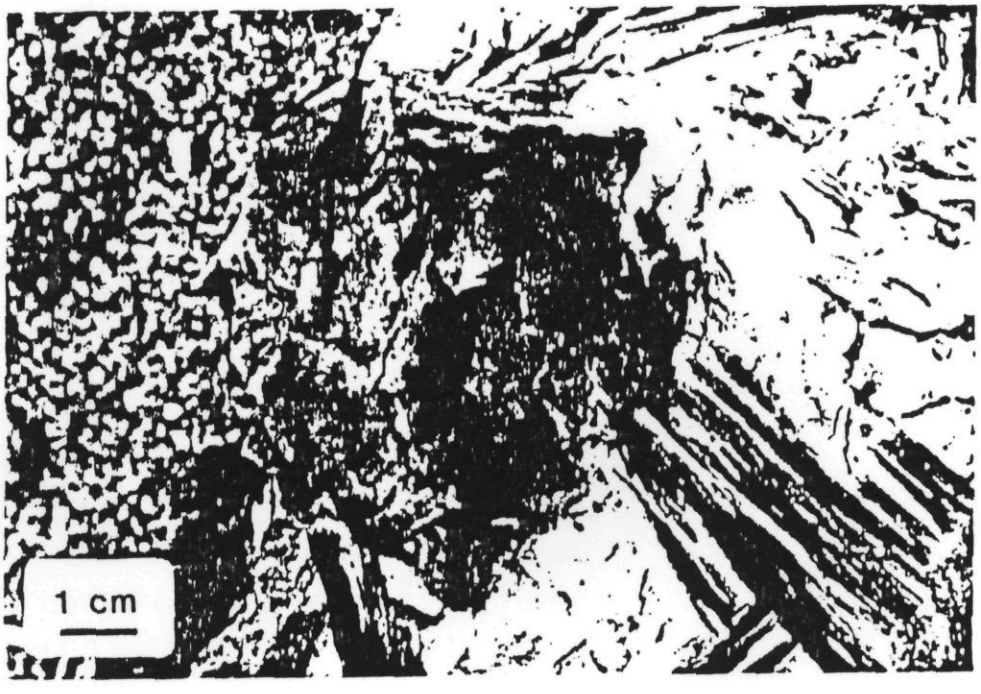

PLATE 3.8: Bladed carbonate in quartz from the Ridge zone. Sample KATR9-1, Wolf prospect.

highest gold and silver values on the property (Holmgren and Cann, 1985) is discussed in section 3.5.2.

The Lookout zone is typified by milky white veins up to 2 m wide (Plate 3.9). These veins have sharp contacts with unaltered host crystal tuff (Eo_6, Fig 3.1). Locally, irregular patches, up to 20 cm in diameter, of bladed quartz carbonate veining occur within broad diffuse pods of white vein quartz.

The Ridge zone is typically in heterolithic breccias within a flow-banded rhyolite (Eo_7, Fig 3.1). The heterolithic fragments comprise grey, green or white, aphanitic to porphyritic volcanic fragments from 1 cm to 4 cm in diameter (Plate 3.4). Some of the fragments are clay-altered. Fragments also include broken chips of banded tan-white chalcedony or quartz. Heterolithic fragments are rimmed by white chalcedony and cemented by translucent quartz. The breccias are crosscut by late stage quartz veinlets (Plate 3.10). Minor quartz-carbonate patches up to 0.5 m occur within larger white veins. These veins are peripheral to breccia areas. The presence of fragments from previous hydrothermal events, rimming of fragments, peripheral veining, and late stage veinlets define a multistage history of mineralization.

The Pond zone is typified by milky white sucrosic quartz, cryptocrystalline grey-white banded chalcedonic veins (Plate 3.11) and veinlets hosted in rhyolite porphyry

PLATE 3.9: Milky white quartz veins as thick as 2 m at the Lookout Zone, Wolf prospect.

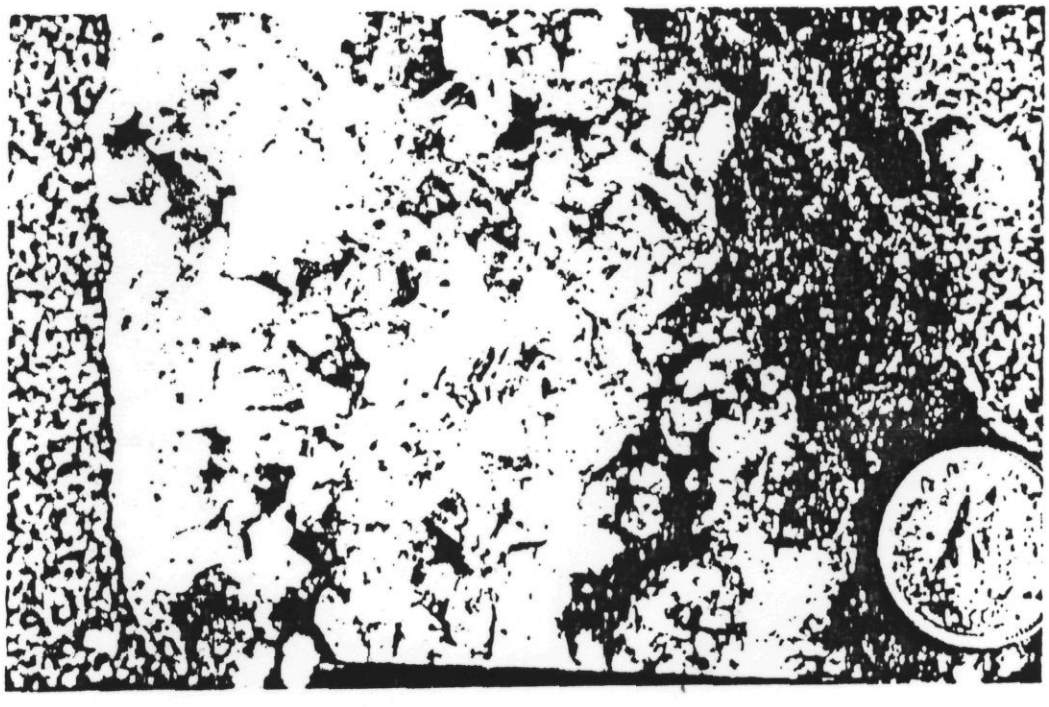

PLATE 3.10: Drusy vein quartz from the East zone. Sample KA188, Wolf prospect.

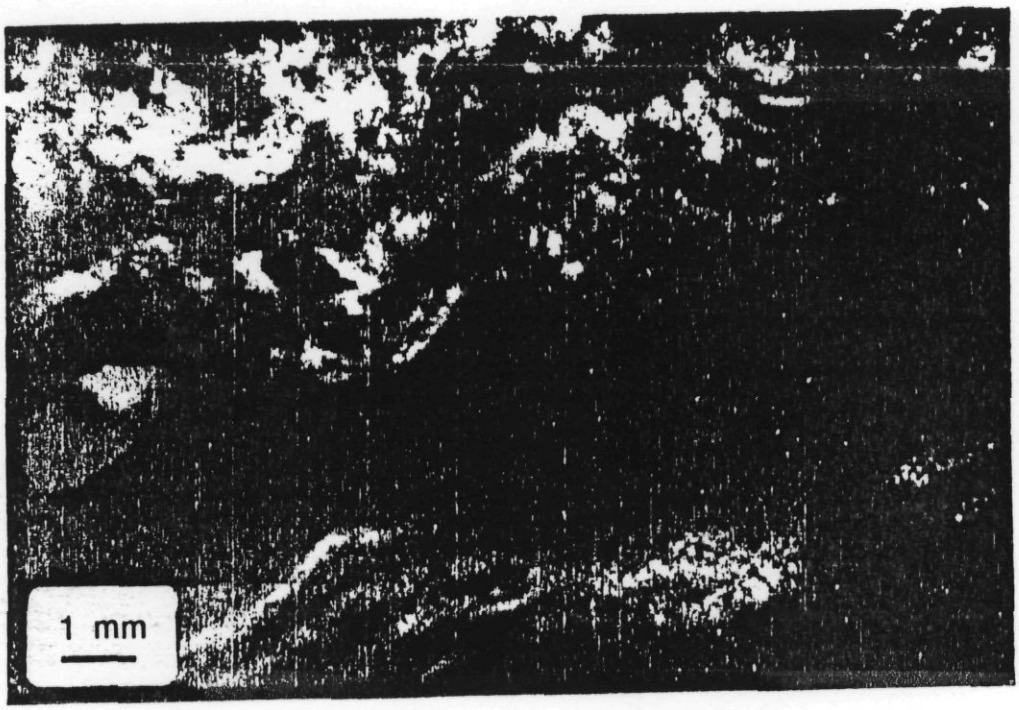

PLATE 3.11: Banded chalcedony veins from the Pond zone. Sample KA4-7, Wolf prospect.

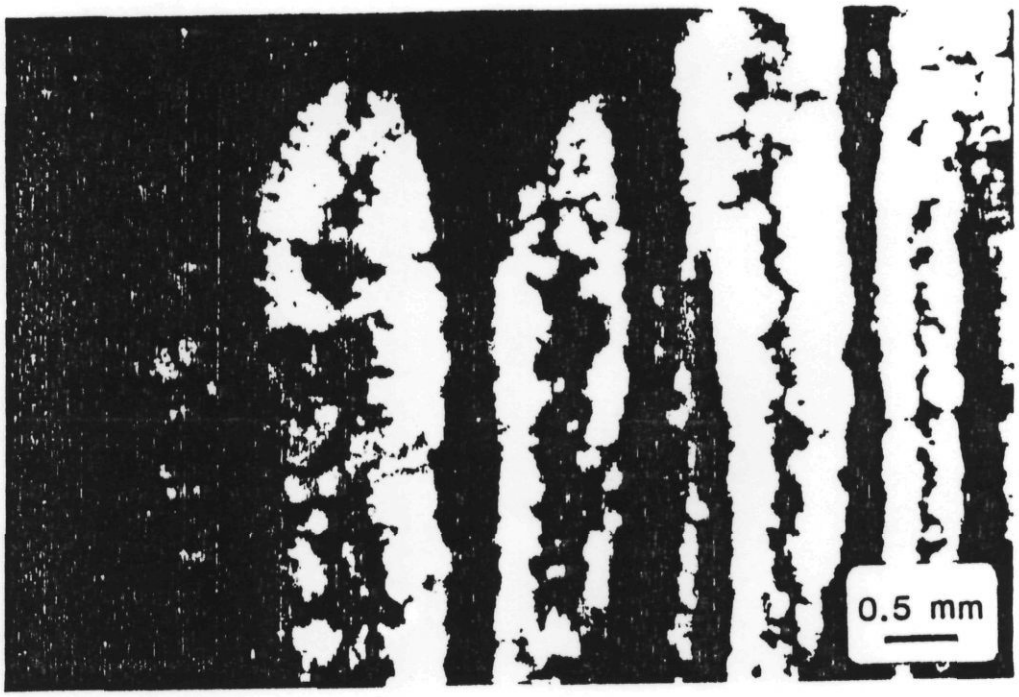

PLATE 3.12: Photomicrograph of clear crystalline quartz interstitial to dark bladed carbonate, Ridge zone. Sample KATR9-1, Wolf prospect.

(Eo_9: Fig 3.1). Locally veinlets are vuggy and contain pods of bladed quartz.

The East zone, on a rise on the East side of the property (Fig. 3.18B), is separated from the other zones by about 1 km. Textures are typified mainly by late stage drusy quartz crystals up to 2 cm long in vugs. The vugs are often crosscut by 2 mm quartz veinlets.

Distribution of chalcedony and drusy quartz and bladed quartz-carbonate vein textures with depth from the Ridge and Pond zones are illustrated on vertical sections (Figs. 3.22 and 3.23). Each section is hand contoured to define the following amounts of vein type: (1) less than 0.1%, (2) between 0.1 and 1%, (3) between 1 and 5%, and (4) greater than 5%. The Ridge zone is characterized on surface by multistage brecciation and veining events (Fig. 3.19). Highest gold grades are associated with veins containing abundant bladed quartz-carbonate (Fig 3.24). At depth, however, the markedly drusy quartz veins are truncated by a north-south, westwardly dipping thrust fault (Fig. 3.23A). Drusy, chalcedonic quartz and bladed quartz-carbonate veins abundant at the Pond zone (Figs. 3.22 and 3.23). The veins extend to depths of at least 100 m from the surface.

A qualititive alteration map (Fig. 3.25) shows the extent of argillic alteration across the property. Zones of high or intense clay alteration generally correspond with the mineralized zones outlined in section 3.5.1.

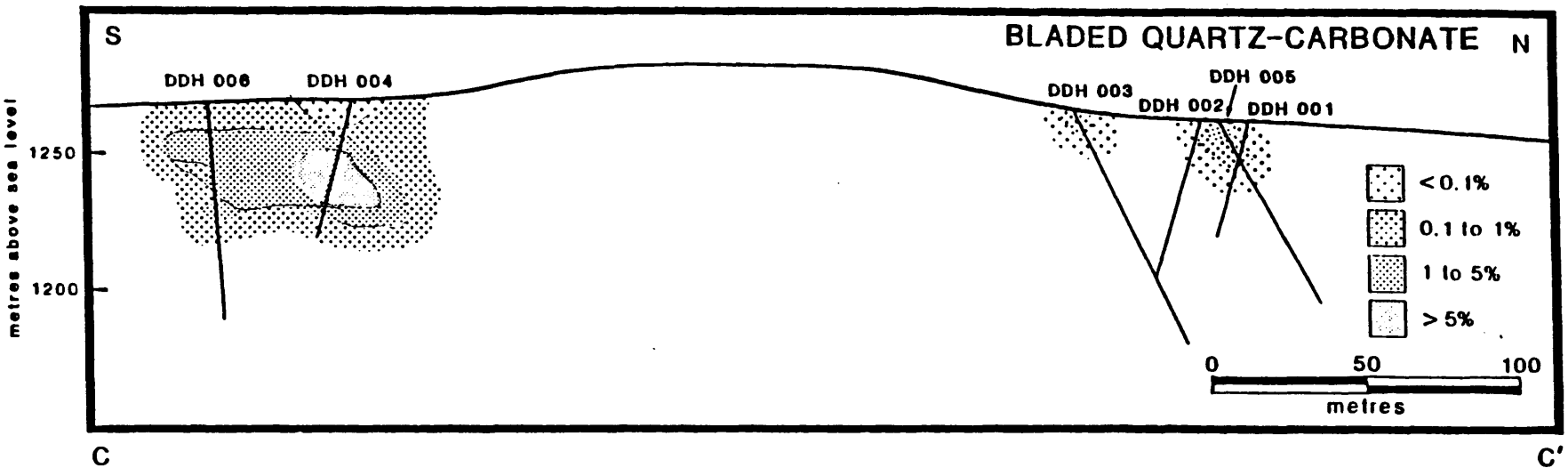

FIGURE 3.22: North-south vertical section (C-C':Fig. 3.1A) of the Wolf prospect showing distribution of vein and breccia phases with depth (refer to Figure 3.20 for geology).

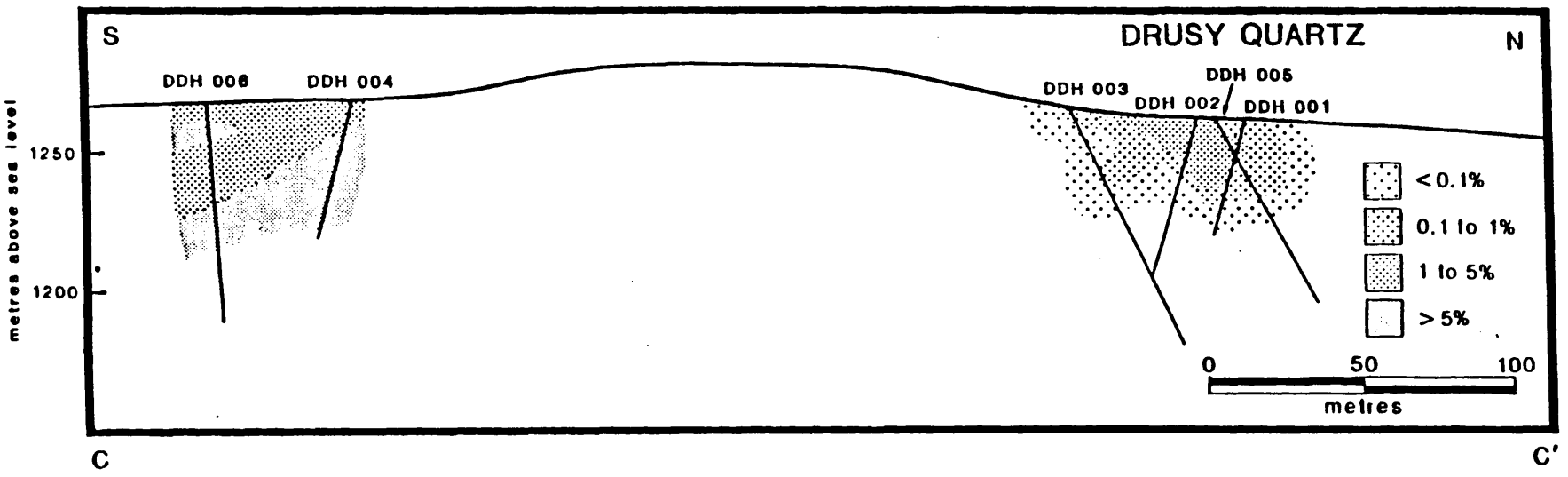

FIGURE 3.22: North-south vertical section (C-C':Fig. 3.1A) of the Wolf prospect showing distribution of vein and breccia phases with depth (refer to Figure 3.20 for geology).

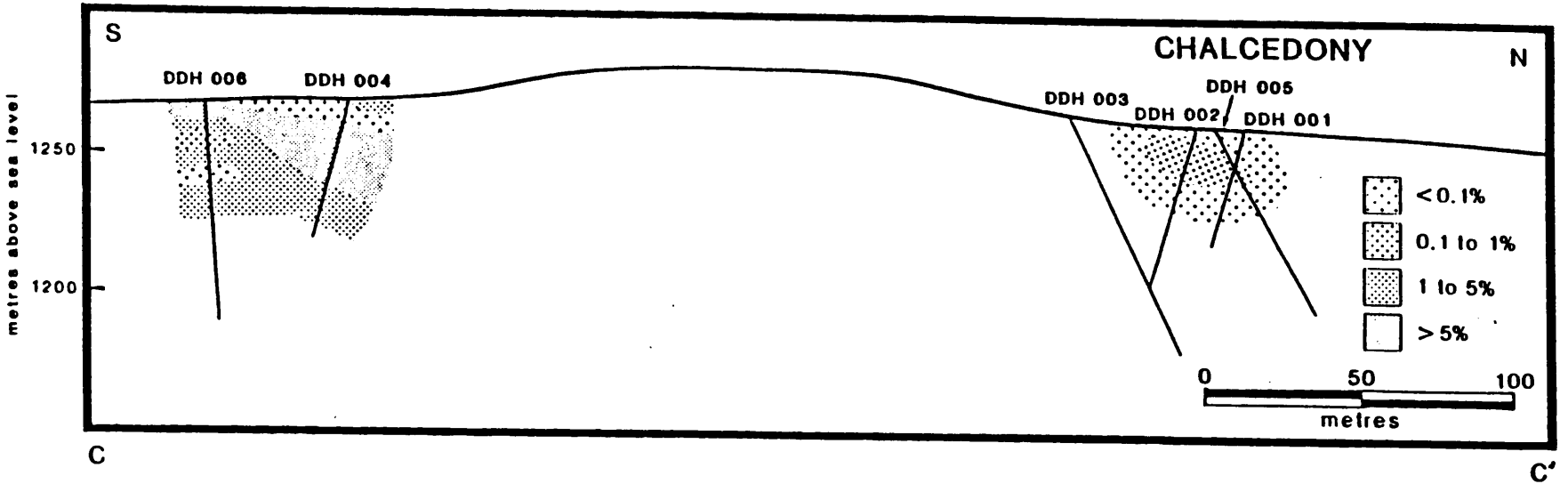

FIGURE 3.22: North-south vertical section (C-C':Fig. 3.1A) of the Wolf prospect showing distribution of vein and breccia phases with depth (refer to Figure 3.20 for geology).

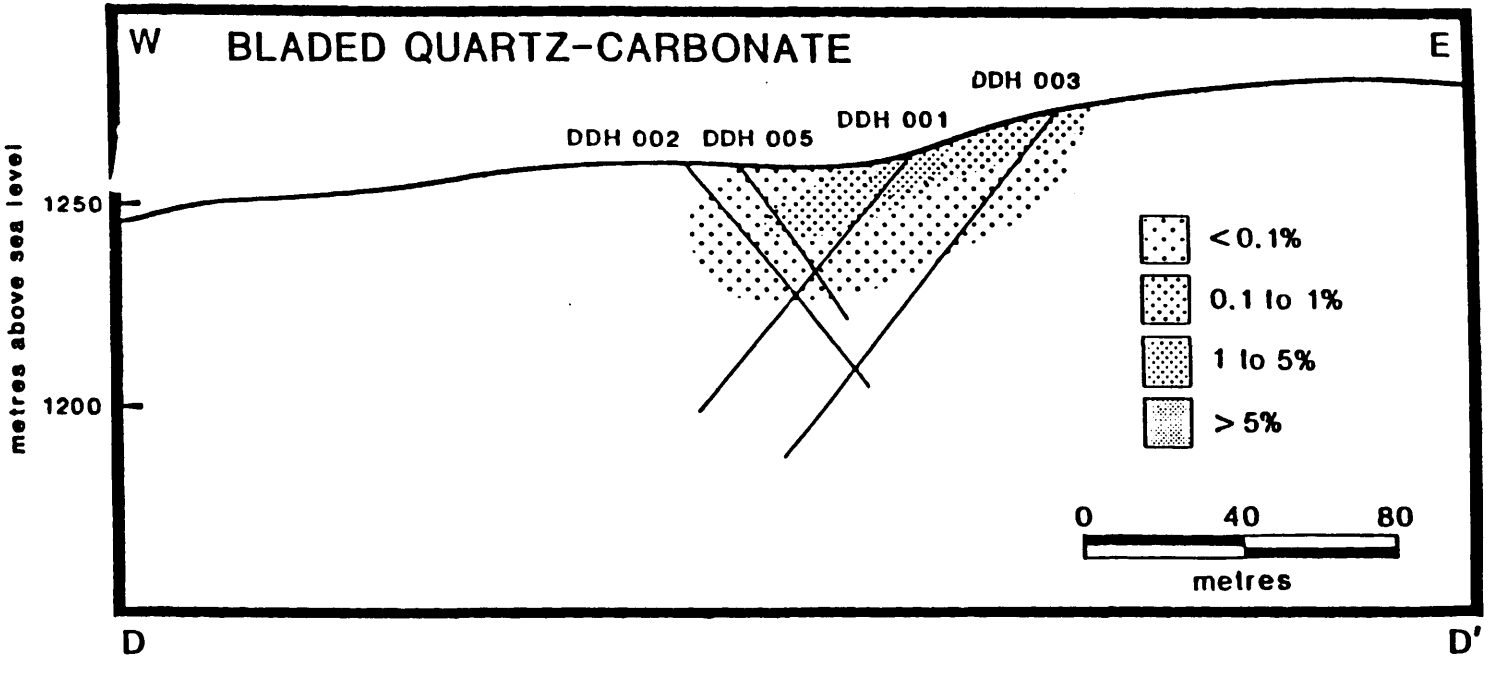

FIGURE 3.23: East-west vertical section (D-D':Fig. 3.1A) of the Wolf prospect showing distribution of vein and breccia phases with depth (refer to Figure 3.23 for geology).

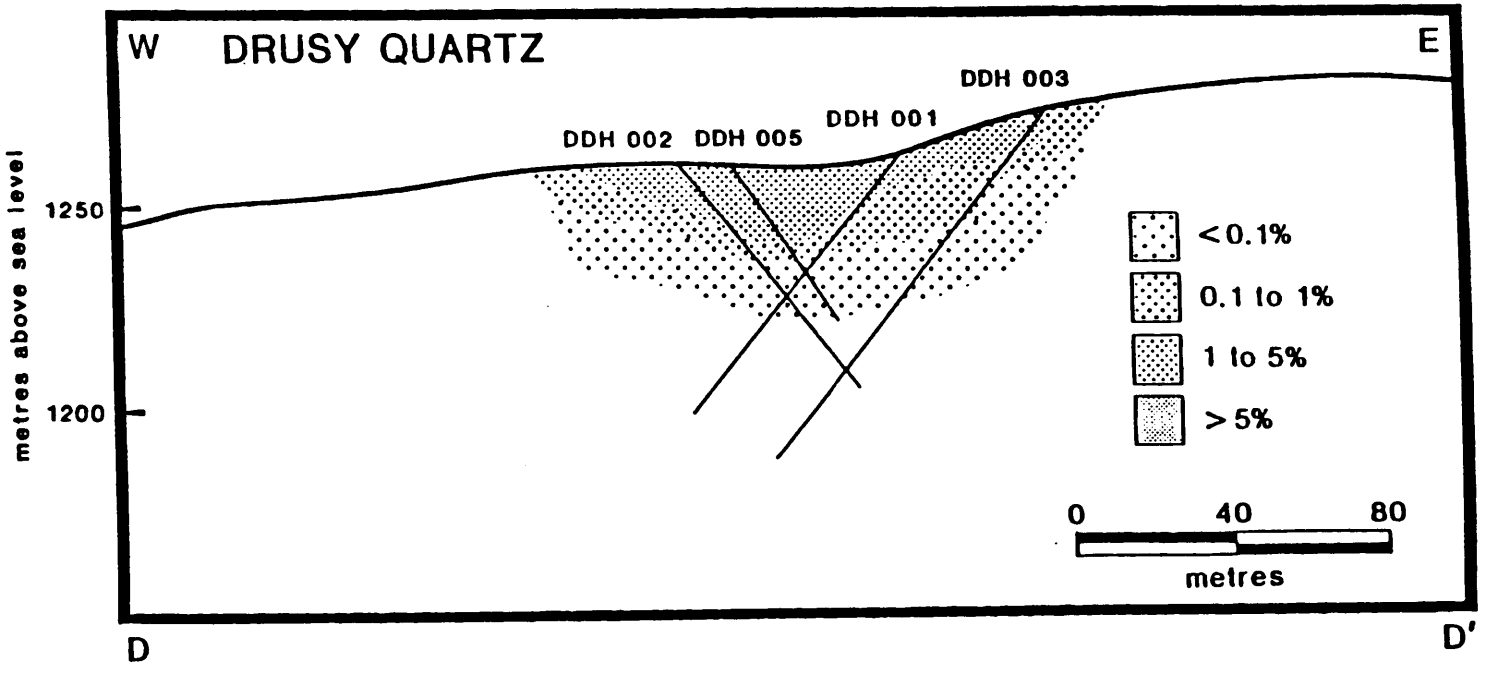

FIGURE 3.23: East-west vertical section (D-D':Fig. 3.1A) of the Wolf prdspect showing distribution of vein and breccia phases with depth (refer to Figure 3.23 for geology).

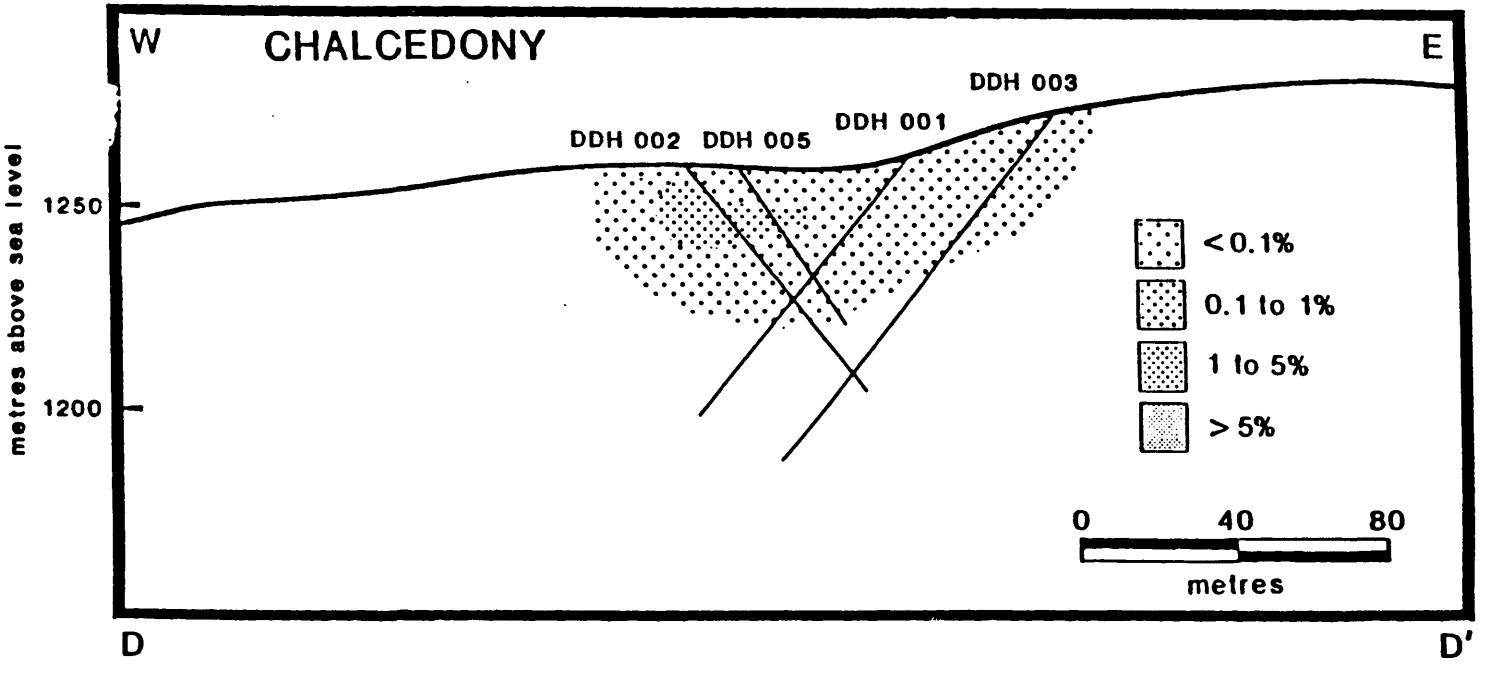

FIGURE 3.23: East-west vertical section (D-D':Fig. 3.1A) of the Wolf prospect showing distribution of vein and breccia phases with depth (refer to Figure 3.23 for geology).

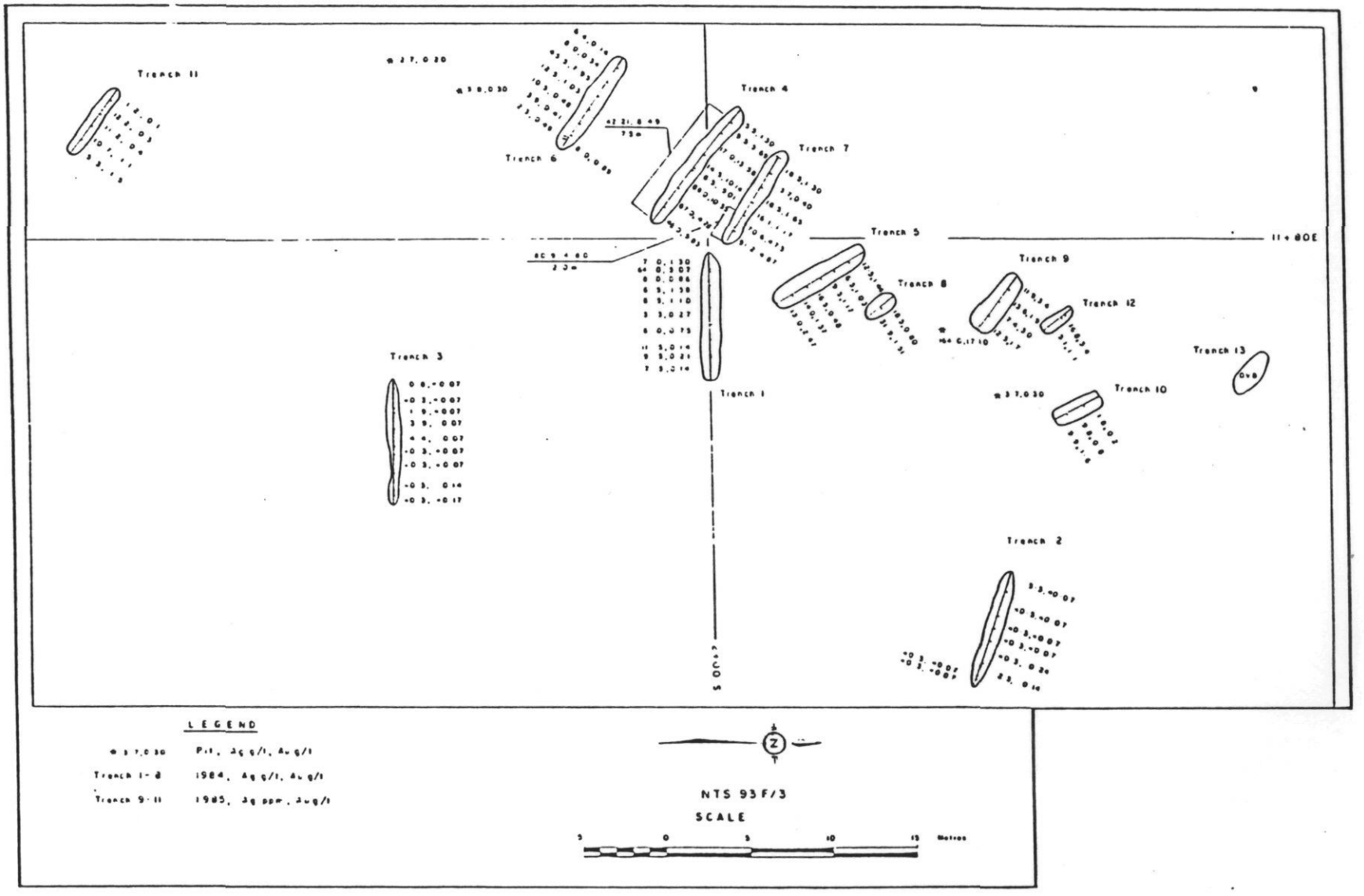

FIGURE 3.24: Trench map of the Ridge Zone (Figs. 3.18 showing distribution of gold and silver grades, Wolf prospect (from Holmgren and Cann, 1985). Refer to Figure 3.19 for distribution of vein and breccia textures.

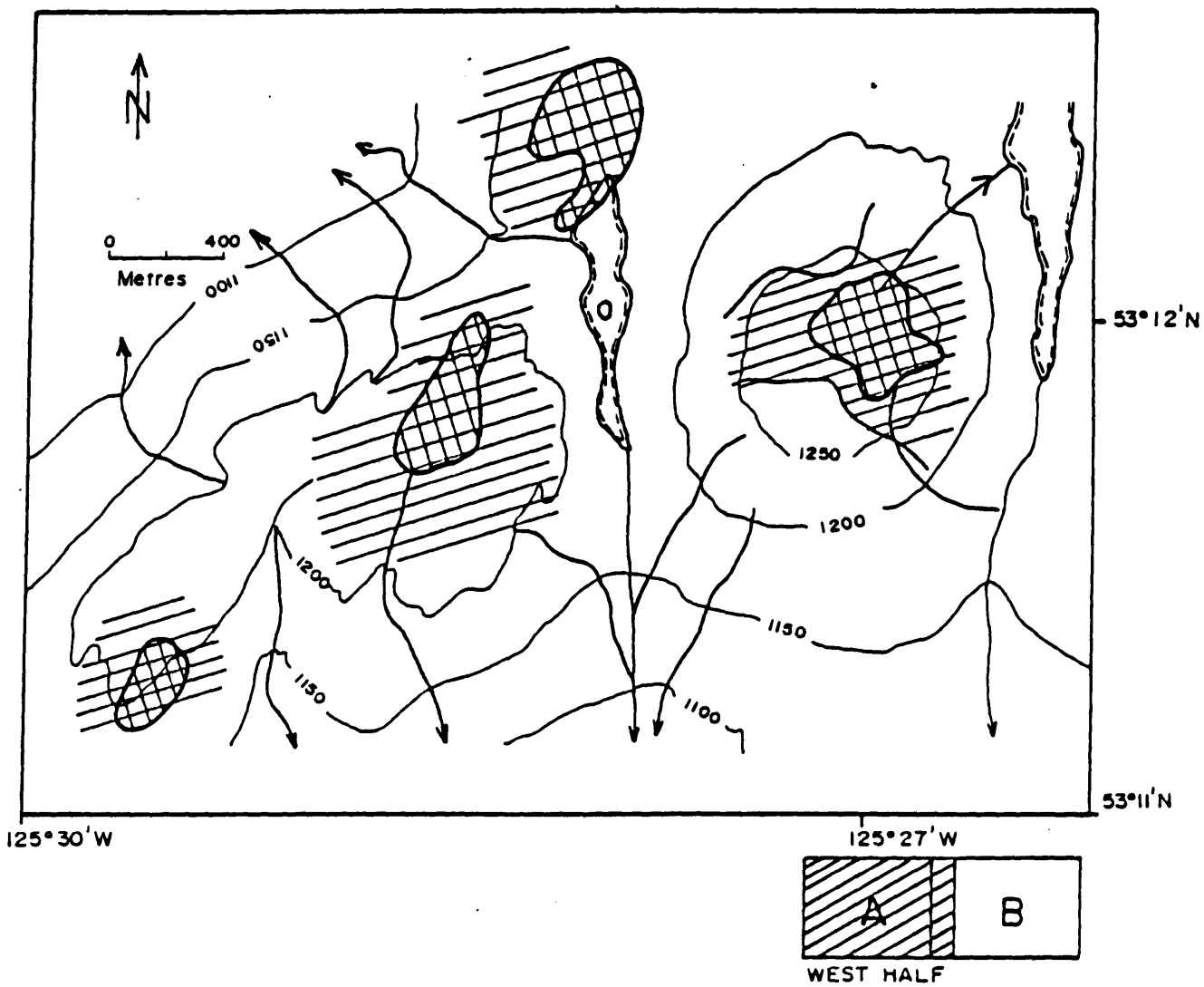

FIGURE 3.25: Qualititive alteration map of the Wolf prospect. Zone of high argillic alteration are indicated by hatched lines; advanced argillic alteration is indicated by crosshatching. A) west half, and B) east half.

3.5.2 CHARACTER OF VEINS AND BRECCIAS

Eight temporally and texturally distinct phases of vein and breccia deposition are recognised at Wolf. These phases are best displayed in trenches on the Ridge zone (Fig. 3.19). The relative timing of these hydrothermal events, modified from Cann (1984), is listed in Table 3.6.

Initiation of hydrothermal events at Wolf is marked by replacement of rhyolite fragments up to 1 cm in diameter in the rhyolite (Eo_7) with black chalcedony. Pervasive silicification of rhyolite accompanied the replacement of these fragments. Brecciation of the rhyolite (Eo_7) followed, perhaps as a result of resurgent doming of Eo_7. The newly opened cavities allowed growth of coarse-grained carbonate minerals which developed blades up to 3 cm long. Influx of silica replaced carbonate blades with translucent to white chalcedonic quartz and rimmed brecciated fragments. Patches of rhyolite (Eo_7) and crystal tuff (Eo_6) were then replaced by massive fine-grained white quartz. White colloform chalcedonic veinlets crosscut the earlier fabrics and were in turn crosscut by massive white quartz veins up to 2 m wide. Finally, clear, colourless, well-formed, drusy quartz infilled cavities containing replaced carbonate blades (Plate 3.12) and formed 1-2 mm veinlets with cockade texture. Heterolithic breccias with a black volcanic matrix (Eo_8) crosscut previous hydrothermal features.

The quartz-carbonate textures at Wolf are similar to those detailed by McDonald (1987) at Mt. Skukum, south-

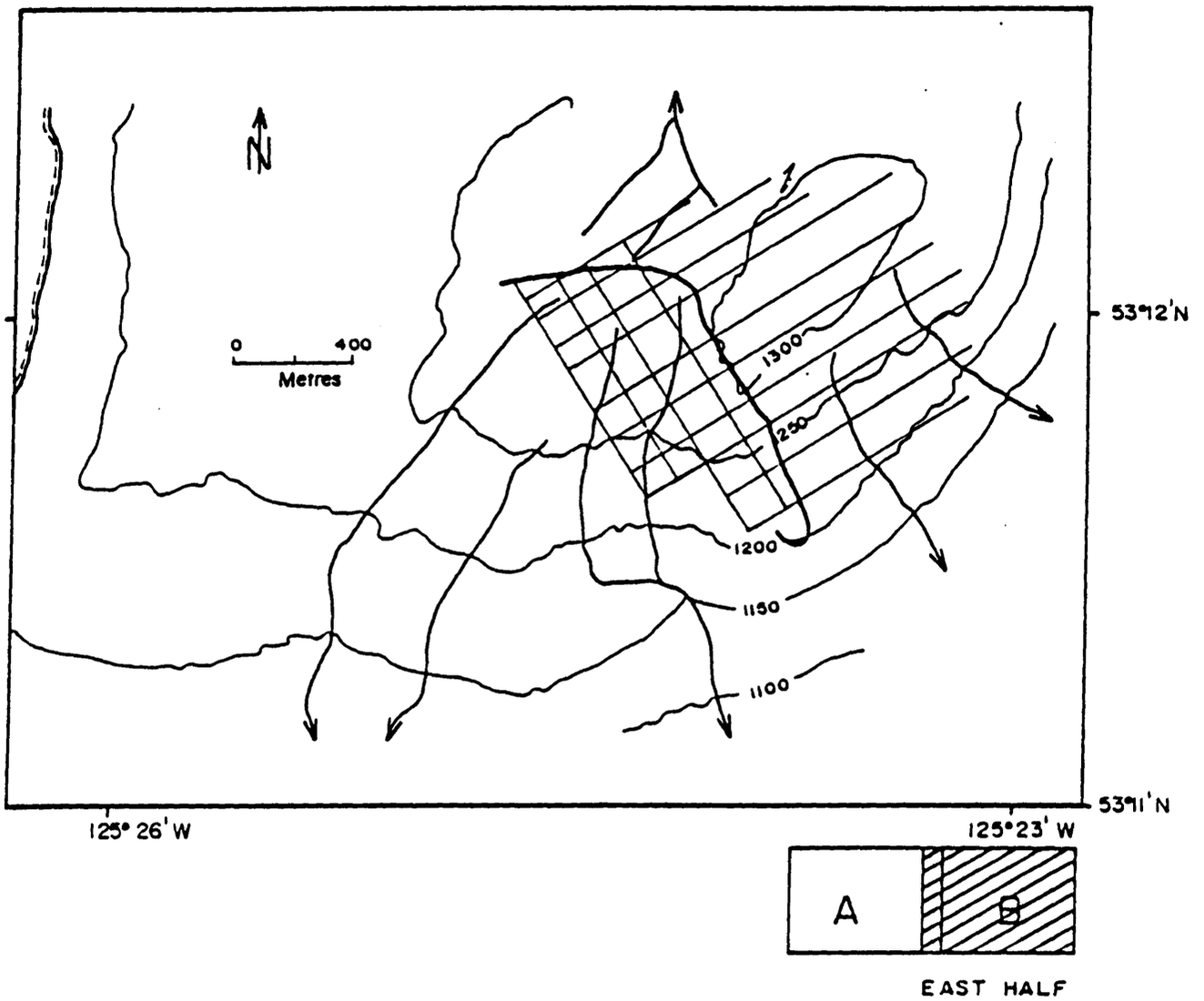

FIGURE 3.25: Qualititive alteration map of the Wolf prospect. Zone of high argillic alteration are indicated by hatched lines; advanced argillic alteration is indicated by crosshatching. A) west half, and B) east half.

TABLE 3.6: Estimated paragenetic sequence of hydrothermal events at the Wolf prospect, central British Columbia (modified from Cann, 1984).

	VEIN OR BRECCIA PHASE	HYDROTHERMAL EVENT
YOUNGEST	8	Black matrix pebble breccia
	7	Drusy quartz fills cavities, cockade quartz textured veinlets
	6	Massive, milky white quartz veins up to 2 m wide
	5	Chalcedonic veining and vein selvages
	4	Massive replacement of volcanic rock and calcite blades by fine-grained quartz
	3	Rimming of breccia fragments by chalcedony and fine-grained quartz
	2	Brecciation of volcanics and growth of carbonate blades in open cavities
OLDEST	1	Replacement of rhyolite fragments with black chalcedony

central Yukon Territory. At Wolf textures more clearly demonstrated that quartz crystal infilling between replaced carbonate blades is a later feature (Plate 3.12).

3.5.3 ORE PETROLOGY

Gold and silver mineralization is associated with: (1) the chalcedonic phase that commonly rims brecciated fragments (phase 3: Table 3.6), (2) the massive replacement of volcanics and the formation of bladed quartz-carbonate veins (phase 4, Table 3.6), and (3) the chaledonic veining and vein selvages (phase 5, Table 3.6). These relationships are inferred from microscopic studies and correlation of highest gold grades with textures. Ore minerals in veins are micron sized and commonly not observed megascopically. Results of scanning electron microscope (SEM) studies undertaken by Cann (1984) and the writer are outlined below.

Electrum (Au,Ag; Fig. 3.26) occurs as free grains from 5-10 u up to 30 u in diameter (Plate 3.13). It is also found as 2-3 u blebs in pyrite (Plate 3.14).

Native Silver (Ag) occurs as free grains varying from 3-9 u up to 20 u in length (Plate 3.15). It also occurs in electrum (see gold above).

Argentite (Ag_4SeS), **naummannite** (Ag_2Se) and/or **acanthite** (AgS_2) are probably present since peaks of Se and S were detected in energy dispersive electron microscope scans (Figs. 3.27).

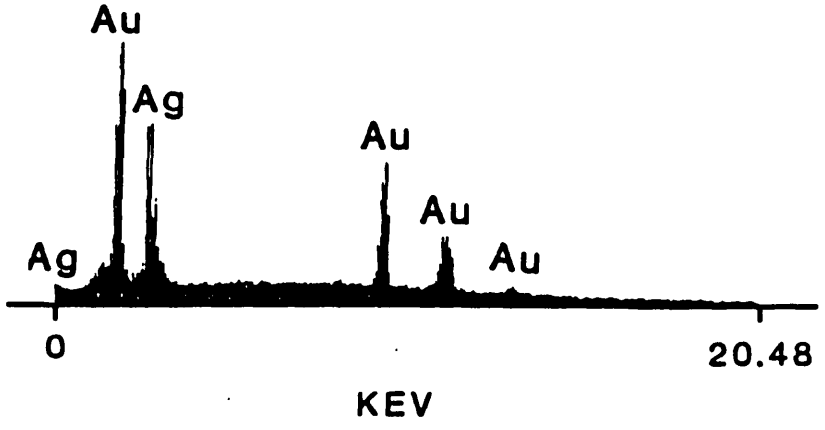

FIGURE 3.26: Scanning electron microscope energy dispersive peaks of electrum (Au, Ag) in quartz-carbonate veins of the Ridge zone (Figs. 3.18, 3.19 and 3.24), Wolf prospect.

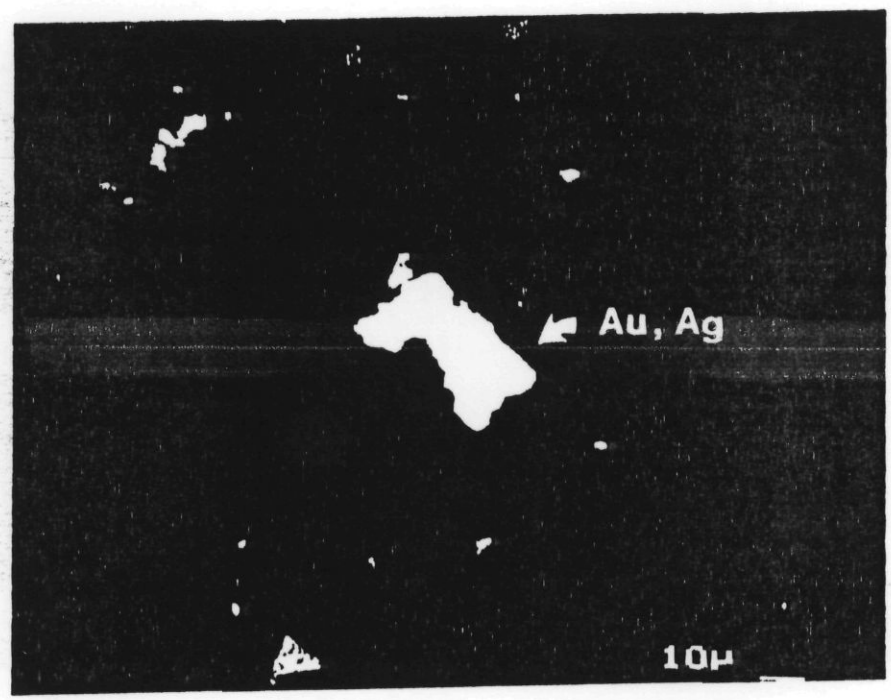

PLATE 3.13 Photomicrograph of electrum in a quartz-carbonate vein from the Ridge zone. Sample KATR9-1, Wolf prospect. Back-scattered electron image.

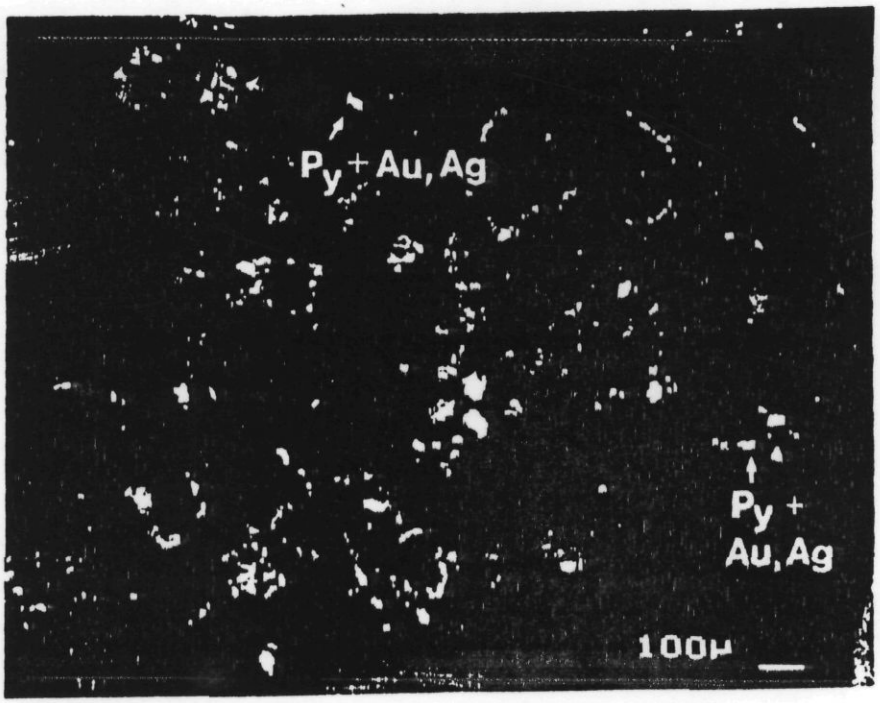

PLATE 3.14: Photomicrograph of electrum within pyrite cubes in a quartz-carbonate vein from the Ridge zone. Sample KATR9-1, Wolf prospect. Back-scattered electron image.

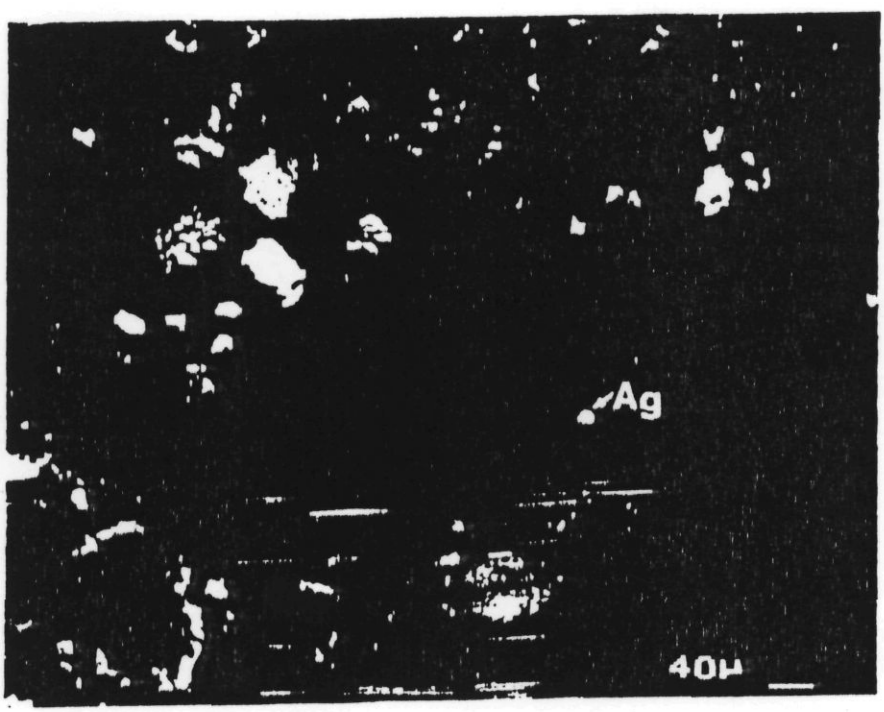

PLATE 3.15: Photomicrograph of native silver in a quartz-carbonate vein from the Ridge zone. Sample KATR9-1, Wolf prospect. Back-scattered electron image.

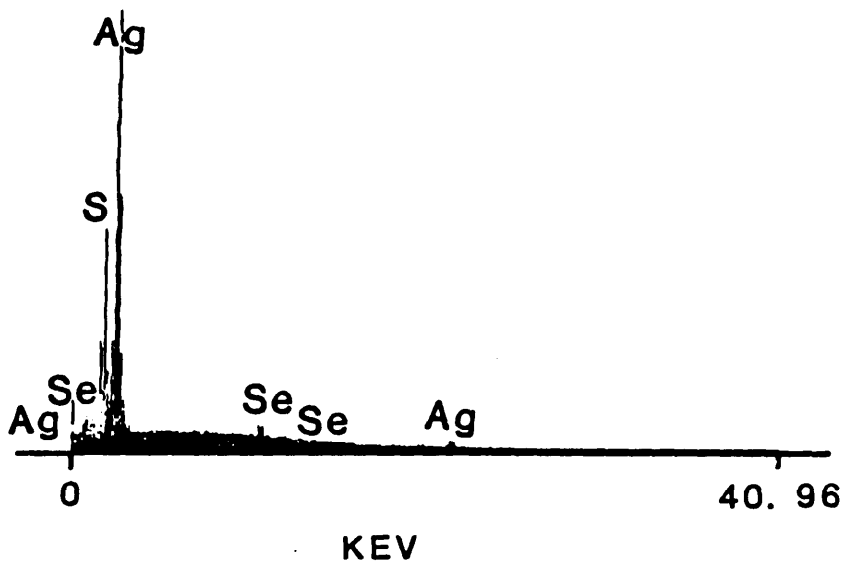

FIGURE 3.27: Scanning electron microscope energy dispersive peaks representing one or a combination of aguilarite (Ag_4SeS), naummannite (Ag_2Se), or acanthite (AgS_2) in quartz-carbonate veins of the Ridge zone (Figs. 3.18, 3.19 and 3.24), Wolf prospect.

Pyrite (Fe_2S) occurs as euhedral disseminations (up to 1 mm) in rhyolite (Eo_7) and rhyolite porphyry (Eo_9) on the Ridge and Pond zones. It contains grains of electrum up to 2 u in diameter.

Chalcopyrite (Cu_5FeS_2) occurs as rare disseminations (up to 1 mm across) in rhyolite (Eo_7) on the Ridge zone. Cubic grains of pyrite can be surrounded by irregular chalcopyrite grains with secondary rims of silver-rich **digenite** (Cu_9S_5; Cann, 1984).

Galena (PbS) has been detected in one sample as a discrete grain 5-10 u in diameter.

Argillic alteration has been quantitatively estimated (Fig. 3.25) for the Wolf property. Zones of high to intense clay alteration occur with mineralized zones outlined in section 3.5.1.

Qualitative X-ray diffraction patterns were used to define the alteration mineral assemblage at Wolf. Seven samples taken from drill core on the Ridge and Pond zones were analysed using standard techniques at The University of British Columbia. Minerals were identified (Table 3.7) based on diffraction chart peak height. Wallrock alteration bordering the silicified zones near veins is typically argillic or sericitic. Chlorite and K-feldspar were also detected adjacent to veins (Table 3.7).

3.5.4 METAL DISTRIBUTION

TABLE 3.7: Alteration minerals in rocks of the Ridge and Pond zones determined by X-ray diffraction analyses of representative specimens at the Wolf prospect, central British Columbia. Numbers in table indicate the relative abundance of the mineral; 1 = most abundant, 4 = least abundant. Sample locations are in Figure 3.5.

SAMPLE NUMBER	UNIT NUMBER	ALTERATION MINERAL[1]						
		OR	PL	MU	KA	MM	CL	IL
KA1-1	Eo_7	1	2			3		
KA2-1	Eo_7			2	1		3	
KA3-6	Eo_7		4		1		2	3
KA4-9	Eo_9				1		3	2
KA5-13	Eo_7				1		2	
KA6-12	Eo_9	1						
KA6-17	Eo_9			2	1		3	

1. Alteration mineral abbreviations: OR = orthoclase, PL = plagioclase, MU = muscovite, KA = kaolinite, MM = montmorillonite, CL = chlorite, IL = illite.

Metal distribution patterns were examined using elements commonly associated with epithermal deposits. These included 25 As, Ba, S and Sb values from the geochemical sample suite (Table 3.8A) as well as 373 Au and Ag values (Table 3.8B; Cann, 1984; Holmgren and Cann, 1985).

Data plotted on logarithmic probability paper (Fig. 3.28) were partitioned into respective populations using the procedure outlined by Sinclair (1976). The means and standard deviations for partitioned populations are in Table 3.9. Ba, S and Sb consist of mixtures of two lognormal distributions. Au, Ag and As represent single lognormal distributions. The Wolf property is characterized by gold to silver ratios of 1:20 based on the means of these populations.

3.5.5 DISCUSSION

The Wolf prospect is typified by precious metal mineralization hosted in zones of silicified rhyolite and rhyolite porphyry, quartz and rhyolite breccias, and quartz veins. Formation of open spaces by block faulting and doming acted as conduits, and focused hydrothermal fluid deposition. At least eight distinct phases of veining and brecciation are recognised (Table 3.6). Association of breccia textures, vuggy vein textures, chalcedony and mineralization implies that vein emplacement was explosive and at shallow levels. Evidence for boiling of hydrothermal fluids is documented at Wolf by study of fluid inclusions in

P. 86 is Table 3.5
P. 54A now

87

TABLE 3.8a: Trace element chemistry of As, Ba, S and Sb from rocks of the Wolf property sample suite[1].

SAMPLE NUMBER	ELEMENT As ppm	Ba ppm	S ppm	Sb ppm
KA009	26	50	92	2
KA029	12	47	67	2
KA066	11	261	68	1
KA067	15	588	163	4
KA077	20	24	69	1
KA078	10	25	51	2
KA087	15	79	144	2
KA090	14	500	66	3
KA104	32	68	72	4
KA106	11	163	98	3
KA108	6	974	74	2
KA112	43	42	89	6
KA128	55	463	150	0
KA133	10	155	77	3
KA135	47	263	153	0
KA141	42	46	79	8
KA163	7	30	48	2
KA178	2	321	125	2
KA184	10	55	73	3
KA195	4	462	114	2
KA200	11	156	94	1
KA220	21	63	86	7
KA221	14	32	58	12
KADDH3-6	48	12	114	4
KADDH4-7	23	182	83	4

1. Analyses were obtained from Midland Earth Science Associates, Nottingham, U.K.

TABLE 3.8b: Trace element chemistry of Ag and Au from rocks of the Wolf prospect, central British Columbia (from Holmgren and Cann, 1985). Silver analyses are in parts per million; gold analyses in parts per billion.

SAMPLE NUMBER	SOURCE 1	Ag (ppm)	Au (ppb)
G-1302	ACME	0.7	10
G-1303	ACME	0.4	25
G-1304	ACME	0.4	5
G-1305	ACME	18.3	2630
G-1306	ACME	0.2	30
G-1307	ACME	0.7	75
G-1308	ACME	4.3	250
G-1309	ACME	3.8	475
G-1310	ACME	0.8	50
G-1311	ACME	0.5	40
G-1312	ACME	0.9	130
G-1313	ACME	0.5	40
G-1314	ACME	0.7	25
G-1315	ACME	0.4	25
G-1316	ACME	0.9	5
G-1317	ACME	0.3	5
G-1318	ACME	0.1	5
G-1319	ACME	6.2	1510
G-1320	ACME	54.7	7100
G-1321	ACME	63.7	5840
G-1322	ACME	7.1	430
G-1323	ACME	0.4	25
G-1324	ACME	0.4	5
G-1325	ACME	0.2	15
G-1326	ACME	0.2	5
G-1327	ACME	1.2	25
G-1328	ACME	0.9	40
G-1331	ACME	0.3	55
G-1332	ACME	0.3	65
G-1333	ACME	1.3	165
G-1334	ACME	4.4	210
G-1335	ACME	0.2	5
G-1329	ACME	0.2	5
G-1330	ACME	0.1	5
G-1336	ACME	0.5	20
G-1337	ACME	0.1	5
G-1338	ACME	0.6	15
G-1339	ACME	0.1	20
G-1340	ACME	0.1	5
G-1341	ACME	0.6	125
G-1342	ACME	1.1	10
G-1343	ACME	0.4	25
G-1344	ACME	5.9	430
G-1345	ACME	0.5	15
G-1346	ACME	0.3	20

TABLE 3.8b: (continued p2.)

		Ag ppm	Au ppb
G-1347	ACME	0.5	20
G-1348	ACME	0.2	5
G-1349	ACME	0.8	25
G-1350	ACME	0.1	20
G-1351	ACME	0.1	5
G-1352	ACME	0.1	30
G-1353	ACME	0.1	5
G-1354	ACME	0.1	5
G-1355	ACME	0.2	5
G-1356	ACME	4.1	330
G-1357	ACME	1.4	85
G-1358	ACME	2.4	70
G-1359	ACME	1.2	130
G-1360	ACME	0.4	25
G-1361	ACME	0.1	40
G-1362	ACME	0.1	15
G-1363	ACME	0.2	20
G-1364	ACME	0.8	105
G-1365	ACME	0.4	50
G-1366	ACME	1.1	60
G-1367	ACME	0.1	10
G-1368	ACME	0.1	5
G-1369	ACME	0.1	35
G-1370	ACME	0.1	25
G-1371	ACME	0.7	50
G-1372	ACME	0.1	5
G-1373	ACME	0.4	5
G-1374	ACME	0.3	10
G-1375	ACME	0.6	60
G-1376	ACME	1.5	155
G-1377	ACME	1.8	140
G-1378	ACME	0.6	100
G-1379	ACME	1.2	95
G-1380	ACME	0.8	20
G-1381	ACME	1.6	245
G-1382	ACME	0.5	5
G-1383	ACME	0.5	25
G-1384	ACME	1.6	95
G-1385	ACME	1.1	55
G-1386	ACME	1.7	60
G-1387	ACME	0.6	65
G-1388	ACME	0.3	30
G-1389	ACME	2	160
G-1390	ACME	3.3	415
G-1391	ACME	4.7	620
G-1392	ACME	12.6	985
G-1393	ACME	1.7	280
G-1394	ACME	1.2	125
G-1395	ACME	0.8	70
G-1396	ACME	0.2	15
G-1397	ACME	9.7	565
G-1398	ACME	1.3	25
G-1399	ACME	0.4	20

TABLE 3.8b: (continued p3.)

		Ag ppm	Au ppb
G-1400	ACME	2	10
G-1451	ACME	1.6	585
G-1452	ACME	0.7	60
G-1453	ACME	1.1	25
G-1454	ACME	1.8	70
G-1455	ACME	0.6	55
G-1456	ACME	0.6	5
G-1457	ACME	0.4	20
G-1458	ACME	0.3	40
G-1459	ACME	0.2	5
G-1460	ACME	0.9	5
G-1461	ACME	0.3	5
G-1462	ACME	0.5	5
G-1463	ACME	0.4	5
G-1464	ACME	0.7	5
G-1465	ACME	0.8	165
G-1466	ACME	2.2	5
G-1467	ACME	0.4	5
G-1468	ACME	0.3	5
G-1469	ACME	0.2	10
G-1470	ACME	0.1	5
G-1471	ACME	0.2	5
G-1472	ACME	0.3	5
G-1473	ACME	0.1	5
G-1474	ACME	0.1	5
G-1475	ACME	0.2	5
G-1476	ACME	0.2	5
G-1477	ACME	0.1	5
G-1478	ACME	0.1	5
G-1479	ACME	0.1	5
G-1480	ACME	0.1	5
G-1481	ACME	0.2	5
G-1482	ACME	0.1	5
G-1483	ACME	0.3	5
G-2601	ACME	0.5	65
G-2602	ACME	1.7	250
G-2603	ACME	0.2	18
G-2604	ACME	0.2	20
G-2605	ACME	0.6	34
G-3606	ACME	0.1	5
G-2607	ACME	0.3	3
G-2608	ACME	0.4	7
G-2609	ACME	0.2	4
G-2610	ACME	0.2	8
G-2611	ACME	0.2	3
G-2612	ACME	2.7	20
G-1613	ACME	0.1	2
G-2614	ACME	0.1	3
G-2615	ACME	0.3	43
G-2616	ACME	0.3	27
G-2617	ACME	0.1	4
G-2618	ACME	2	140
G-2619	ACME	1.2	28

TABLE 3.8b: (continued p4.)

		Ag ppm	Au ppb
G-2520	ACME	1	17
G-2621	ACME	0.9	11
G-2622	ACME	0.6	9
G-2623	ACME	0.8	45
G-2624	ACME	1	47
G-2625	ACME	0.5	39
G-2626	ACME	0.1	40
G-2627	ACME	0.7	17
G-2628	ACME	3.2	51
G-2629	ACME	2.3	22
G-2630	ACME	1.5	23
G-2631	ACME	0.9	29
G-2632	ACME	0.5	25
G-2633	ACME	1.1	1
G-2634	ACME	0.8	15
G-2635	ACME	2.6	14
G-2636	ACME	2.2	32
G-2637	ACME	7.4	2
G-2638	ACME	2.1	4
G-2639	ACME	3.5	14
G-2640	ACME	3	12
G-2641	ACME	1.4	12
G-2642	ACME	0.4	35
G-2643	ACME	0.6	26
G-2644	ACME	0.1	24
G-2645	ACME	0.1	10
G-2646	ACME	0.1	16
G-2647	ACME	0.9	15
G-2648	ACME	0.3	23
G-2649	ACME	0.3	7
G-2650	ACME	1.5	35
G-2651	ACME	12.2	170
G-2652	ACME	1	27
G-2653	ACME	0.2	19
G-2654	ACME	0.3	14
G-2655	ACME	1.3	26
G-2656	ACME	0.4	39
G-2657	ACME	0.3	42
G-2658	ACME	0.8	40
G-2659	ACME	0.5	29
G-2660	ACME	0.2	10
G-2661	ACME	0.5	9
G-2662	ACME	0.4	9
G-2663	ACME	0.4	12
G-2664	ACME	0.2	17
G-2665	ACME	0.3	25
G-2666	ACME	0.3	11
G-2667	ACME	0.3	13
G-2668	ACME	0.5	22
G-2669	ACME	0.6	14
G-2670	ACME	0.4	36
G-2671	ACME	0.6	17
G-2672	ACME	0.5	18

Ag ppm Au ppb

TABLE 3.8b: (continued p5.)

G-2673	ACME	0.2	2
G-2674	ACME	0.3	25
G-2675	ACME	0.3	7
G-2676	ACME	0.2	4
G-2677	ACME	10.3	340
G-2678	ACME	0.2	28
G-2679	ACME	0.4	65
G-2680	ACME	0.6	42
G-2681	ACME	0.8	4
G-2682	ACME	0.6	5
G-2683	ACME	0.7	36
G-2684	ACME	0.3	16
G-2685	ACME	0.6	85
G-2686	ACME	0.4	44
G-2687	ACME	1	38
G-2688	ACME	0.7	42
G-2689	ACME	0.3	9
G-2690	ACME	0.6	44
G-2691	ACME	0.4	455
G-2692	ACME	0.4	59
G-2693	ACME	20.5	2100
G-2694	ACME	0.4	19
G-2695	ACME	0.3	59
G-2696	ACME	1	85
G-2697	ACME	0.3	40
G-2698	ACME	0.2	32
G-2699	CDN	1.3	5
G-2700	CDN	1.4	15
G-2701	CDN	0.4	40
G-2702	CDN	1.4	35
G-2703	CDN	0.1	25
G-2704	CDN	0.1	60
G-2705	CDN	1.5	170
G-2706	CDN	0.4	185
G-2707	CDN	1.3	170
G-2708	CDN	0.1	30
G-2709	CDN	3.4	330
G-2710	CDN	3.7	210
G-2711	CDN	1.4	75
G-2712	CDN	1.2	140
G-2713	CDN	1.3	90
G-1679	ACME	0.7	230
G-1680	ACME	1.8	290
G-1681	ACME	0.9	135
G-1682	ACME	0.9	190
G-1683	ACME	1.1	280
G-1684	ACME	2.1	190
G-2714	ACME	1	105
G-2715	ACME	0.9	210
G-2716	ACME	1.3	110
G-2717	ACME	1.5	225
G-2718	ACME	15.1	1800
G-2719	ACME	3.4	610

TABLE 3.8b: (continued p6.) Ag ppm Au ppb

G-2720	ACME	1.6	250
G-2721	ACME	3.2	360
G-2722	ACME	3.7	470
G-2723	ACME	6.1	940
G-2724	ACME	6.7	680
G-2725	ACME	2.7	480
G-2726	ACME	0.3	35
G-2727	ACME	1.3	265
G-2728	ACME	2.5	320
G-2729	ACME	11.5	1800
G-2730	ACME	2.2	850
G-2731	ACME	1.4	230
G-2732	ACME	2.3	225
G-2733	ACME	2.1	235
G-2734	ACME	1.6	40
G-2735	ACME	0.4	30
G-2736	ACME	3.2	330
G-2737	ACME	3.8	410
G-2738	ACME	1.7	240
G-2739	ACME	4.5	985
G-2740	ACME	6	1550
G-2741	ACME	4.7	200
G-2742	ACME	1.3	90
G-2743	ACME	0.4	16
G-2744	ACME	2.2	75
G-2745	ACME	12.2	780
G-2746	ACME	6.1	310
G-2747	ACME	2	310
G-2748	ACME	1.6	165
G-2749	ACME	1.5	250
G-2750	ACME	1.4	265
G-2765	ACME	0.7	5
G-2766	ACME	1.2	10
G-2767	ACME	0.2	2
G-2768	ACME	0.2	5
G-2769	ACME	0.1	2
G-2770	ACME	0.4	3
G-2771	ACME	0.4	2
G-2772	ACME	0.1	5
G-2773	ACME	0.7	2
G-2774	ACME	0.2	1
G-2775	ACME	0.1	1
G-2776	ACME	0.6	2
G-2777	ACME	0.3	1
G-2778	ACME	0.1	1
G-2779	ACME	0.3	2
G-2780	ACME	0.1	1
G-2781	ACME	0.4	2
G-2782	ACME	2.5	7
G-2783	ACME	0.2	2
G-2784	ACME	0.2	3
G-2785	ACME	1	2
G-2786	ACME	0.2	1

TABLE 3.8b: (continued p7.) Ag ppm Au ppb

G-2787	ACME	0.1	1
G-2788	ACME	0.2	1
G-2789	ACME	0.1	2
G-2790	ACME	0.1	4
G-2791	ACME	0.2	1
G-2792	ACME	0.1	1
G-2793	ACME	0.3	11
G-2794	ACME	0.1	2
G-2795	ACME	0.1	1
G-2796	ACME	0.1	1
G-2797	ACME	0.1	1
G-2798	ACME	0.1	4
G-2799	ACME	1.1	9
G-2800	ACME	0.1	1
G-3301	ACME	2.3	450
G-3302	ACME	2.5	730
G-3303	ACME	0.2	9
G-3304	ACME	4.9	430
G-3305	ACME	38.6	2200
G-3306	ACME	1.8	270
G-3307	ACME	2.2	300
G-3308	ACME	6	250
G-3309	ACME	5.9	500
G-3310	ACME	6.7	290
G-3311	ACME	8.4	510
G-3312	ACME	3.6	980
G-3313	ACME	12.5	2000
G-3314	ACME	11.5	2100
G-3315	ACME	1.1	150
G-3316	ACME	5.6	930
G-3317	ACME	0.6	90
G-3318	ACME	3.4	750
G-3319	ACME	0.9	155
G-3320	ACME	1.2	310
G-3321	ACME	0.5	115
G-3322	ACME	0.6	90
G-3323	ACME	3.3	1600
G-3324	ACME	2.9	460
G-3325	ACME	1.2	100
G-3326	ACME	12	800
G-3327	ACME	1.8	75
G-3328	ACME	2.3	410
G-3329	ACME	7.7	700
G-3330	ACME	1.6	100
G-3331	ACME	5.9	290
G-3332	ACME	36.7	1300
G-3333	ACME	2.7	180
G-3334	ACME	0.8	90
G-3335	ACME	1.2	100
G-1685	ACME	1.5	155
G-1686	ACME	1	210
G-1687	ACME	1.2	135

TABLE 3.8b: (continued p8.)

TABLE 3.8b: (continued p8.) Ag ppm Au ppb

G-1688	ACME	0.3	80
G-1689	ACME	0.2	65
G-1690	ACME	0.1	75
G-1691	ACME	0.1	7
G-1692	ACME	0.1	8
G-1693	ACME	0.6	90
G-1694	ACME	1.3	110
G-1695	ACME	0.3	125
G-1696	ACME	1	24
G-1697	ACME	0.3	130

I. Geochemical ICP analyses were obtained from Acme Analytical Laboratories, Vancouver, and CDN Resource Laboratories Ltd., Delta, B.C. Samples were digested with 3 ml 3-1-2 HCl-HNO3-H2O at 95 degrees for one hour and dilited to 10 ml with water.

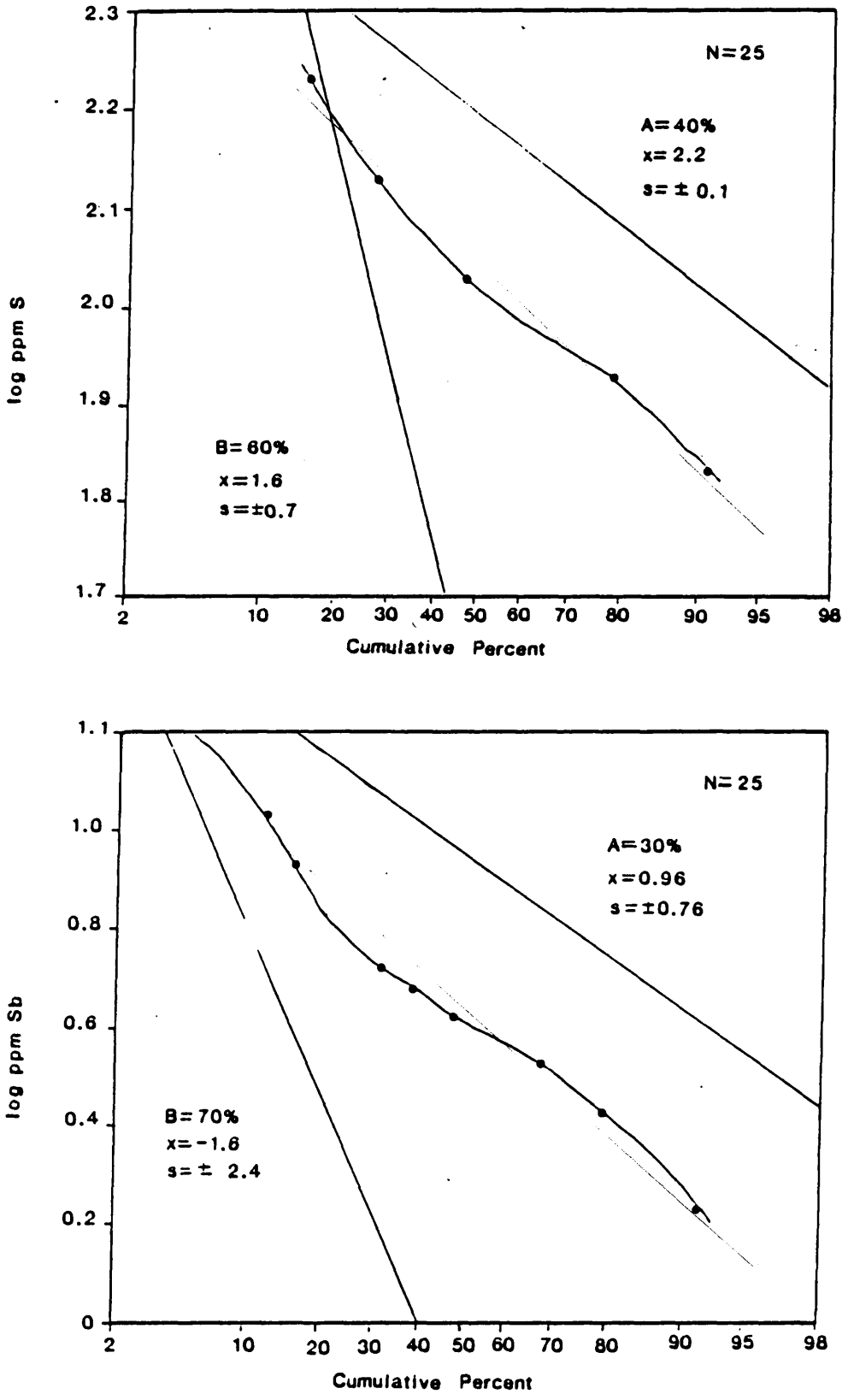

FIGURE 3.28: Logarithmic probability plots illustrating distribution of: A = Au, B = Ag, C = S, D = Sb, E = B from the Wolf prospect. Means and standard deviations are in Table 3.9.

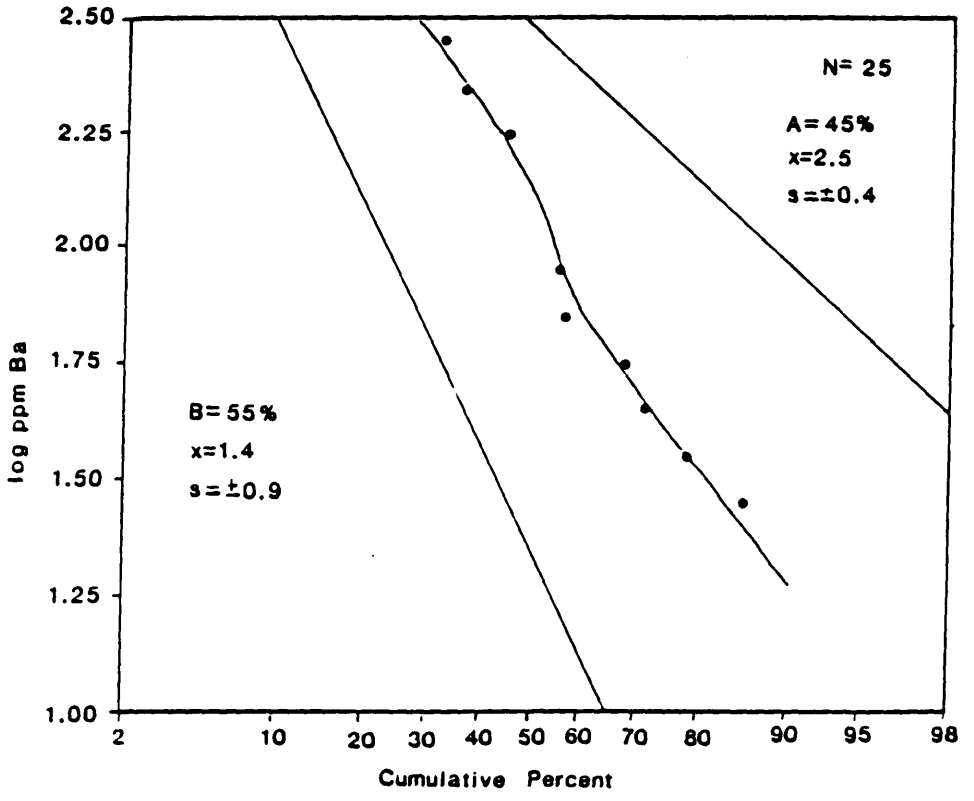

FIGURE 3.28: Logarithmic probability plots illustrating distribution of: A = Au, B = Ag, C = S, D = Sb, E = B from the Wolf prospect. Means and standard deviations are in Table 3.9.

TABLE 3.9: Means and standard deviations determined graphically for partitioned metal values at the Wolf prospect, central British Columbia.

ELEMENT	UNITS	POPULATION	%[1]	b[2]	b+s[3]	b-s[4]
Au	ppb	A	100	31.6	251	4.47
Ag	ppm	A	100	0.63	2.82	0.13
As	ppm	A	100	16.6	35.5	7.59
Ba	ppm	A	45	300	750	126
	ppm	B	55	23.7	178	3.2
S	ppm	A	40	158	214	115
	ppm	B	60	42	200	8.9
Sb	ppm	A	30	9.1	15.1	5.25
	ppm	B	70	0.7	40	0.13

1. % of data in population
2. antilog of mean of lognormal population
3. antilog of mean plus one standard deviation of lognormal population
4. antilog of mean plus one standard deviation of lognormal population

quartz veins and breccias (section 3.6). Boiling releases volatiles such as CO_2, H_2S and H_2O promoting silica saturation (Fournier, 1985) and argillic alteration in the wallrock adjacent to silicified zones. Abundant chalcedony implies that hydrothermal fluids were silica saturated. Rapid precipitation of gold from silica saturated hydrothermal fluids has been related to boiling in several epithermal deposits (Barnes, 1979; Henley and Brown, 1985).

Native silver and electrum of micron size are associated with pyrite and silver sulphosalts in silicified zones. Probability graphs indicate that the partititioning of Au and Ag into a single population contrasts with partitioning of other elements. It should be noted that Au and Ag analyses are from a large population (N = 373) whereas As, Ba, S and Sb are from a small one (N = 25). The difference in partitioning of the Au and Ag, compared to Ba, Sb and S could be related to contrasting population size and/or sampling of different populations. If a difference in number of populations exists, Ba, S and Sb could represent background values in the Ootsa Lake Group as well as anomalous values related to mineralization at Wolf. Background gold and silver values in the Ootsa Lake Group on the Whitesail Lake sheet are markedly low (Diakow, oral comm., 1988). The Au and Ag values at Wolf are from samples in known areas of mineralization and probably represent anomalous populations related to hydrothermal processes rather than background populations. Because As does not

correlate with the other elements, it might not be a reliable geochemical pathfinder at Wolf.

Geologic setting, vein and breccia textures, alteration and metal distribution patterns at Wolf resemble those of a low sulphur hot-spring or silicified stockwork deposit (Berger and Eimon, 1983; Silverman and Berger, 1985). Examples of this type of a deposit include Round Mountain, Nevada; Borealis, Nevada; and McLaughlin, California.

3.6. HYDROTHERMAL ENVIRONMENT OF DEPOSITION

Fluid inclusion and oxygen isotope studies examine some features of the hydrothermal environment of deposition at Wolf. Specifically, these studies constrain: (1) the temperature and salinity of the depositional fluid, (2) the oxygen and hydrogen isotopic composition and source of the hydrothermal fluid, (3) the depth of mineral emplacement, (4) the water to rock ratio in the hydrothermal system, and (5) the fluid evolution of the system with time. Defining the hydrothermal environment of deposition at Wolf allows comparison to similar deposits hosted in Eocene volcanic rocks in British Columbia, as well as to world-class deposits.

3.6.1. FLUID INCLUSION STUDY

The fluid inclusion study of 17 vein and breccia samples from five zones on the Wolf property allows estimates of: (1) the temperature of deposition of

hydrothermal fluids, (2) the salinity of the hydrothermal fluids, (3) the composition of vapour or solid phases present, (4) the significance of boiling as a precipitation mechanism in the hydrothermal system, and (5) the depth of mineral emplacement. Samples mainly taken from drill core on the Ridge and Pond zones and from the Lookout, Chopper Pad and East zones allow representation of ore fluids over a significant vertical and lateral extent. Sample locations are plotted in Figures 3.29 and 3.30, detailed descriptions of samples are in Table 3.10.

3.6.1.1. Sample preparation and analysis

Seventeen doubly polished thin sections were prepared closely following the procedure outlined by Holland et al. (1978). Sections were cut 50 to 100 um thick and polished with tin oxide. Of the original 17 samples, usable inclusions were available in only eight sections. The remaining sections were choked with minute inclusions (< 2 um across) which could not be adequately resolved at 1250x magnification with the petrographic microscope.

Fluid inclusion analysis was carried out using a Chiaxmeca heating/freezing stage. A total of 41 fluid inclusions were analysed (Table 3.11). Measurements were corrected using calibration curves from McDonald (1987). These curves demonstrate an accuracy of measurement to within 6.7°C with a precision of 0.6°C (1σ) for the temperature range -100°C to +40°C, and to within 5.3°C with

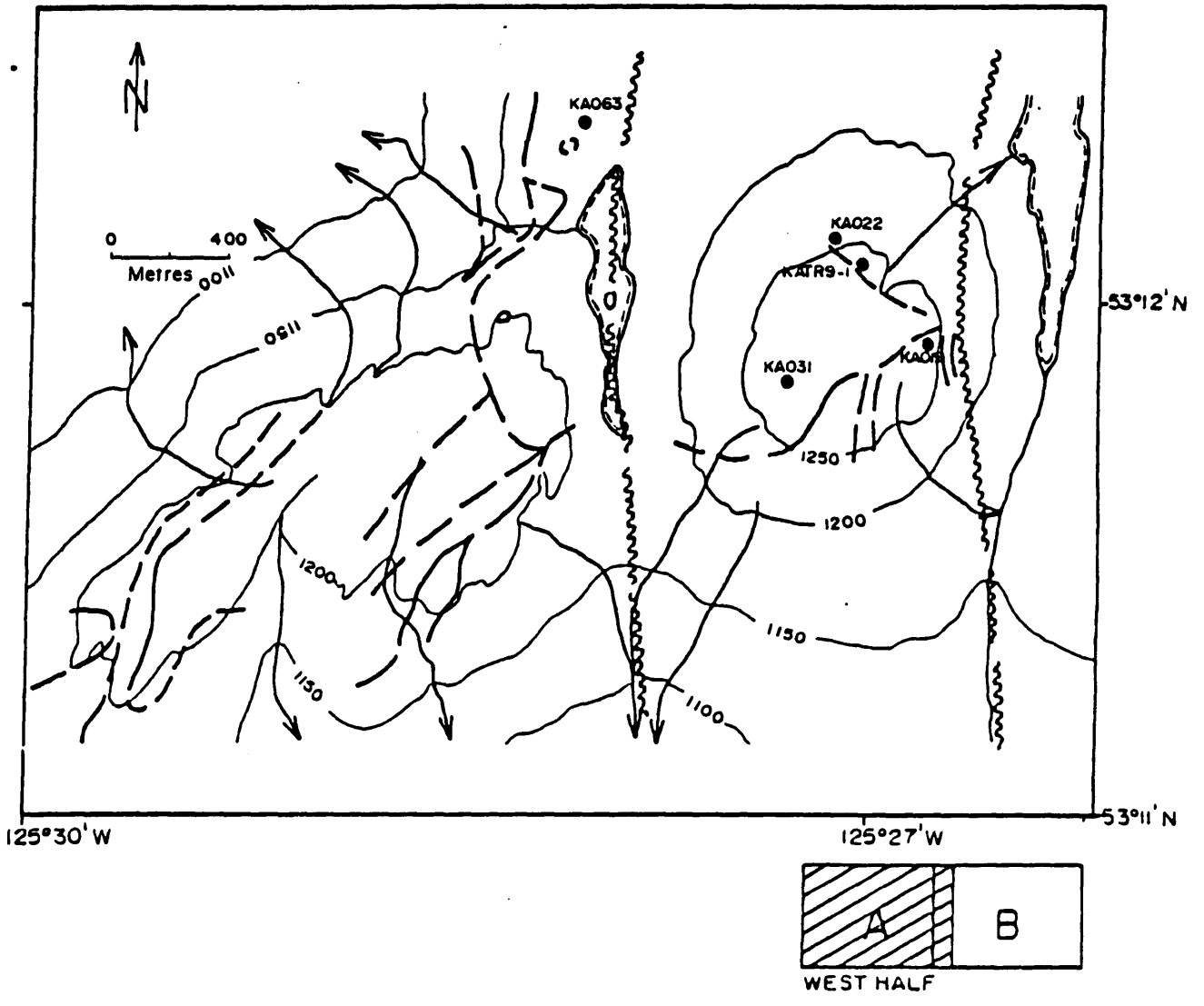

FIGURE 3.29: Sample locations of surface veins used for fluid inclusion analyses from the Wolf prospect. A) west half, and B) east half. Sample descriptions are in Table 3.10.

TABLE 3.10: Descriptions of vein samples used for fluid inclusion analyses at the Wolf property, central British Columbia. Samples are located in Figures 3.29 and 3.30.

ZONE	SAMPLE NUMBER	VEIN TYPE	HOST ROCK	SAMPLE DESCRIPTION
RIDGE	KATR9-1	BLADED	RHYOLITE	Densely bladed quartz-carbonate vein (blades up to 2 cm long
RIDGE	KA1-1	BLADED	RHYOLITE	Myriad of densely bladed quartz-carbonate veins (blades up to 5 mm long)
RIDGE	KA1-2	BLADED	RHYOLITE	Densely bladed quartz-carbonate veinlet (1 cm wide, blades up to 0.5 cm long)
RIDGE	KA2-2	BRECCIA INFILLS	RHYOLITE	Heterolithic breccia fragments rimmed by fine-grained, translucent quartz
RIDGE	KA3-4	BRECCIA INFILLS	RHYOLITE	Clear, colourless, fine-grained quartz rims on rhyolite breccia fragments
RIDGE	KA5-5	COCKADE	RHYOLITE	Quartz veinlet up to 2 mm wide rims rhyolite breccia fragments
RIDGE	KA022	MASSIVE REPLACE-MENT	CRYSTAL	Replacement of host crystal tuff by fine silica with relict shadows of former minerals remaining
POND	KA4-8	BLADED	RHYOLITE PORPHYRY	Bladed quartz-carbonate, rimming of host rock by quartz and drusy quartz cavities
POND	KA4-15	CHALC-EDONIC BANDING	RHYOLITE PORPHYRY	Banded chalcedonic veins sealed by milky white sucrosic quartz

TABLE 3.10: (continued)

POND	KA4-19	QUARTZ	RHYOLITE	Repeated infilling and sealing of veinlet by fine-grained quartz and chalcedony.
POND	KA6-2	COCKADE QUARTZ VEIN	RHYOLITE PORPHYRY	Comb quartz, quartz infilling, chalcedonic banding and rimming of vein walls by quartz.
POND	KA6-6	BLADED	RHYOLITE PORPHYRY	Bladed quartz-carbonate crosscut by 2mm veinlets of drusy quartz.
POND	KA6-14	BLADED	RHYOLITE PORPHYRY	Densely bladed quartz-carbonate veinlet (blades up to 0.5 cm long).
POND	KA019	QUARTZ VEIN	CRYSTAL TUFF	Sample from large massive, milky-white quartz vein.
LOOKOUT	KA031	BLADED	CRYSTAL TUFF	Bladed quartz-carbonate within broad patch of milky white vein quartz.
CHOPPER PAD	KA063	BRECCIA INFILLS	RHYOLITE	Infilling around rhyolite breccia by clear, translucent fine-grained quartz
EAST	KA188	DRUSY	RHYOLITE PORPHYRY	Drusy quartz fills open cavities and lines fractures.

TABLE 3.11: Petrographic, homogenization and freezing data for fluid inclusions from quartz veins at the Wolf prospect, central British Columbia. Sample locations are in Figure 3.30 and 3.31.

ZONE	SAMPLE NUMBER	ELEV (m)	VEIN[1] TYPE	INCLUSION[2] TYPE	INCLUSION[2] SIZE	INCLUSION[2] BS	INCLUSION[2] V%	TEMPERATURE[3] HOMG.	TEMPERATURE[3] EUT.	TEMPERATURE[3] LAST
RIDGE	KATR9-1	1250	BL	S	24.6 16.4	5	5	176		
				PS	16.4 16.4	5	10	288		
				PS	16.4 16.4	5	10	289		
				P	24.6 16.4	5	5	270		
				S	10.9 8.2	5	5	191		
				S	10.9 8.2	5	5	183		
				S	8.2 5.5	3	10	180		
				P	81.9 27.3	10	15	265	-28	-2
				PS	24.6 16.4	5	10	267		
RIDGE	KA3-4	1265	BR	P	16.4 16.4	10	5	250		
				S	24.6 16.4	10	5	100		
				PS	24.6 16.4	10	10	285		
RIDGE	KA022	1240	MR	PS	13.7 8.2	5	40	145		
				PS	13.7 8.2	5	30	145		
POND	KA4-8	1247	BL	P	41.0 32.8	10	2	265		
				S	65.5 41.0	10	2	82		
				P	16.4 16.4	5	10	183		

1. VEIN TYPE: BL = bladed, BR = breccia infilling, MR = massive replacement, CQ = cockade quartz veinlet, DQ = drusy quartz veinlet.
2. INCLUSION TYPE: P = primary, PS = pseudosecondary, S = secondary.
   INCLUSION SIZE: maximum by minimum; in microns.
   INCLUSION BS: BS = bubble size; in microns.
   INCLUSION V%: V% = volume percent (Vl/Vl + Vv)
3. TEMPERATURE HOMG. = homogenization temperature; ^{o}C
   TEMPERATURE EUT. = eutectic temperature; ^{o}C
   TEMPERATURE LAST = last melting temperature; ^{o}C

TABLE 3.11: (continued p2.)

ZONE	SAMPLE NUMBER	ELEV (m)	VEIN[1] TYPE	INCLUSION[2] TYPE	SIZE	BS	V%	TEMPERATURE[3] HOMG.	EUT.	LAST
POND	KA4-15	1235	BL	P	16.4 16.4	5	20	155		
				PS	16.4 16.4	5	5			
				PS	24.6 16.4	5	10	145		
POND	KA6-6	1245	BL	S	54.6 16.4	10	5	181		
				S	16.4 16.4	5	10	137		
				P	32.8 24.6	10	5	262	-26.5	-2.1
				P	16.4 16.4	5	10	180	-26.5	-2.3
POND	KA6-2	1250	CQ	P	16.4 16.4	5	30	162		
				P	16.4 10.9	5	20	188		
				PS	24.6 10.9	5	5	170		
				S	16.4 10.9	5	5	179		
EAST	KA188	1250	DQ	P	41.0 24.6	10	10	249		
				PS	57.3 24.6	10	2	249		
				PS	65.5 16.4	10	2	235		
				P	81.9 32.8	15	2	258	-27	-1.3
				S	65.5 41.0	15	5	243		
				S	65.5 32.8	15	10	242		
				S	65.5 41.0	15	5	230		

1. VEIN TYPE: BL = bladed, BR = breccia infilling, MR = massive replacement, CQ = cockade quartz veinlet, DQ = drusy quartz veinlet.
2. INCLUSION TYPE: P = primary, PS = pseudosecondary, S = secondary.
   INCLUSION SIZE: maximum by minimum; in microns.
   INCLUSION BS: BS = bubble size; in microns.
   INCLUSION V%: V% = volume percent (Vl/Vl + Vv)
3. TEMPERATURE HOMG. = homogenization temperature; ^{o}C
   TEMPERATURE EUT. = eutectic temperature; ^{o}C
   TEMPERATURE LAST = last melting temperature; ^{o}C

TABLE 3.11: (continued p3.)

ZONE	SAMPLE NUMBER	ELEV (m)	VEIN[1] TYPE	INCLUSION[2] TYPE	INCLUSION[2] SIZE	INCLUSION[2] BS	INCLUSION[2] V%	TEMPERATURE[3] HOMG.	TEMPERATURE[3] EUT.	TEMPERATURE[3] LAST
EAST	KA188	1250	DQ	S	65.5 16.4	10	2	253		
				P	54.6 54.6	15	2	210		
				P	81.9 49.1	15	10	286	-24	-1.0
				PS	81.9 32.8	15	5	162		
				PS	24.6 16.4	10	5	277		
				P	81.9 32.8	15	5	264	-28.1	-0.9

1. VEIN TYPE: BL = bladed, BR = breccia infilling, MR = massive replacement, CQ = cockade quartz veinlet, DQ = drusy quartz veinlet.
2. INCLUSION TYPE: P = primary, PS = pseudosecondary, S = secondary.
   INCLUSION SIZE: maximum by minimum; in microns.
   INCLUSION BS: BS = bubble size; in microns.
   INCLUSION V%: V% = volume percent (Vl/Vl + Vv)
3. TEMPERATURE HOMG. = homogenization temperature; ^{o}C
   TEMPERATURE EUT. = eutectic temperature; ^{o}C
   TEMPERATURE LAST = last melting temperature; ^{o}C

a precision of 2.2°C (1σ) for the temperature range +40°C to +420°C.

3.6.1.2. Error analysis

Consecutive heating and freezing runs were made to test reproducibility of homogenization and last melting temperatures. Heating rates of about 5°C/minute were used to within 30°C of homogenization, at which time rates were decreased to 1-2°C/minute. Repeated measurements demonstrate a reproducibility to within 5°C and 2°C for homogenization and last melting temperatures respectively.

3.6.1.3. Fluid Inclusion Petrography

Fluid inclusions were observed from bladed quartz-carbonate veins, cockade quartz veinlets, drusy quartz lined cavites and quartz infilling around brecciated fragments (Table 3.11). An estimated paragenetic sequence for these phases of vein and breccia deposition is in Table 3.6. Recognition of these textures allows clear documentation of fluid inclusion data with respect to hydrothermal events at Wolf.

Primary (P), pseudosecondary (PS), or secondary (S) origin was identified carefully for each fluid inclusion measured from Wolf (Table 3.11). Wherever possible, primary fluid inclusions tracing growth zones in the quartz crystals were measured (Plate 3.16). These inclusions are assumed to represent samples of fluids trapped at the same time of

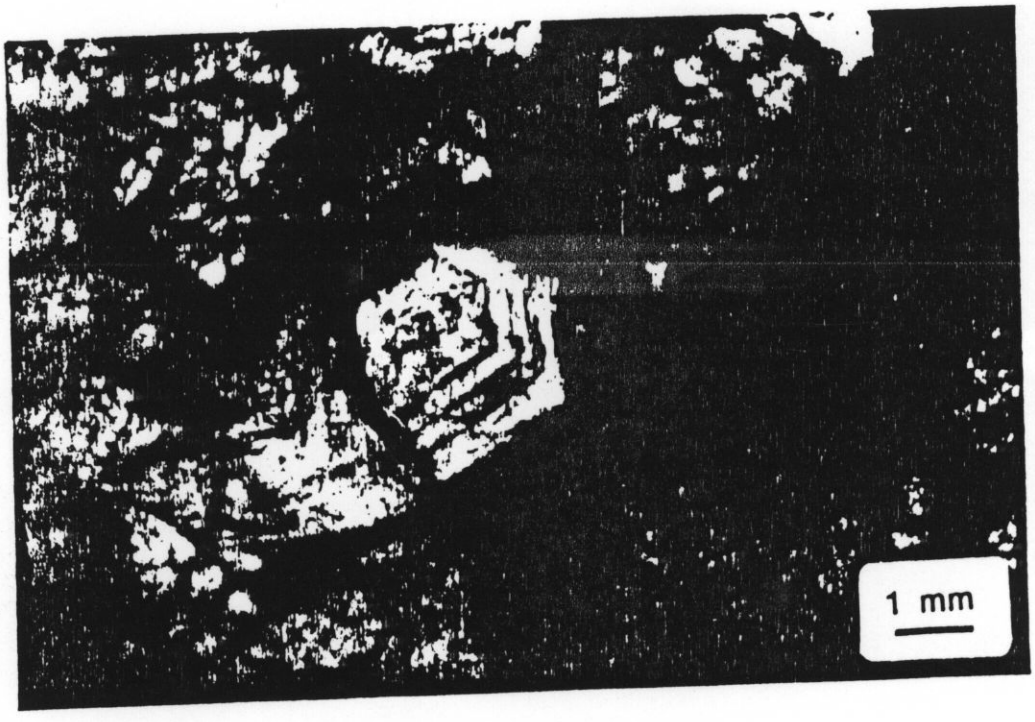

PLATE 3.16: Photomicrograph of growth zones in quartz defined by primary fluid inclusion concentrations. Quartz-carbonate vein from the Pond zone. Sample KA4-8, Wolf prospect. Transmitted light, plane polarized light.

formation as the quartz host. Secondary fluid inclusions lying along planes crosscutting crystal boundaries were also measured (Plate 3.17). These inclusions are preserved in healed microfractures and provide information on fluids present after growth of the quartz host. Pseudosecondary fluid inclusions lying along planes terminating at crystal boundaries represent fluids trapped in fractures during growth of the quartz host. Assignment of fluid inclusion origin is crucial to interpretation of fluid inclusion data within a paragenetic framework (Roedder, 1976).

Most fluid inclusions at Wolf have two phases with the dominant phase being liquid (Plate 3.18). The most conspicuous single feature of all inclusions studied is a vapour bubble. The diameter of the vapour bubble in each inclusion was measured at room temperature (Table 3.11) before and after each heating so that any leakage induced by subsequent cooling could be measured (cf. Hollister et al., 1981). No change in vapour bubble diameter was observed in the study. Visual estimations of the amount of vapour phase present, made by comparison to a chart in Roedder (1976), are in Table 3.11, and vary from 2% to 40% with a mode of 10%. Evidence for boiling was observed in one quartz-carbonate vein sample (KA4-8, Plate 3.19) where growth zones in quartz are defined by two phase liquid and vapour-rich inclusions.

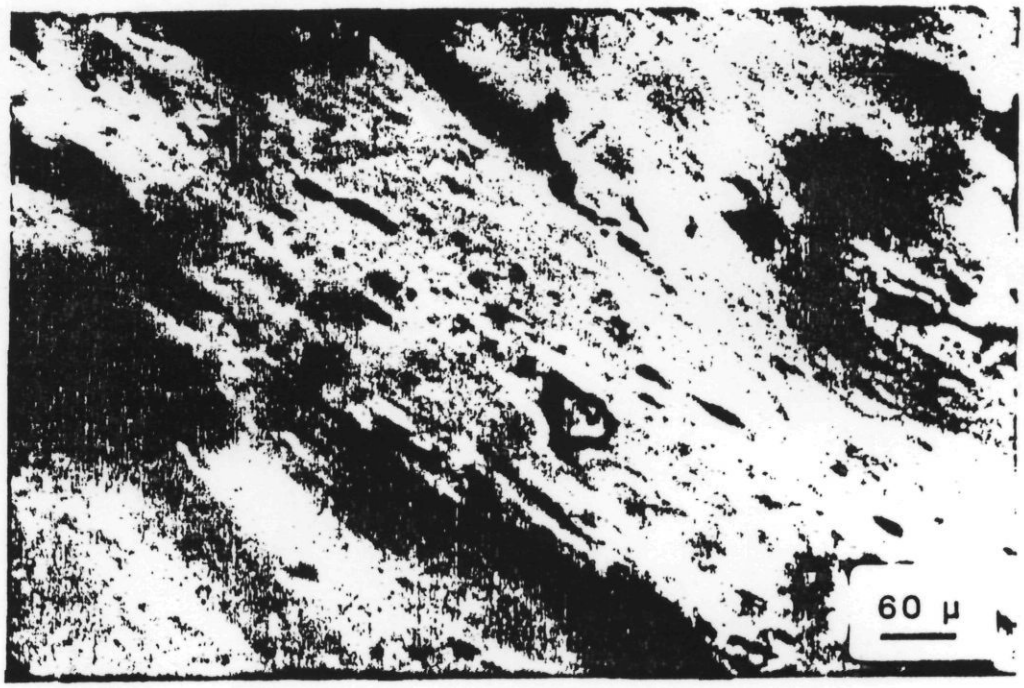

PLATE 3.17: Photomicrograph of planes of secondary fluid inclusions in quartz from the Pond zone. Sample KA6-2, Wolf prospect. Transmitted light, plane polarized light.

PLATE 3.18: Photomicrograph of typical two-phase fluid inclusions in vein quartz from the Ridge zone. Sample KA022, Wolf prospect. Transmitted light, plane polarized light.

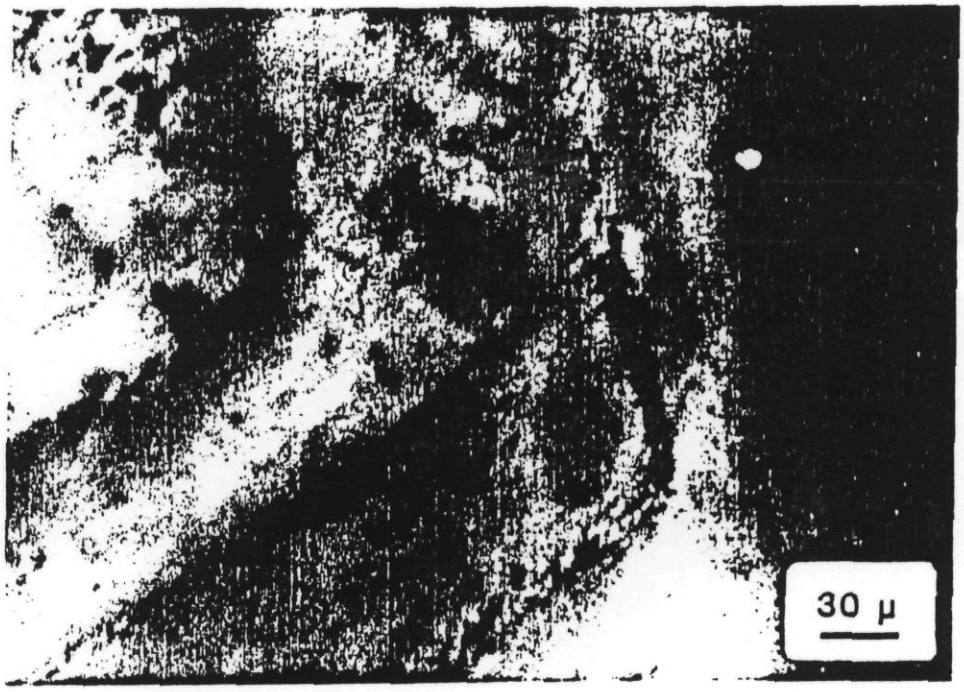

PLATE 3.19: Photomicrograph of growth zones in a quartz crystal defined by primary fluid inclusion concentrations. Pond zone. Sample KA4-8, Wolf prospect. Transmitted light, plane polarized light.

The size of measured fluid inclusions ranged from 8.2 um to 81.9 um across in their longest dimension. Most inclusions were less than 30 um long.

Two phase fluid inclusions from Wolf were crushed to test for the presence of CO_2 vapour using methods described in Roedder (1984). CO_2 is a common volatile component in most fluid inclusions in the epithermal environment (Bodnar et al., 1985); the presence of CO_2 can be recognised by expansion of the vapour bubble when the inclusions are opened by crushing a sample thick section in oil. The minimum amount of CO_2 required before the vapour bubble will expand during crushing studies is 0.1 mol percent (Bodnar et al., 1985). Evidence of noncondensed gases was not seen during crushing studies from Wolf samples. Thus, less than 0.1 mol percent CO_2 is present in the fluid inclusions at Wolf. This is typical for most bonanza-type epithermal systems (Bodnar et al., 1985), although the dominant volatile component in most fluid inclusions from the epithermal environment is CO_2 (Bodnar et al., 1985).

3.6.1.4 Freezing and heating data

Freezing and heating studies were conducted on the Chiaxmeca stage following operating procedures outlined by Bloom (1979). Because freezing is less likely to distort inclusions in quartz, all observations were completed in the freezing mode before proceeding to the heating phase.

All inclusions used for freezing studies were supercooled to approximately -100°C. Slow heating (averaging 2°C/minute) from -100°C to about +5°C enabled determination of the temperature of initial melting (eutectic temperature, Table a1) and the temperature of last melting. Due to the opacity of several quartz plates and the small size of many inclusions, freezing temperatures and phase changes could only be observed in six fluid inclusions. Eutectic and last melting points for inclusions from each vein type are plotted in Figures 3.31 to 3.32 and summarized in Table 3.12.

Eutectic tempertures, which represent the first ice melting, range from -24°C to -28.1°C (Table 3.12). No meaningful distinction can be made between eutectic temperatures from fluid inclusions hosted in drusy or bladed quartz (Fig. 3.31). Last melting temperatures range from -0.9°C down to -2.3°C. Fluid inclusions hosted in early formed bladed quartz yielded lower last melting temperatures, and therefore higher salinities, than those hosted in later formed drusy quartz (Fig. 3.32).

Homogenization temperatures were determined for 41 inclusions from different vein types (Table 3.13). Heating rates of about 10°C/minute were used to within 30°C of homogenization at which time rates were decreased to 2°C/minute.

Homogenization data are plotted, using a class interval of 20°C, for each vein type (Fig. 3.33) and for each origin

TABLE 3.12: Summary of eutectic and last melting temperatures from fluid inclusions, Wolf prospect, central British Columbia. Sample locations are in Figures 3.30 and 3.31. Data are presented in Figures 3.32 and 3.33.

SAMPLE NUMBER	VEIN TYPE	NUMBER OF MEASUREMENTS	EUTECTIC TEMPERATURE ^{o}C	LAST MELTING TEMPERATURE ^{o}C
KATR9-1	BLADED	1	-28	-2.0
KA6-6	BLADED	2	-26.5 $\pm$ 0	-2.2 $\pm$ 0.1
KA188	DRUSY	3	-26.4 $\pm$ 1.7	-1.3 + 0.2

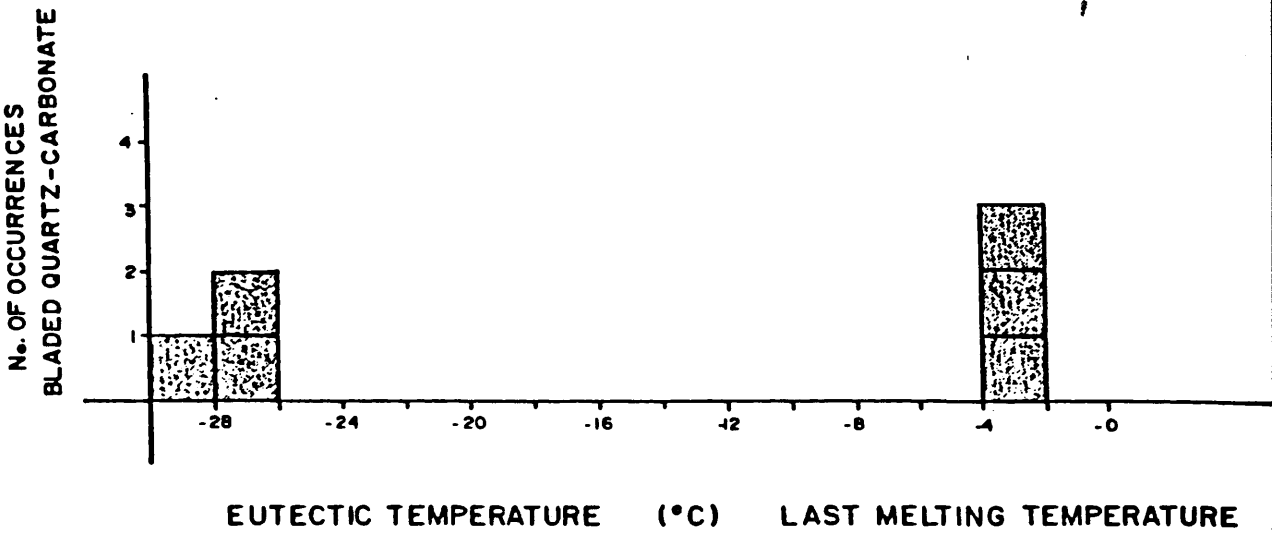

FIGURE 3.31: Eutectic and last melting temperatures of inclusion from bladed quartz-carbonate veins from the Wolf prospect. Freezing data are in Table 3.12.

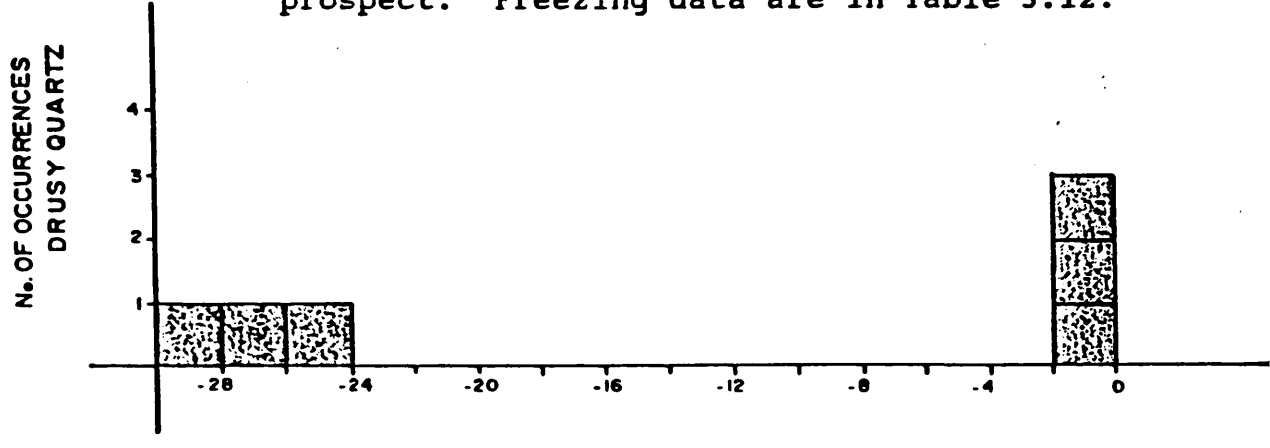

FIGURE 3.32: Eutectic and last melting temperatures of inclusi from drusy quartz infillings from the Wolf prospe Freezing data are in Table 3.12.

TABLE 3.13: Summary of homogenization temperatures from fluid inclusions from different vein types, Wolf prospect, central British Columbia. Sample locations are in Figures 3.30 and 3.31. Data are presented in Figures 3.34 to 3.38.

VEIN TYPE	INCLUSION TYPE	NUMBER OF MEASUREMENTS	AVERAGE TEMPERATURE OF HOMOGENIZATION
BLADED	P	8	229 ± 45 °C
QUARTZ-	PS	5	225 ± 65 °C
CARBONATE	S	7	162 ± 36 °C
COCKADE	P	2	175 ± 13 °C
QUARTZ	PS	1	170°C
VEINLETS	S	1	179°C
DRUSY	P	5	253 ± 25 °C
QUARTZ	PS	4	231 ± 43 °C
	S	4	242 ± 8 °C
BRECCIA	P	1	250°C
INFILLING	PS	1	285°C
BY QUARTZ	S	1	100°C
MASSIVE REPLACEMENT	PS	2	145 ± 0 °C

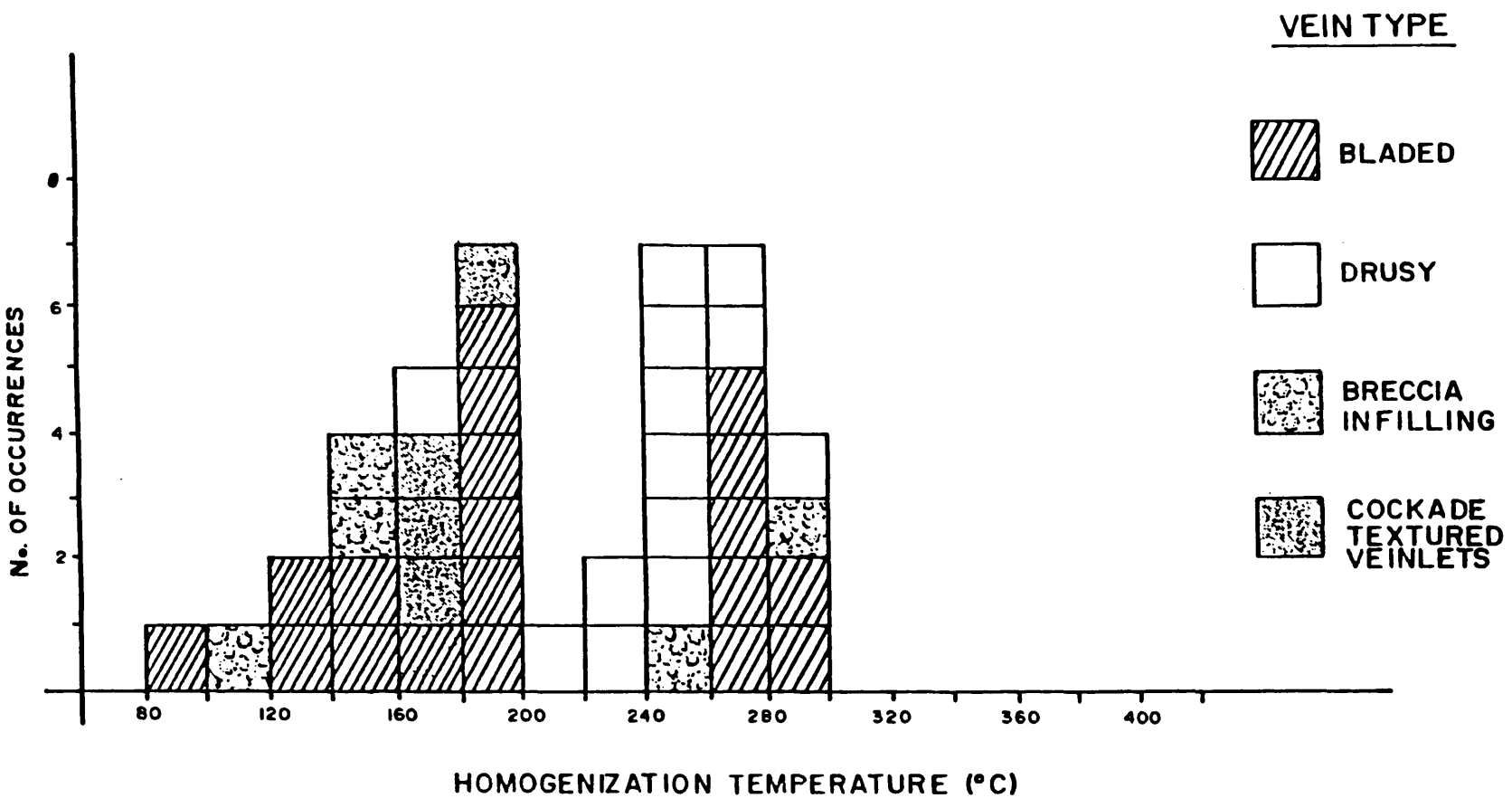

FIGURE 3.33: Homogenization temperature vs. vein type for fluid inclusion samples from the Wolf prospect. Data are in Table 3.12.

type (Fig. 3.34). Primary, pseudosecondary and secondary fluid inclusions from all vein types are bimodally distributed with peaks at 260°C and 180°C (Fig. 3.34). Inclusions in early-formed bladed quartz-carbonate veins have bimodally distributed homogenization temperatures with peaks at 280°C and 180°C (Fig. 3.33). Homogenization temperatures from quartz infilling breccias are unevenly spread from 100°C to 289°C (Fig. 3.33). Cockade textured veins have homogenization temperatures centred at 180°C (Fig. 3.33). Secondary fluid inclusions hosted in drusy quartz infillings, which formed late in the paragenetic sequence of hydrothermal events at Wolf, have unimodally distributed homogenization temperatures with a dominant peak at 250°C (Fig. 3.33).

3.6.1.5 Interpretation

Fluid inclusions from the Wolf property have low concentrations of dissolved salts as determined from last melting temperatures ranging from -2.3°C to -0.9°C (Table 3.12). Eutectic melting in these inclusions (-24°C up to -28.1°C) closely approximates the metastable eutectic melt in the H_2O-NaCl system (about -28°C) which suggests that salinity can be largely attributed to NaCl (Roedder, 1984). Last melting temperatures correspond to dissolved salt contents of between 4.9 and 1.5 weight percent NaCl equivalent. Most epithermal deposits have salinities of between 0.1 and 3.6 weight percent NaCl equivalent (Spooner,

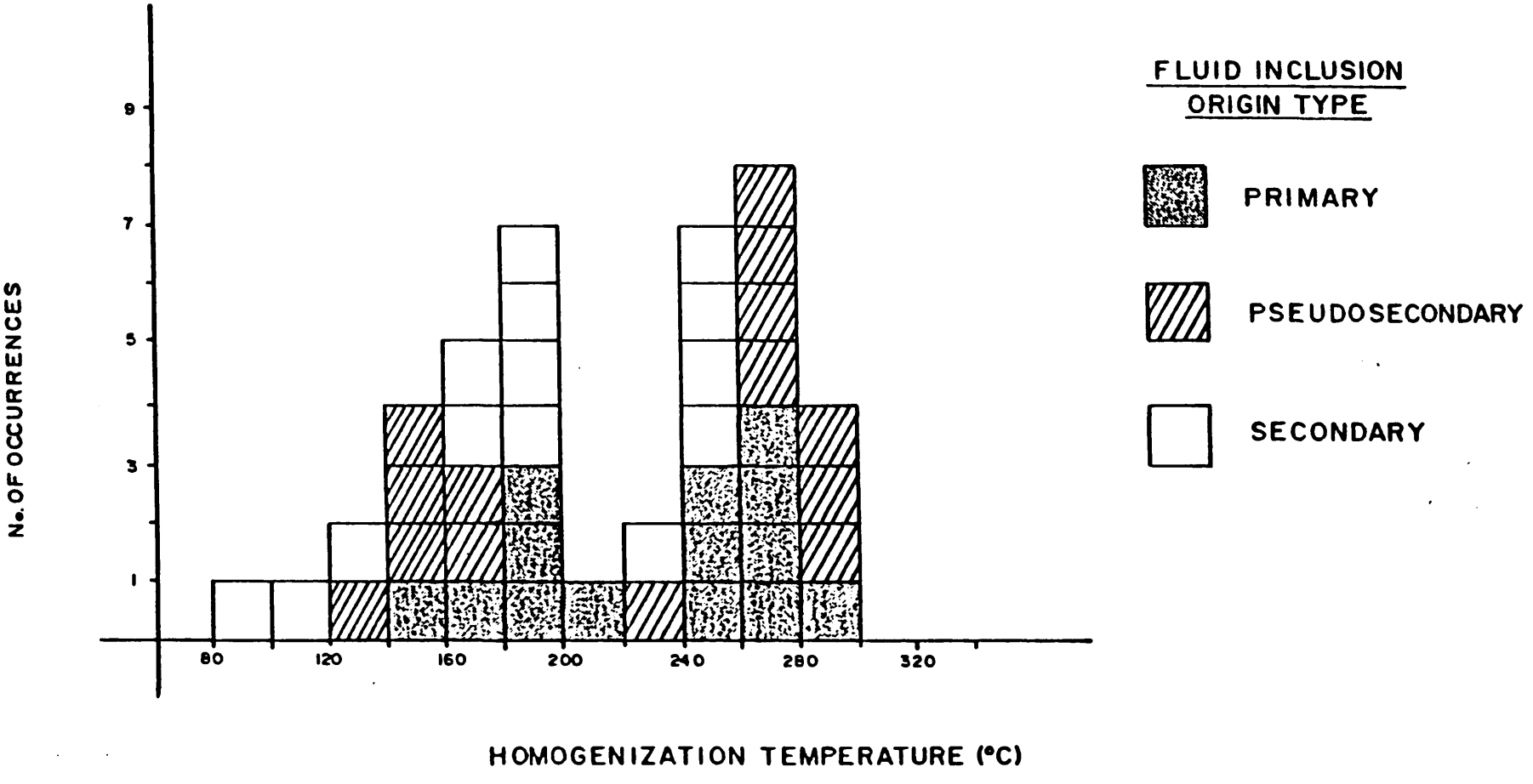

FIGURE 3.34: Homogenization temperature vs. origin type for fluid inclusion samples from the Wolf prospect. Data are in Table 3.12.

1981). Thus salinities of fluid inclusions at Wolf are within expected limits for epithermal deposits, and represent samples of the large amounts of hydrothermally driven, low salt content waters that passed through these rocks.

Less than 0.1 mol percent CO_2 is present in fluid inclusions from the Wolf property. Such low partial pressures of CO_2 are typical for epithermal deposits (figure 5.14 in Bodnar, 1985).

Homogenization temperatures (all to the liquid phase), represent the minimum temperature of trapping of the fluids at the time of formation of the host quartz. On the basis of characteristic epithermal textures (section 3.5.2), the Wolf system formed at shallow depths. Pressure correction to measured temperatures are therefore negligible, and temperature of homogenization is approximately equal to the temperature of trapping.

Fluid inclusion homogenization temperatures at Wolf range from a maximum of 289°C to a minimum of 100°C and show a bimodal distribution (Fig. 3.34). Analysis of each vein type and respective fluid inclusion origin type follows.

Of the estimated eight hydrothermal events at Wolf (Table 3.6), four episodes of veining are documented using fluid inclusion data. These episodes, from oldest to youngest, are: (1) formation of bladed quartz-carbonate veins, (2) rimming of breccia fragments by quartz, (3) formation of cockade textured veinlets, and (4) infilling of

cavities by drusy quartz. Gold and silver mineralization is associated with formation of bladed quartz-carbonate veins and rimming of breccia fragments by quartz (section 3.5.3). Early-formed bladed quartz-carbonate veins show a bimodal distribution of homogenization temperatures in primary fluid inclusions with peaks at 270°C and 180°C (Fig. 3.33). Quartz rimming breccia fragments shows no distinct distribution of homogenization temperatures. Formation of cockade textured veinlets seems to have occurred at temperatures close to 170°C. Drusy quartz is unimodally distributed with primary fluid inclusion peaks at 250°C. These modal temperatures are consistent with characteristic temperatures for epithermal deposits of between 140°C and 300°C (Roedder, 1984).

Evidence for boiling at Wolf is implied by three separate lines of evidence. Macroscopically, breccia textures within veins associated with precious metals indicate that boiling might have occurred during mineralization. Microscopically, primary fluid inclusions with similar homogenization temperatures (Fig. 3.35) have widely varying liquid to vapour ($V_{liquid}/(V_{liquid}+V_{vapour})$) ratios (Fig. 3.36), which is generally indicative of boiling. The most compelling evidence comes from sample KA4-8 (Table 3.11) where growth zones in quartz are defined by two phase liquid and vapour-rich inclusions. Epithermal deposits commonly are characterized by boiling (Roedder, 1984).

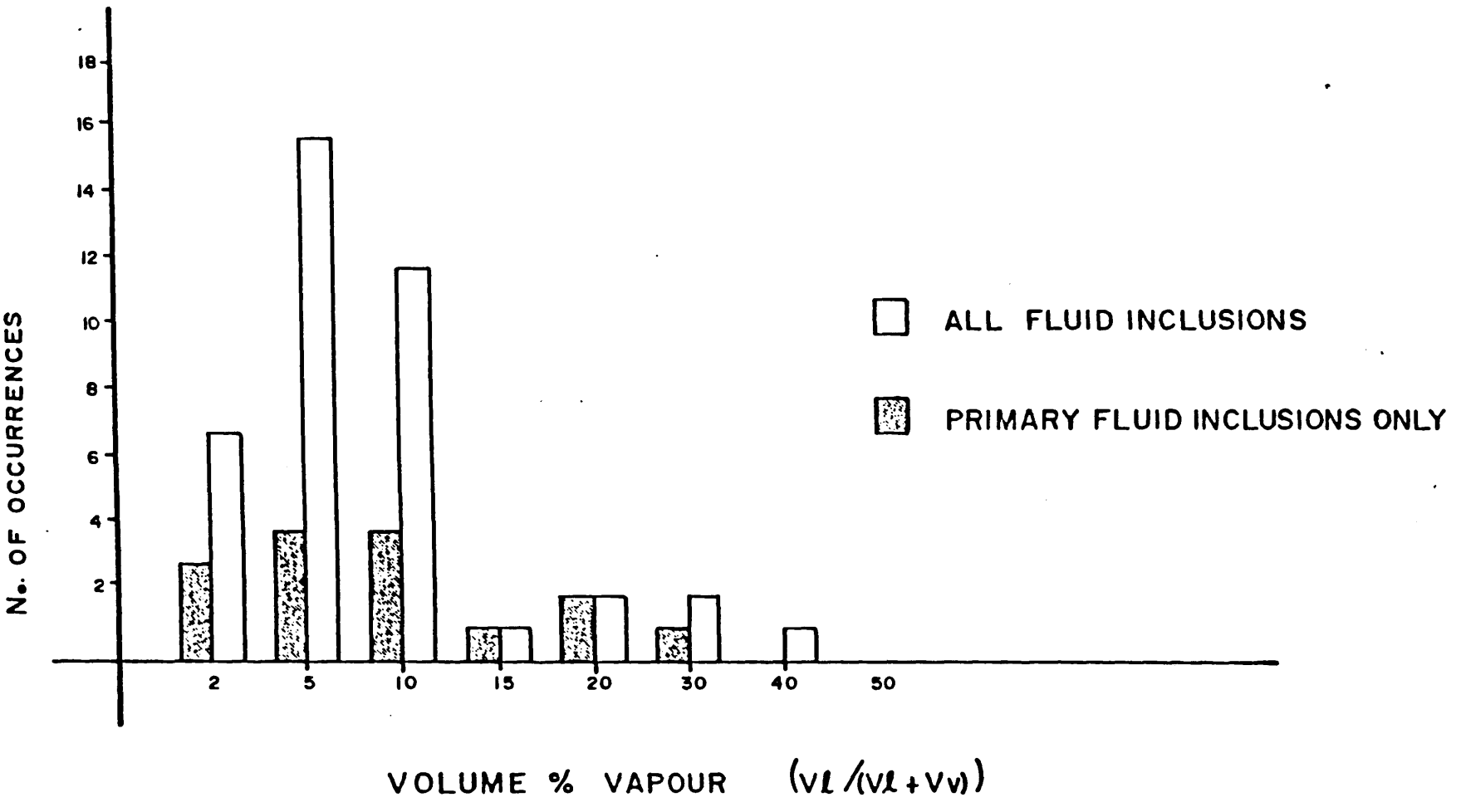

FIGURE 3.36: Frequency distribution of volume percent vapour in fluid inclusions from veins, Wolf prospect, showing the wide variation in L:V ratios. Data are in Table 3.12.

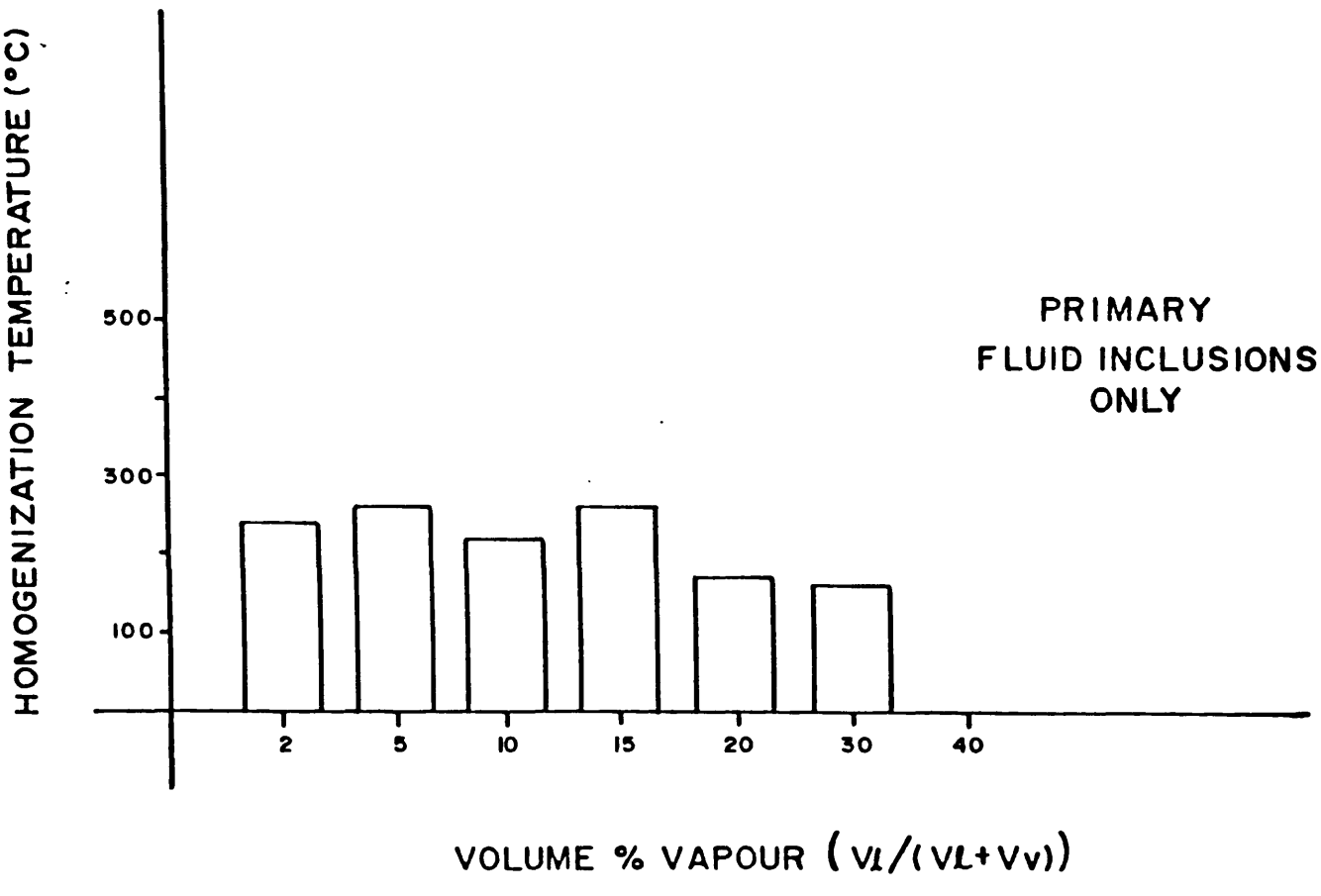

FIGURE 3.35: Homogenization temperature vs. liquid to vapour ratios of primary fluid inclusions from the Wolf prospect. Data are in Table 3.12.

At least two different fluids were responsible for precipitation of veins at Wolf. Fluids characteristic of early formed bladed quartz-carbonate veins are more saline and deposited over a wider temperature range than those of late drusy quartz (Fig 3.37).

The respective modal temperatures and salinities for each vein type might reflect mineralizing events related to periods of peak fluid flow. The first event, probably related to gold and silver mineralization, began at temperatures of 270°C and 180°C, and formed low sulphide, precious metal-rich, bladed quartz-carbonate veins from relatively saline fluids. With cooling, quartz might have rimmed brecciated fragments, and at 170°C, precipitated cockade textured veinlets. Since temperatures near 250°C seem most favourable for gold deposition in an epithermal environment (Cathles, oral comm., 1986), the lower temperature vein quartz understandably is not known to be associated with precious metals. The formation of drusy quartz from relatively low salinity fluids within a confined temperature range of 250°C to 300°C represents a second event apparently unrelated to significant mineralization at Wolf since it contains no gold or silver values (section 3.5).

Calculation of depths of emplacement for quartz-carbonate veins at Wolf are possible assuming the fluids were boiling (Haas, 1971) and using experimental homogenization temperatures of 270°C and 180°C. Fluids that

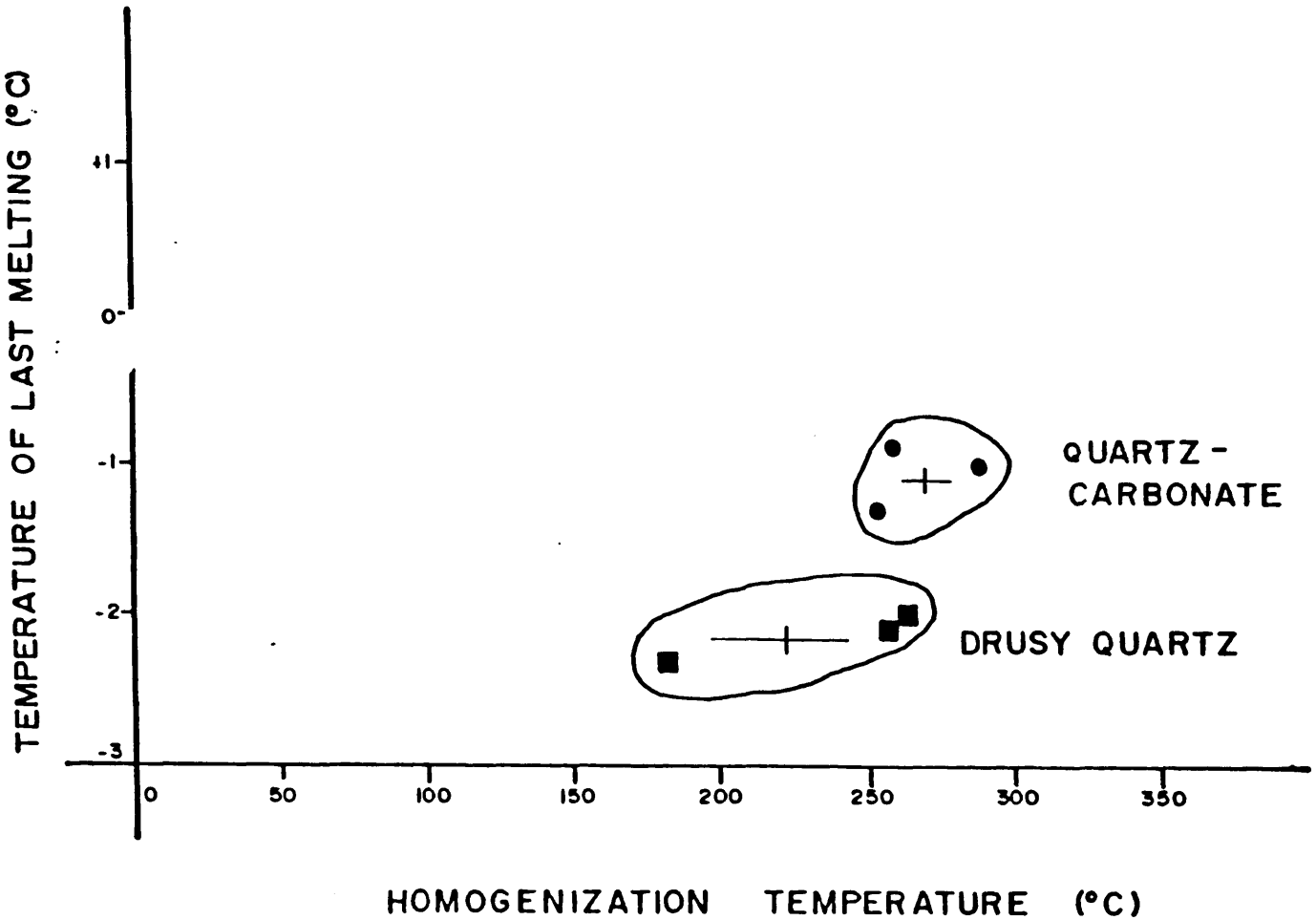

FIGURE 3.37: Homogenization temperature vs. salinity for fluid inclusions from the Wolf prospect. Two fluid populations (bars represent standard error of the means) are observed: (a) fluids characteristic of early formed bladed quartz-carbonate veins which have higher homogenization temperatures and salinities, and (b) fluids characteristic of late drusy quartz which have lower homogenization temperatures and salinities.

formed early quartz-carbonate veins had densities of about 0.80 g/cm^3 and 0.91 g/cm^3. Calculated vapour pressures for quartz-carbonate veins are about 9.8 and 53.9 bars respectively.

Calculated vapour pressures represent confining pressures on fluids that are boiling during deposition. In most natural situations, confining pressures are between hydrostatic and lithostatic limits (Roedder, 1984). Under extreme hydrostatic conditions (Fig. 3.38A), maximum depths of emplacement are approximately 100 m and 625 m for low and high temperature quartz-carbonate veins, respectively. Under extreme lithostatic conditions (Fig. 3.38B), using a mean rock density of 2.7 g/cm^3, the maximum depths of emplacement for low and high temperature quartz-carbonate veins are approximately 200 m and 40 m. These calculated depths are consistent with the epithermal character of the veins (section 3.5) and are less than one kilometre which is typical for epithermal deposits.

The bimodal character of quartz-carbonate homogenization temperatures can be explained by considering a system that alternates from a condition intermediate between hydrostatic and lithostatic (Fig. 3.38C), to a condition that is essentially hydrostatic (Fig. 3.39A). Using a mean rock density of 0.8 g/cm^3, the depth of emplacement for low and high temperature quartz-carbonate veins are 18 m and 97 m respectively. The calculated depth of about 96 m for high temperature quartz-carbonate veins

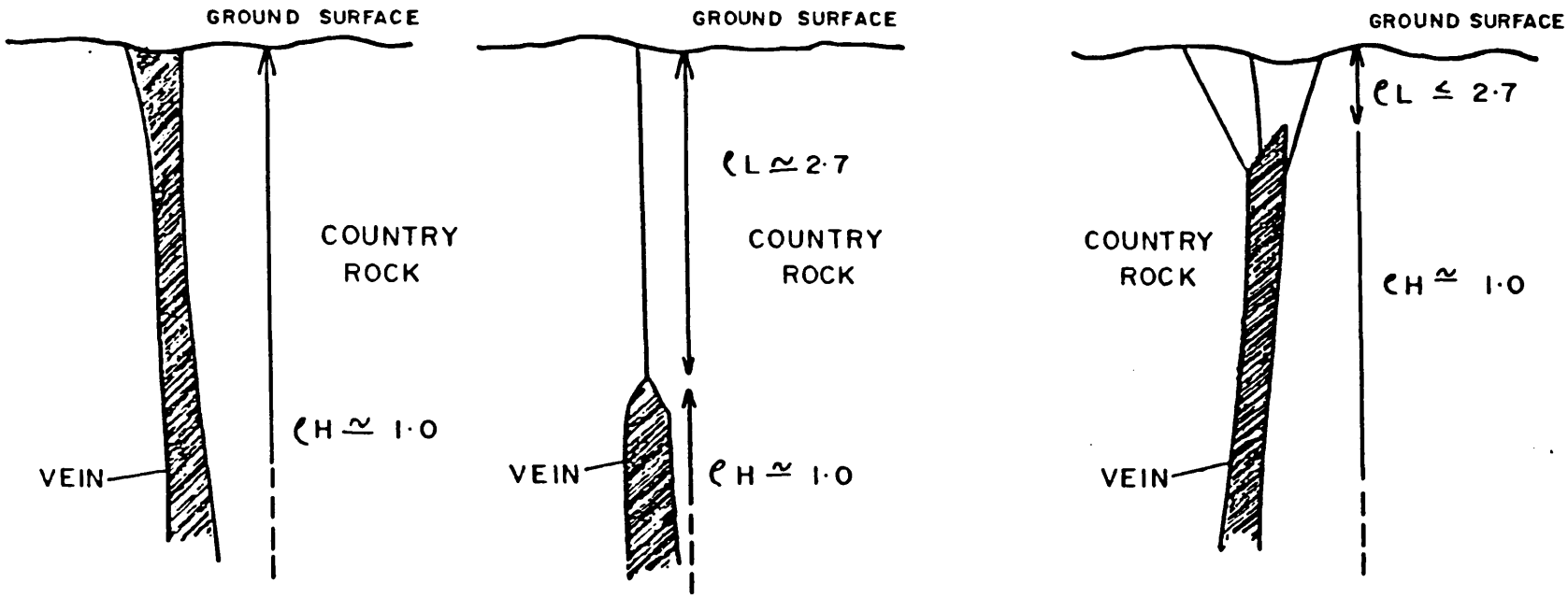

A: HYDROSTATIC CONDITIONS (open to surface)

B: LITHOSTATIC CONDITIONS (virtually closed to surface)

C: INTERMEDIATE CONDITIONS (partially open to surface)

FIGURE 3.38: Sketches illustrating possible hydrostatic, lithostatic or intermediate conditions of vein precipitation at the Wolf prospect. Shaded area represents subsequently filled vein opening.

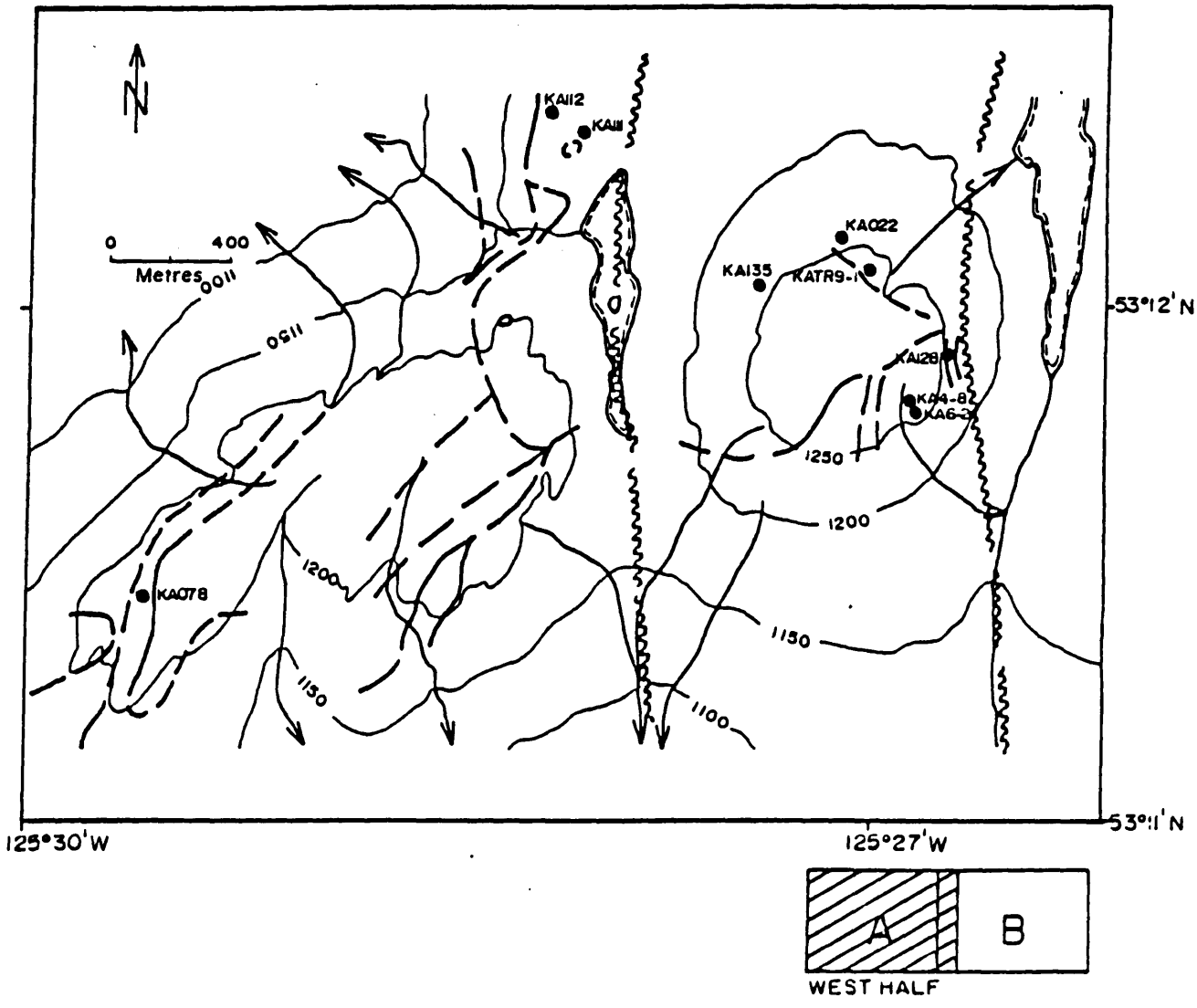

FIGURE 3.39: Locations of samples of whole rock, vein and mineral separate samples used for oxygen isotope analyses from the Wolf property. A)west half, and B) east half.

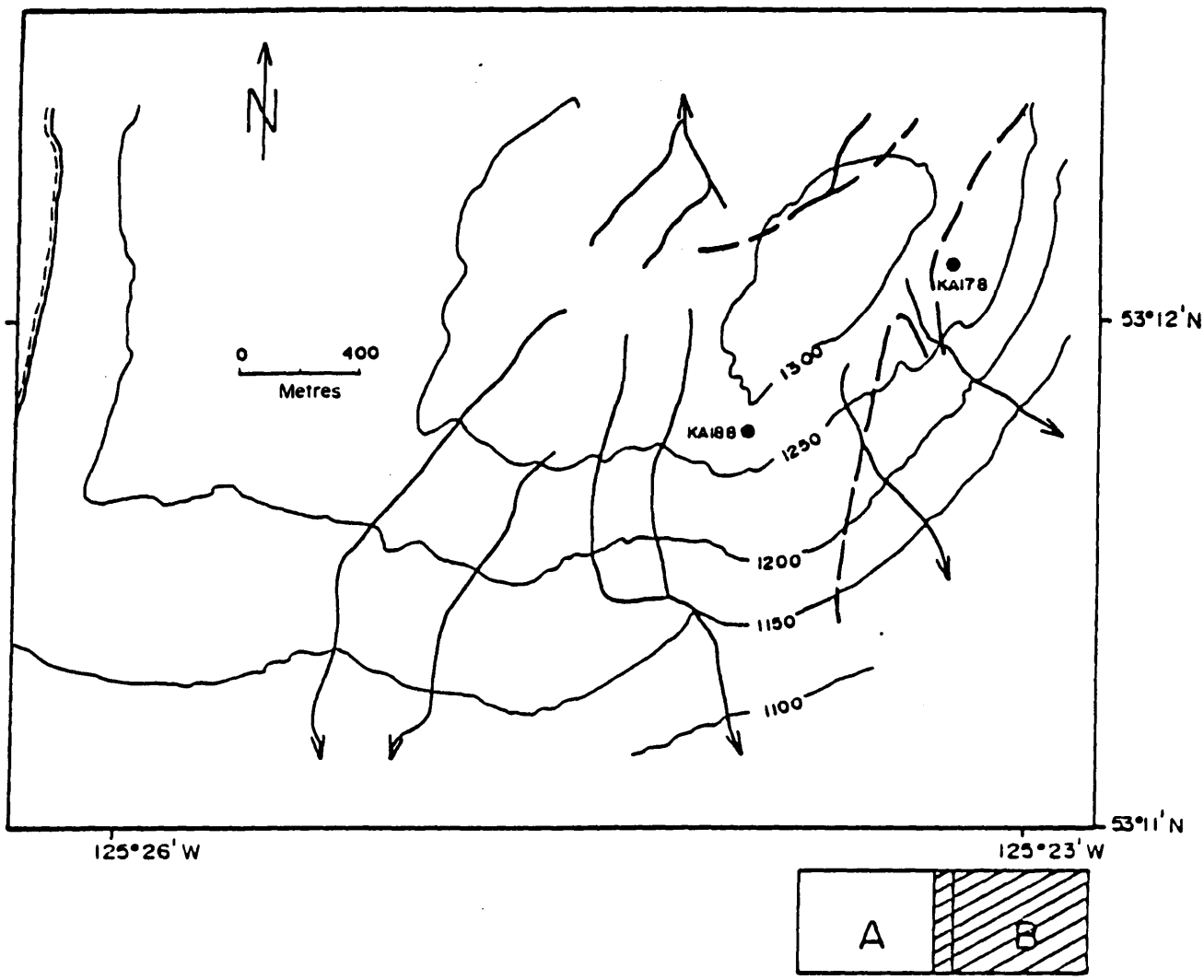

FIGURE 3.39: Locations of samples of whole rock, vein and mineral separate samples used for oxygen isotope analyses from the Wolf property. A)west half, and B) east half.

precipitated under intermediate conditions (Fig. 3.38C) is coincident with that calculated for low temperature quartz-carbonate veins precipitated under hydrostatic conditions. This suggests that quartz-carbonate veins were precipitated from high and low pressure equivalents of the same hydrothermal fluid. Moreover, bladed quartz-carbonate textures seems to reflect alternating hydrostatic and lithostatic pressures at the boiling point. Formation of a silica cap sealing fluid movement at Wolf would cause an increase in fluid pressure approaching lithostatic conditions. Minerals deposited in partially sealed periods reflect higher pressure conditions and higher temperatures of emplacement. Release of pressure, by breaking a silica cap, could induce production of abundant vapour. Subsequent loss of volatiles and decrease in fluid temperature initiated rapid precipitation of minerals, including gold.

3.6.2 STABLE ISOTOPE STUDY

The stable isotope study of 12 samples was done under the supervision of T.K. Kyser at the University of Saskatchewan, Saskatoon. The objectives of the study were to: (1) calculate the oxygen and hydrogen isotopic compositions of hydrothermal fluids which formed the deposit, (2) determine the source of hydrothermal fluids, (3) estimate the water to rock ratio in the fossil hydrothermal system, and (4) constrain the fluid evolution of the system with time.

Hydrogen isotope compositions were measured directly from waters extracted from fluid inclusions in quartz vein samples. Separate paragenetic vein stages (section 3.5) were hand picked. Fluid inclusions from each stage were studied in detail (section 3.6.1) and assumed to represent single populations.

The direct approach for measuring oxygen isotope compositions was not taken because water present in fluid inclusions of oxygen-bearing minerals undergoes exchange with the host mineral during cooling, thus changing the $^{18}O/^{16}O$ ratio of the fluid (Rye and O'Neil, 1968). Therefore, oxygen isotope compositions of the mineralizing fluids at Wolf were measured indirectly by isotopic analysis of mineral assemblages, calculation of temperatures of formation using fluid inclusions and published experimental data (Carmichael et al., 1974), and application of experimentally derived fractionation factors.

3.6.2.1 Sample preparation and analysis

Twenty analyses of 12 samples from Wolf were used, including seven quartz vein sample, five whole rock samples and five mineral separates (Table 3.14; Fig. 3.39). Mineral separation for quartz was achieved by coarse crushing in an agate mortar followed by heating the sample in strong HCl. Whole rock samples were pulverized to less than 200 mesh size in a tungsten carbide ring mill. Mineral separates, hand-picked from a -30 to +60 mesh size under a binocular

TABLE 3.14: Oxygen isotope compositions[1] from samples of whole rock, quartz vein and phenocrysts, Wolf prospect, central British Columbia. Sample locations are in Figures 3.40. Data are plotted in Figures 3.42 and 3.43.

SAMPLE NUMBER	SAMPLE DESCRIPTION	$d^{18}O$
VEIN SAMPLES		
KA 022	QUARTZ VEIN - RIDGE ZONE Massive replacement of crystal tuff by fine silica with only relict shadows of former minerals remaining.	-1.5
KA 111	QUARTZ VEIN - CHOPPER PAD ZONE Grey-white banded chalcedonic quartz. hosted by rhyolite.	1.6
KA 188	QUARTZ VEIN - EAST ZONE Silicified textures within rhyolite porphyry include: comb quartz veinlets, drusy cavities lined by quartz crystals and quartz veinlets crosscutting fragments of rhyolite porphyry.	-6.7
KADDH3-4	QUARTZ VEIN - RIDGE ZONE Clear fine-grained quartz rims breccia fragments in rhyolite.	-4.3
KADDH4-8	QUARTZ VEIN - POND ZONE Rhyolite porphyry shows the following textures: bladed quartz-carbonate, rimming of host rock fragments by quartz, open space filling by milky quartz, and drusy cavities lined by quartz.	-0.1
KADDH6-2	QUARTZ VEIN - POND ZONE Silicified textures in rhyolite porphyry include: comb quartz, quartz infilling, chalcedonic banding and rimming of vein walls and drusy cavities lined by quartz crystals.	1.4
KATR9-1	QUARTZ VEIN - TRENCH 9, RIDGE ZONE Densely bladed quartz vein sample (blades up to 2 cm long) within rhyolite.	0.8

TABLE 3.14: (continued)

SAMPLE NUMBER	SAMPLE DESCRIPTION	$d^{18}O$
WHOLE ROCK SAMPLES		
KA 078	WHOLE ROCK - K-FELDSPAR QUARTZ PORPHYRY The rock contains 5% quartz phenocrysts (1mm in diameter) and 5% orthoclase phenocrysts (less than 2 mm in diameter) suspended in a cryptocrystalline groundmass. No hydrothermal alteration is evident.	-1.6
KA 112	WHOLE ROCK - RHYOLITE The rock contains 10% euhedral orthoclase phenocrysts (1 to 2 mm in diameter) and 5% irregular quartz crystals (1 mm in diameter), set in a fine-grained groundmass. Spherulitic textures and flow banding are common. Field relations suggest that the rhyolite could have been emplaced as a dome.	0.2
KA 128	WHOLE ROCK - RHYOLITE PORPHYRY Sample contains 50% euhedral orthoclase crystals (1 cm in diameter) and 10% quartz crystals (2 to 3 mm in diameter) set in a fine groundmass. Field relations indicate that this unit is intrusive.	-1.0
KA 135	WHOLE ROCK - CRYSTAL TUFF 'Crowded' rock with 30% euhedral orthoclase phenocrysts (1 to 3 mm in diameter) and 10% irregular quartz phenocrysts (1 mm in diameter). Many of the crystals are broken.	1.6
KA 178	WHOLE ROCK - PORPHYRITIC ANDESITE Sample contains 10% plagioclase, 10% hornblende, and 20% pyroxene phenocrysts set in a cryptocrystalline groundmass.	-3.6
MINERAL SEPARATES FROM UNITS DESCRIBED ABOVE		
KA 078	QUARTZ PHENOCRYST SEPARATE	6.0
KA 078	FELDSPAR PHENOCRYST SEPARATE	-7.4
KA 112	QUARTZ PHENOCRYST SEPARATE	8.1
KA 135	QUARTZ PHENOCRYST SEPARATE	6.6
KA 135	FELDSPAR PHENOCRYST SEPARATE	0.5

1. All stable isotope analyses were done in the laboratory of T.K. Kyser, Department of Geological Sciences, University of Saskatchewan.

microscope, were washed ultrasonically in distilled water. Quartz vein samples and mineral separates were analysed by XRD to confirm purity of sample powders prior to isotopic analysis. Compositions of whole rock samples were determined by XRF.

Direct analysis of hydrogen isotope compositions by extraction of fluid inclusion waters used 1 g of clean quartz. Indirect analyses of oxygen isotope compositions by analysis of mineral or rock powders used from 5 mg to 18 mg of sample.

Variations in the isotopic ratios of hydrogen and oxygen were measured by mass-spectrometer on H_2 and CO_2 gases, respectively, that were extracted quantitatively from fluid inclusions in crushed minerals. Hydrogen was extracted from fluid inclusions in quartz using the U-technique described by Bigeleisen et al. (1952) as modified by Kyser and O'Niel (1984). Oxygen was extracted by the BrF_5 technique (Clayton and Mayeda, 1963). All stable isotope analyses were made using conventional isotope ratio mass spectrometry and are reported using the d notation in units of per mil ($^{o}/_{oo}$) relative to SMOW standard (Standard Mean Ocean Water).

3.6.2.2 Error analyses

Replicate analyses of vein, whole rock and mineral separate samples are reproducible with a precision of $\pm$ 0.2 per mil (2σ) for $d^{18}O$ (Table 3.15) and $\pm$ 5 per mil (2σ) for

TABLE 3.15: Duplicate data and University of Saskatchwan standard samples used to determine precision and accuracy of oxygen isotope analyses[1] at the Wolf prospect, central British Columbia.

SAMPLE NO.	DUPLICATE 1 ($^{o}/_{oo}$)	DUPLICATE 2 ($^{o}/_{oo}$)	STANDARD ($^{o}/_{oo}$)
KADDH6-2 QUARTZ VEIN	1.4	1.6	
KA135 QUARTZ MINERAL SEPARATE	6.6	6.6	
AGS[2] QUARTZ SAND			9.5

1. All stable isotope analyses were done in the laboratory of T.K Kyser, Department of Geological Sciences, University of Saskatchewan.
2. The value of the AGS standard is $d^{18}O = 9.6\ ^{o}/_{oo}$.

dD (Kyser, pers. comm., 1987). The $d^{18}O$ value of the NBS-28 quartz standard is 9.6 (Kyser, pers. comm., 1987). Standard samples are reproducible with an accuracy of $\pm$ 0.1 per mil (Table 3.17).

3.6.2.3 Isotopic composition of hydrothermal fluids

The hydrogen isotopic compositions of fluids in equilibrium with three quartz veins were directly measured by extracting waters from primary fluid inclusions representing a single population. Values range from -161 per mil to -176 per mil (Table 3.16). Oxygen isotope compositions were calculated indirectly by isotopic analysis of mineral assemblages. Assumptions, techniques and results are below.

At equilibrium, isotopic species partition (fractionate) among available sites in coexisting minerals and fluid through mass-dependent differences in chemical and physical behaviour. The partitioning of two isotopes between two species, X and Y, is described by the fractionation factor, $\alpha_{xy} = R_x/R_y$ (where R is the isotope ratio; for example D/H or $^{18}O/^{16}O$). The degree of fractionation, independent of pressure because of the nearly identical volume of heavy and light isotopes (Sheppard, 1977), but varies inversely with temperature in a predictable way (Urey, 1947; Bigeleisen and Mayer, 1947). Thus, the isotopic composition can be indirectly calculated given: (1) analytical isotope data from a mineral that was

TABLE 3.16: Calculated oxygen isotope compositions (section 3.6.2) and measured hydrogen isotope compositions[1] of hydrothermal fluids at the Wolf prospect, central British Columbia.

SAMPLE NUMBER	SAMPLE MATERIAL	$d^{18}O$ MATERIAL	TEMPERATURE °C	$d^{18}O$ WATER	dD WATER
KA022	VEIN QUARTZ	-1.5	145	-17.9	-176
KA111	VEIN QUARTZ	1.6	<170	-12.7	
KA188	VEIN QUARTZ	-6.7	240	-16.6	-161
KA3-4	VEIN QUARTZ	-4.3	267	-12.9	
KA4-8	VEIN QUARTZ	-0.1	183	-13.5	
KA6-2	VEIN QUARTZ	1.4	170	-12.9	
KATR9-1	VEIN QUARTZ	0.8	279	-7.4	-163
KA078	WHOLE ROCK	-1.6	250	-7.9	
KA112	WHOLE ROCK	0.2	250	-6.1	
KA128	WHOLE ROCK	-1.0	250	-7.3	
KA135	WHOLE ROCK	1.6	250	-4.7	
KA178	WHOLE ROCK	-3.6	250	-9.9	
KA078	FELDSPAR SEPARATE	-7.4	250	-11.5	
KA135	FELDSPAR SEPARATE	0.5	250	-3.6	

1. All stable isotope analyses were done in the laboratory of T.K. Kyser, Department of Geological Sciences, University of Saskatchewan.

in equilibrium with the hydrothermal fluid, (2) the fractionation coefficient (α) between that mineral and water, and (3) an independent estimate of temperature of formation of the mineral through fluid inclusions or other geothermometers.

The oxygen isotope compositions of hydrothermal fluids in equilibrium with quartz veins at Wolf were calculated using: (1) the analytical isotope data from the veins (Table 3.16), (2) the experimental quartz-water fractionation curves of Clayton et al. (1972), and (3) averaged homogenization temperature from primary fluid inclusion data (section 3.6.1).

Equation 3.1. QUARTZ-WATER (Clayton et al, 1972):

$1000\ln\alpha_{(quartz\text{-}water)} = 3.38(10^6/T^2) - 2.90$

where T = temperature (K), and the temperature range = 200 to 500°C.

Results of these calculations (Table 3.16) show a wide spread of isotopic compositon in the depositional fluids of between $d^{18}O = -7.4$ and $-17.9\ ^{o}/_{oo}$.

The oxygen isotope composition of depositional fluids was also calculated using the assumption of Taylor (1979) that the measured $d^{18}O$ whole rock value is equal to the $d^{18}O$ value of plagioclase (An_{30}). Calculations were made using: (1) the whole rock analytical isotope data (Table 3.16), (2) the plagioclase (An_{30})-water curves of O'Neil and Taylor (1967), and (3) an estimated temperature of formation of the rock of 800°C (from Fig. 6-12 in Carmichael et al., 1974).

Equation 3.2. PLAGIOCLASE(An_{30})-WATER (O'Neil and Taylor, 1967):

$1000\ln\alpha_{(plag.-\ water)} = 2.68(10^6/T^2)-3.53$

where T = temperature (K), and the temperature range = any geologically reasonable temperature

Results of these calculations (Table 3.16) show a spread of isotopic composition in the depositional fluids of between $d^{18}O = -2.4$ and $+2.8\ ^{o}/_{oo}$. These values are higher than those calculated from quartz veins.

3.6.2.4 Water to Rock ratio

The water to rock ratio of the fossil hydrothermal system at Wolf can be estimated assuming isotopic equilibrium between wallrock and fluids (Ohmoto and Rye, 1974). Unaltered rhyolite rocks typically have a $d^{18}O$ value of about $7\ ^{o}/_{oo}$ (Field and Fifarek, 1985). Rhyolitic rocks from Wolf that have been exposed to hydrothermal fluids have $d^{18}O$ values lower than this norm (Table 3.16). The water to rock ratio is dependent on temperature, the $d^{18}O$ value of the hydrothermal fluid, and the difference between altered and unaltered values.

Calculation of the original ^{18}O content of the hydrothermal fluids at Wolf from $d^{18}O$ values for quartz veins gave values ranging from -7.4 to $-17.9\ ^{o}/_{oo}$. These values represent the equilibration of hydrothermal fluids with wallrock of considerably higher ^{18}O content. Thus, the original isotopic composition of the fluids must have been

less than $d^{18}O = -17.9\ ^{o}/_{oo}$. The initial $d^{18}O$ of meteoric waters prior to exchange with wallrock is best calculated using D/H analyses of fluid inclusions and equation 3.3.

Equation 3.3. INITIAL METEORIC WATER (Craig, 1961):

$$dD = 8d^{18}O + 10$$

The average dD value as measured from fluid inclusion waters is $-166\ ^{o}/_{oo}$ (Table 3.16). The dD value for meteoric water in the Wolf area today is approximately $-160^{o}/_{oo}$ (figure 6.3 in Taylor, 1979). This meteoric isotope composition reflects latitude and elevation. Since hydrogen isotopic compositions of meteoric waters have undergone only a 1 to 2% shift toward heavier values since Tertiary time (Taylor, 1974; O'Neil and Silberman, 1974), the $-166\ ^{o}/_{oo}$ value determined experimentally from fluid inclusions at Wolf is reasonable. By using the dD value of $-166\ ^{o}/_{oo}$, the initial $d^{18}O$ of waters at Wolf is calculated as $-22\ ^{o}/_{oo}$ from equation 3.

Assuming continuous recirculation and re-equilibration of hydrothermal fluids in a closed system, the water to rock ratio at Wolf is calculated using the relationships in equation 3.4.

Equation 3.4. CLOSED SYSTEM W/R (Ohmoto and Rye, 1974; Taylor, 1979):

$$w/r = \frac{d^{f}rock - d^{i}rock}{d^{i}water - (d^{f}rock - \Delta)}$$

where: $\Delta = d^{f}rock - d^{f}water$, i = initial value and f = final value after exchange.

Results of these calculations (Table 3.17) indicate water to rock ratios of 0.21 to 0.46 at Wolf. Calculated water to rock ratios do not account for boiling and mixing of unexchanged meteoric water (Field and Fifarek, 1985).

Assuming hydrothermal fluids make only one pass through an open system, the water to rock ratios at Wolf are 0.19 to 0.42 (Table 3.17) as calculated from equation 5.

Equation 3.5. OPEN SYSTEM W/R (Taylor, 1979):

$$w/r = \ln\left[\frac{d^{i}water + \Delta - d^{i}rock}{d^{i}water - (d^{f}rock - \Delta)}\right]$$

where: $\Delta = d^{f}rock - d^{f}water$, i = initial value, and f = final value after exchange.

Both open and closed system models give only minimum water to rock ratios because: (1) a lot of water may pass through the rocks without equilibrating, and (2) the water entering the volume of rock under consideration could have become depleted in ^{18}O from the original isotopic composition it had before entering the rock system (Sheppard, 1977).

3.6.2.5 Geothermometry

Mineral separates of quartz and potassium feldspar phenocryst pairs were analyzed to estimate the temperature of formation of their host rocks. Fractionation factors ($1000\ln\alpha = \Delta$) for mineral pairs have been determined experimentally (e.g. Blattner and Bird, 1974; Sheppard and Schwarcz, 1970), and derived empirically (e.g. Bottinga and

TABLE 3.17: Calculated water to rock ratios (section 3.5.2) assuming closed and open systems at the Wolf prospect, central British Columbia.

SAMPLE NUMBER	d18O WHOLE ROCK	d18O WATER	W/R CLOSED SYSTEM	W/R OPEN SYSTEM
KA078	-1.6	-7.9	0.61	0.48
KA112	0.2	-6.1	0.43	0.36
KA128	-1.0	-7.3	0.54	0.43
KA135	1.6	-4.7	0.31	0.27
KA178	-3.6	-9.9	0.88	0.63

Javoy, 1974; Field and Fifarek, 1985) assuming preservation of isotopic equilibrium between minerals. Given the fractionation factor ($\Delta_{quartz\text{-}K\text{-}feldspar}$) between these two minerals, the temperature of deposition is expressed by equation 3.6:

Equation 3.6. QUARTZ-KFELDSPAR (Matsuhisa et al., 1979):

$$T(K) = \frac{(0.68(10^3))}{(\Delta_{quartz\text{-}Kfeldspar} - 0.02)^{1/2}}$$

where T = temperature (K), temperature range = 500 to 800°C, and $\Delta_{quartz\text{-}kfeldspar} = d^{18}O_{quartz} - d^{18}O_{kfeldspar}$.

At Wolf, quartz phenocrysts have values from 6.0 to 8.1 $^{o}/_{oo}$ and potassium feldspar phenocrysts have values between -7.4 and +0.5 $^{o}/_{oo}$ (Table 3.16). Common unaltered rock forming minerals such as quartz, carbonates and alkali feldspars have large $d^{18}O$ values of 6 to 13$^{o}/_{oo}$ (Field and Fifarek, 1985). Consequently, it appears that quartz phenocrysts have retained the original composition of the magma which formed rhyolites at Wolf, whereas K-feldspar phenocrysts are depleted in ^{18}O. The temperature of formation of rhyolites at Wolf cannot be calculated using quartz-feldspar mineral pairs because feldspar compositions are depleted in ^{18}O and reflect the composition of hydrothermal fluids that passed through the rocks at Wolf.

The oxygen isotope composition of hydrothermal fluids in equilibrium with potassium feldspar phenocrysts are calculated using: (1) analytical isotope data from the potassium feldspar phenocrysts (Table 3.16), (2) the

experimental feldspar-water fractionation curves of Equation 3.7, and (3) an estimated temperature of formation of the rock of 800°C (from figure 6-12 in Carmichael et al., 1974).

Equation 3.7. ALKALI FELDSPAR-WATER (O'Neil and Taylor, 1967):

$1000\ln \alpha$ (alkali feldspar-water) $= 2.91(10^6/T^2) - 3.41$

where T = temperature (K) and temperature range = 350 to 800°C.

Results of these calculations (Table 3.16) show isotopic compositions in the depositional fluids of $d^{18}O = -6.5$ and 1.4 $^{o}/_{oo}$. These compositions are similar to those calculated from whole rock data (section 3.6.2.3).

3.6.2.6 Interpretation

Quartz veins, whole rock samples and alkali feldspar phenocrysts are depleted in ^{18}O by 3.9 to 9.1 $^{o}/_{oo}$ (Table 3.16), assuming that normal igneous rocks on the earth have minimum $d^{18}O$ of +5.5 $^{o}/_{oo}$ (Taylor, 1968). This depletion is indicative of alteration of wall rock by large volumes of low ^{18}O content hydrothermal fluids at elevated temperatures. Thus, the high degree of isotopic exchange reflects complete saturation of the host rocks with hydrothermal fluids.

Original depositional fluids at Wolf had an initial $d^{18}O$ of -22 $^{o}/_{oo}$ prior to exchange with wallrock. These fluids were enriched in ^{18}O by almost the same amount as wallrock was depleted in ^{18}O. Such reciprocal shifts in

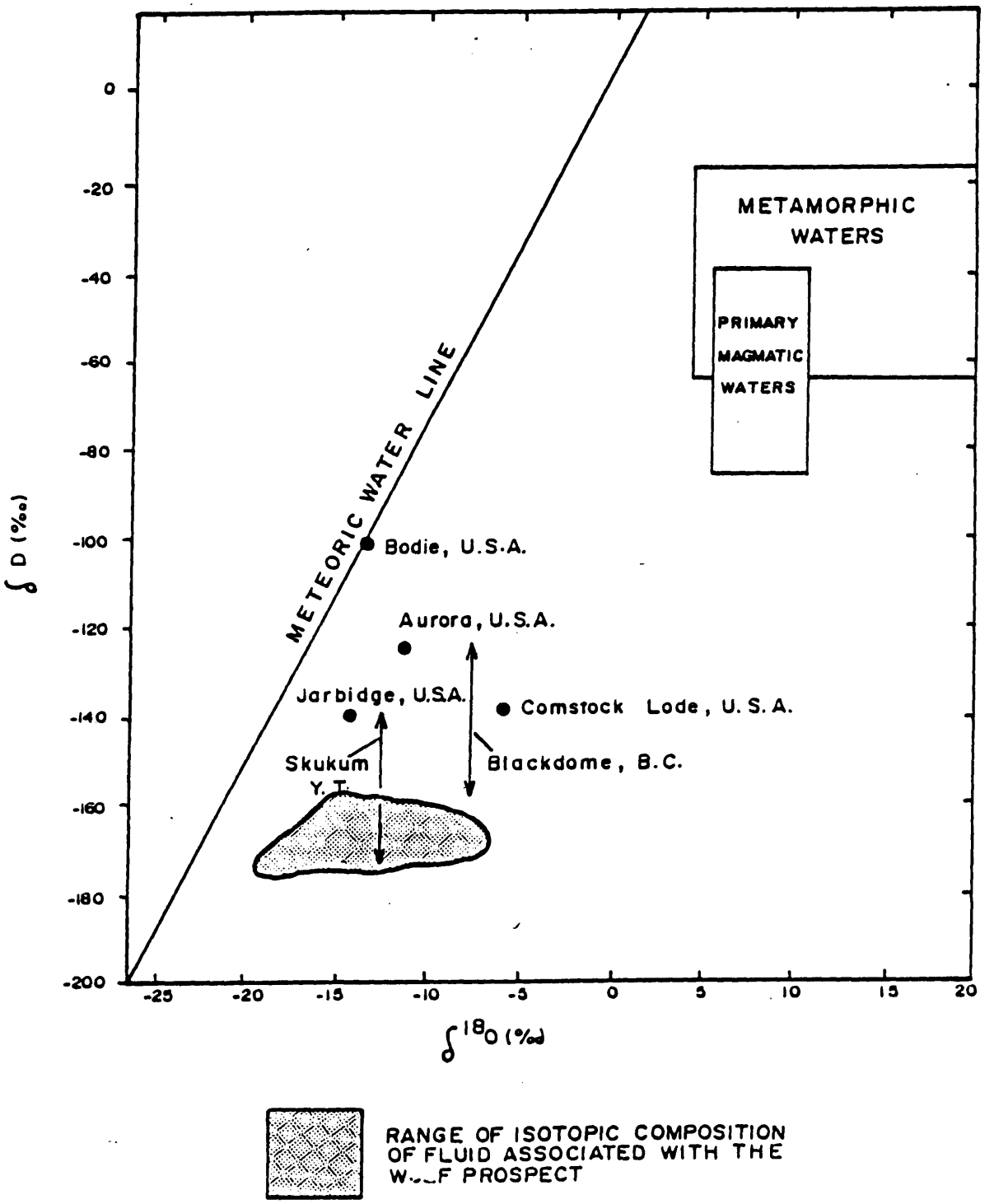

FIGURE 3.40: dD vs. $d^{18}O$ values showing fields for magmatic and metamorphic water and the range of depositional fluid composition at Wolf, central B.C. Values for other Tertiary volcanic-hosted epithermal deposits in B.C., Yukon Territory, and western U.S.A. are also shown.

consistant with reported ratios of 0.2 to 2 from epithermal districts in the U.S.A. (Taylor, 1974). The low salinities in fluid inclusions (section 3.6.1) also support a high water to rock ratio that would maintain dilution of solutions.

The abundance of veining at Wolf (section 3.5) implies that mineral deposition must have occurred in an open system of fractures and fault zones to allow passage of large quantities of fluid. Such evidence, combined with characteristically low background values of gold and silver in Ootsa Lake Group rocks (section 3.5), makes incoming hydrothermal fluids a plausible source for mineralization at Wolf.

Evolution of hydrothermal fluids at Wolf can be charted using the three quartz vein analyses that plot along a horizontal line in Figure 3.41. Sample KATR9-1, collected from the Ridge Zone, is from an early-formed quartz-carbonate vein associated with precious metal mineralization. Isotopes of oxygen and hydrogen plot (Fig. 3.41) furthest from the present day meteoric water line. Sample KA188, collected from the East Zone, is of late-formed drusy quartz (section 3.5); isotopes plot (Fig. 3.41) closest to the meteoric water line. Large volumes of hydrothermal fluids probably carried precious metals in solution from source rocks distant from the property, depositing most precious metals initially when temperatures were hot enough to cause boiling which in turn is related to

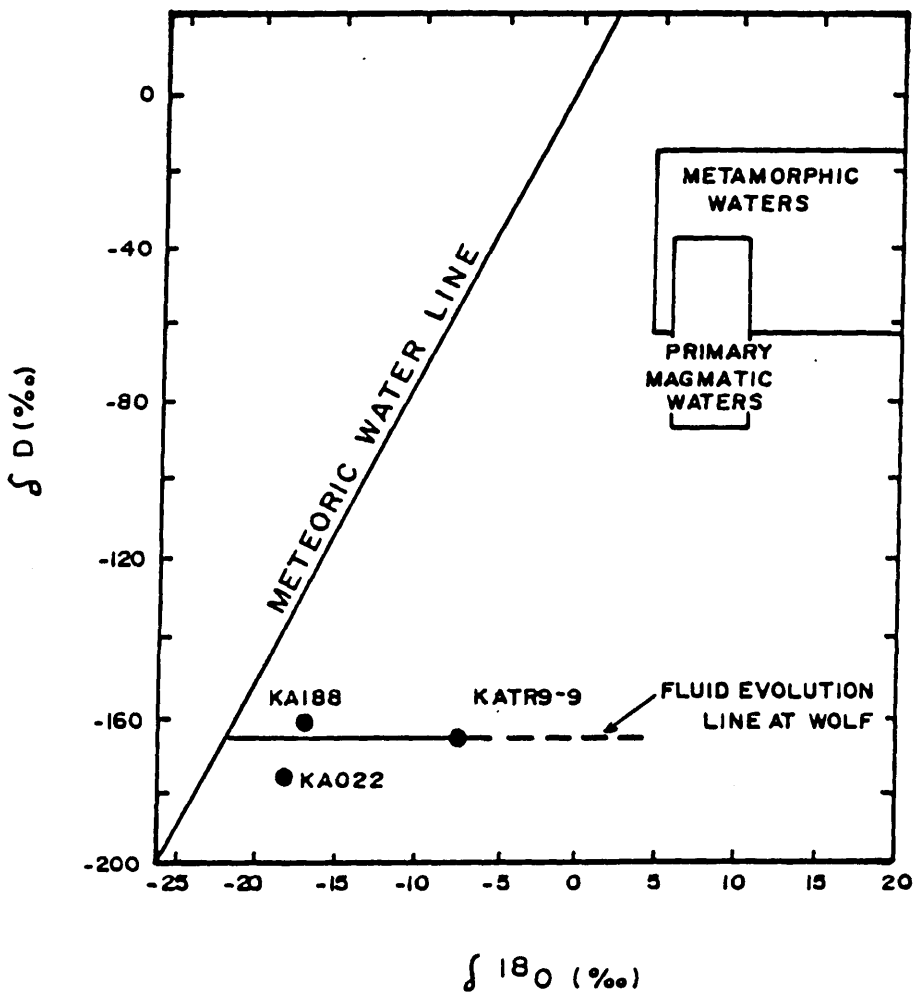

FIGURE 3.41: dD vs. $d^{18}O$ for quartz vein samples from the Wolf prospect with proposed fluid evolution line.

eruption, brecciation, and rapid cooling of the fluid, and evolving to later precious metal poor fluids with the waning of hydrothermal activity.

3.7 CONCLUSIONS

3.7.1 ORIGIN

The Wolf epithermal gold-silver prospect occurs in mid-Eocene Ootsa Lake Group volcanic rocks in central British Columbia (Fig. 2.1). The Ootsa Lake Group unconformably overlies Lower and Middle Jurassic rocks of the Hazelton Group and is preserved as a block-faulted erosional remnant in the Capoose Lake area. Ootsa Lake Group rocks in central British Columbia represent widespread volcanism of short duration in the Eocene (Nelson, 1985).

Ootsa Lake Group rocks at Wolf are grouped into five assemblages (section 3.2) possibly related to a maar (Fisher and Schmincke, 1984; Sillitoe and Bonham, 1984; Sillitoe et al., 1984). Figure 3.42 illustrates interpretation of Ootsa Lake Group rocks at Wolf using a maar model (Andrew and Godwin, 1986). However, the interpretation is limited by the sparce outcrop in the area. Assemblage one, steeply dipping conglomeratic and tuffaceous units, contains reworked material of both volcanic and plutonic provenance. These units might reflect proximity to a major ring fault that could define the boundary of the maar with adjacent Hazelton volcanic rocks. Assemblage two, mainly flat-lying pyroclastic units, represents magmatic differentiation to

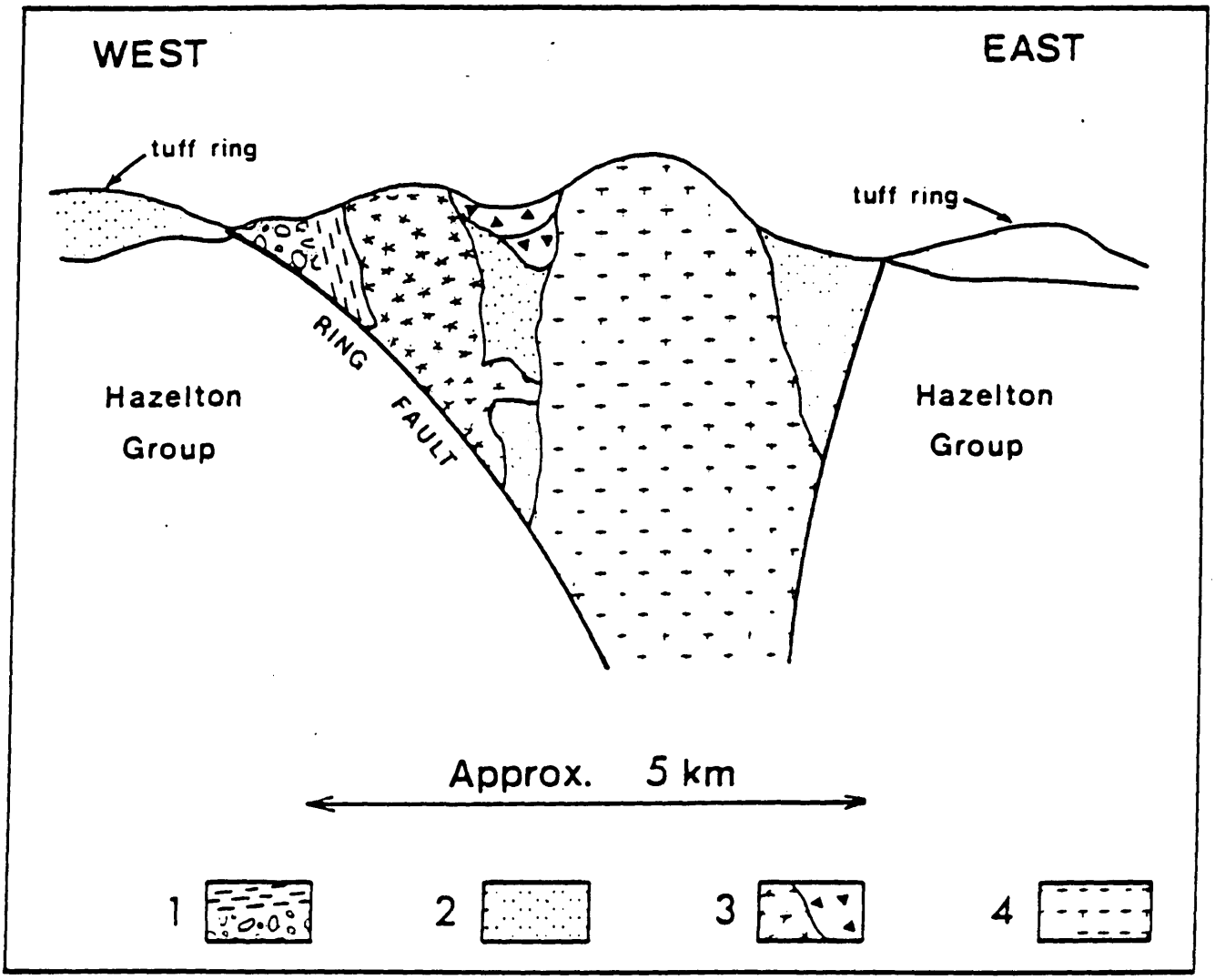

FIGURE 3.42: Schematic diagram illustrating Ootsa Lake Group volcanic setting at Wolf using a maar model. 1 = conglomerate and tuffs, 2 = pyroclastic assemblage, 3 = rhyolite dome, flows and breccia, and 4 = intrusions.

felsic, explosive volcanism forming a tuff ring and deposits within a caldera. Assemblage three, rhyolite flows and breccias, represents doming and associated hydrothermal products related to felsic volcanism within the caldera. Assemblage four, represents final magmatic resurgence causing emplacement of rhyolite porphyry and dykes through the volcanic pile. This intrusion was the last event prior to block faulting and the formation of mineralized veins.

Pearce element ratio diagrams are used to establish that the Eocene volcanic rocks at Wolf are comagmatic and may have formed in part by feldspar differentiation (section 3.3.5). Andesites, on the western side of the property (Fig. 3.1) are not comagmatic with the Eocene felsic volcanic rocks (Figs. 3.15 and 3.16).

A period of erosion from mid-Eocene to mid-Miocene time was followed by deposition of poorly consolidated mid-Miocene epiclastic rocks with a palynomorph assemblage correlative to the Fraser Bend Formation (G. Rouse, pers. comm., 1988). Post mid-Miocene low-angle thrusting of Ootsa Lake Group rocks over the sedimentary rocks at Wolf is similar to that described by Mathews and Rouse (1984) in the Gang Ranch-Big Bar area.

3.7.2 DEPOSIT MODEL

The model proposed for the Wolf epithermal gold-silver prospect is depicted in Figure 3.43 Geological setting, vein and breccia textures, alteration and metal distribution

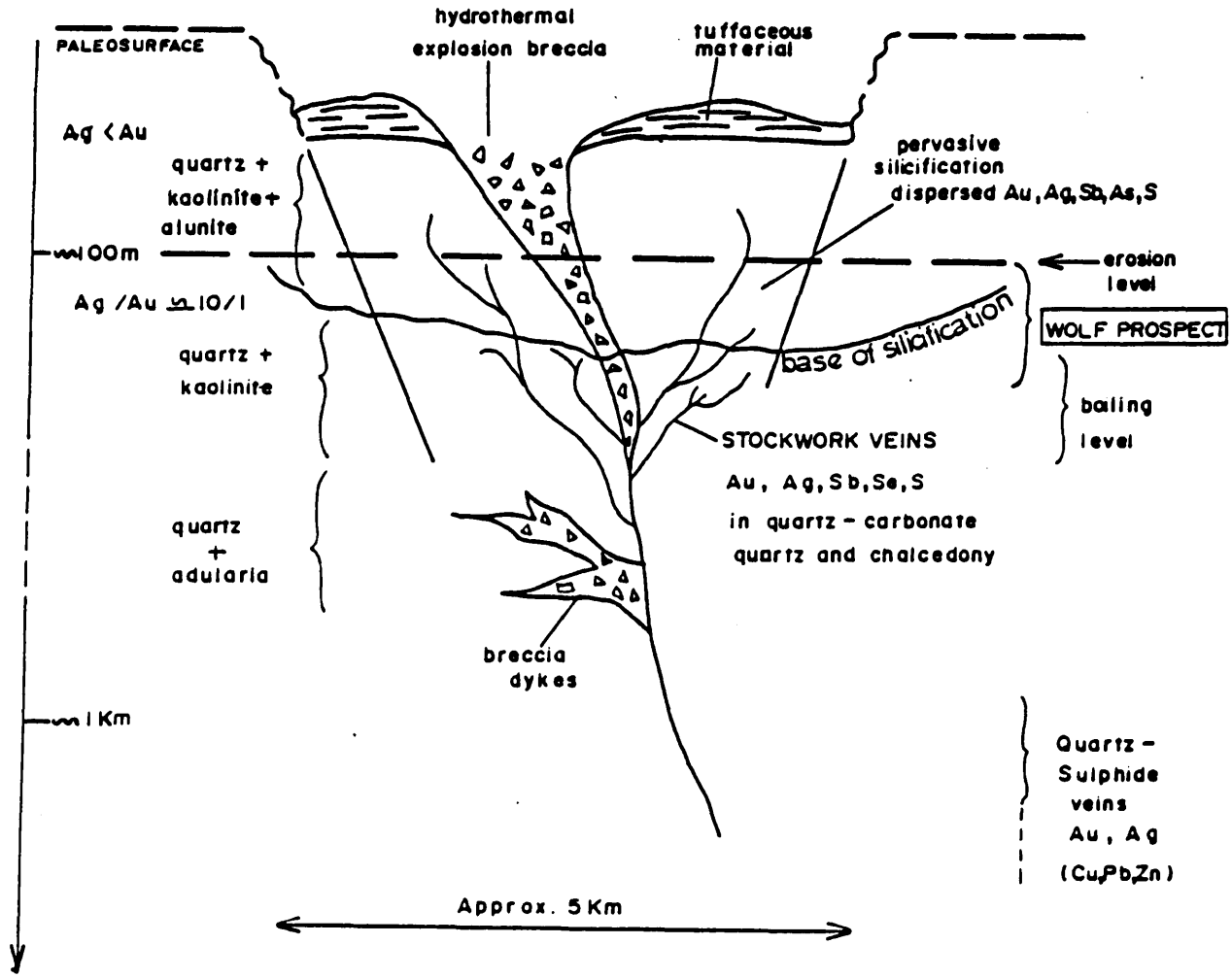

FIGURE 3.43: Schematic cross-section of low sulphur, hot-spring type silicified stockwork model for the genesis of the Wolf prospect, central British Columbia.

patterns at Wolf resemble those of a low sulphur, hot spring or silicified stockwork deposit (Berger and Eimon, 1983; Silverman and Berger, 1985; Hayba et al., 1985). Vein emplacement was probably caused by resurgent magmatic activity which produced a rhyolite porphyry stock and could have initiated hydrothermal circulation. Hydrothermal outflow was centred on at least five zones at Wolf, several of which were accompanied by significant mineralization (section 3.5).

Mineralization at Wolf is hosted in zones of silicified rhyolite and rhyolite porphyry, quartz and rhyolite breccias and quartz vein stockworks. Block faulting provided conduits for circulating hydrothermal fluids and structurally controlled deposition of veins. At least eight distinct phases of repeated, episodic and explosive stockwork veining and brecciation are recognised (section 3.5.2). Vein textures indicate deposition in a near-surface environment where lithostatic pressures were low enough to maintain open spaces produced by faulting. Breccia textures indicate explosive pressure release leading to local rock fracture and precipitation of mineralization. Metal distribution graphs and correlation matricies indicate only one mineralizing event on the property. This event is associated with formation of bladed quartz-carbonate veins and breccia infilling which host native silver, electrum and silver sulphosalts.

Fluid inclusion studies indicate that at least two different fluids were responsible for precipitation of veins at Wolf. Early-formed, mineralized quartz carbonate veins are characterized by homogenization temperatures of 170°C and 270°C and salinities of approximately 4 weight percent NaCl. Late cockade textured veinlets and drusy quartz are characterized by homogenization temperatures of 250°C and 170°C respectively, and salinities of approximately 2 weight percent NaCl. These high homogenization temperatures support the presence of an igneous body at depth which supplied thermal energy to drive the hydrothermal circulation. Both fluids, characterized by less than 0.1 mol percent CO_2, are typical of epithermal deposits. Compelling evidence for boiling at Wolf is the definition of growth zones in quartz by two phase liquid and vapour-rich inclusions. A wide variation in liquid to vapour ratios in inclusions and breccia textures within veins associated with precious metals also supports the occurrence of boiling. Depths of emplacement for boiling fluids were calculated using equations developed by Haas (1971). Considering conditions between extreme hydrostatic or lithostatic (Fig. 3.38C), using a rock density of 0.8 g/cm^3, early-formed quartz carbonate veins deposited at depths near 96 m. This calculated depth is less than one kilometre which is consistant with the epithermal character of the veins.

Stable isotope compositions of minerals at Wolf indicate that a high degree of isotopic exchange between

wallrock and large volumes of low ^{18}O content hydrothermal fluids (section 3.6.2). Oxygen and hydrogen isotope evidence shows that hydrothermal solutions at Wolf were meteoric in origin with virtually no contribution from magmatic sources (Fig. 3.40). Fluid evolution is documented in Figure 3.41 as a horizontal line with early-formed quartz carbonate veins plotting furthest from and late-formed drusy quartz plotting closest to the present day meteoric water line. The size of the hydrothermal circulation cell is predicted by water to rock ratios which indicate that for every gram of altered rock in the area of the prospect, at least 0.27 to 0.54 grams of water moved through the system in its lifetime. Conservatively, assuming an altered area of 10 km^2 to a depth of 700 m, the minimum amount of water that passed through 50 percent of these rocks is $2.55 * 10^{12}$ kg. The paleoclimate in the mid-Eocene was subtropical (Rouse, 1977; Rouse and Mathews, 1979) which probably contributed to the vast quantities of circulating fluids at Wolf.

The source of mineralization at Wolf is probably the host Ootsa Lake Group volcanic rocks with minor contribution from "basement" Hazelton Group rocks. Henley (1985) and McDonald (1987) have suggested that any rock type contains sufficient quantities of precious metals, in trace amounts, to supply the total metallic content typically found in most epithermal deposits many times over.

Field evidence, laboratory studies, and theoretical considerations suggest that large volumes of boiling, meteoric-hydrothermal fluids carrying scavanged precious metals from country rocks were focused into suitable structures, such as block and ring faults, causing pervasive argillic alteration and depletion of the rocks in ^{18}O at the site of hydrothermal discharge. Precious metals were precipitated in response to sudden pressure release accompanying fracturing and brecciation of a partially sealed cap (P_{lith} P_{hyd}). Periodic re-activation of faults, as a result of lithostatic pressure build-up, fractured previous silica sealed caps and/or veins, and lead to repetitive deposition of gold and quartz from boiling hydrothermal fluids and re-sealing of faults. Precipitation of significant gold mineralization is most closely associated with early-formed quartz carbonate veins. With time and waning of the hydrothermal system, fluids evolved to non-boiling lower salinity, extremely ^{18}O depleted, precious metal-poor variety which precipitated late drusy quartz.